東海大学大学院　令和四年度博士論文

Study on the reactivity of active oxygen species with the composite films of methylene blue/water-soluble polymers using quantum chemical calculation

（量子化学計算を用いた活性酸素種とメチレンブルー／水溶性ポリマー複合膜との反応性に関する研究）

指導　岩森　暁　教授

東海大学大学院総合理工学研究科

総合理工学専攻

PASIKA TEMEEPRASERTKIJ

Contents

Chapter 1

INTRODUCTION

1-1 Research background

AOS play pivotal roles in the oxidation reactions of organic compounds. AOS, such as singlet oxygen ($^1O_2$), ozone (O_3), and hydroxyl radicals (OH*), are of interest and value in surface modification, cleaning, and oxidation processes [(1-1)]. AOS is widely used to clean equipment in medical laboratories, including sterilization against Escherichia coli, and is considered more environmentally friendly than conventional methods used to clean packages in industrial environments. AOS can be generated by various techniques and applied for various industrial processes according to their strong oxidative properties [(1-2)]. Accordingly, there are several studies that recently developed an AOS indicator [(1-3), (1-4), (1-5), (1-6)]. The action of ozone as a vigorous oxidizing agent of elastomers and other polymers is well known [(1-7)].

In the previous paper, several methods for the design and application of developing a sensor that can visually determine the presence or absence of AOS via the decolorization of MB. We have reported the occurrence of indicators as well as the decolorization mechanism generated under specific AOS conditions. We have succeeded in preparing uniform MB-dyed water-soluble polymer thin films and investigating their decolorization characteristics upon their exposure to the AOS generated under the high-humidity condition. Moreover, the previous results of methylene blue/water-soluble polymer namely, pullulan and sodium alginate. Furthermore, the decolorization mechanism was investigated by comparing the nuclear magnetic resonance (NMR) spectra of MB mixed with water-soluble polymers before and after exposure to AOS [(1-8)]. The results indicate that film decolorization is caused by the decomposition of MB upon OH* exposure. Moreover, the MB-dyed pullulan and sodium alginate uniform thin films selectively reacted with OH*, which is the AOS generated under the high-humidity conditions. However, information concerning intermolecular interactions between MB and pullulan remains insufficient. To develop a target sensor for detecting OH* [(1-9), (1-10)], which has the strongest oxidative ability among AOS. MB is a convenient indicator for detecting AOS as it decolors after exposure to AOS due to the dye's degradation. MB component became weaker with reaction time. This phenomenon indicated that MB molecules were degraded and removed in the presence of OH radicals,

which is the degradation mechanism of MB in the photocatalytic oxidation process. However, in the above studies, none have focused on the degradation mechanism of MB.

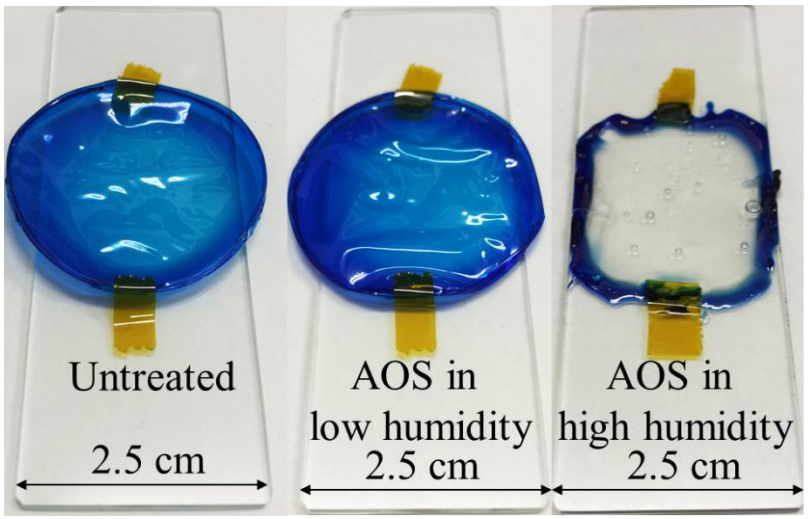

Fig 1-1 The methylene blue /pullulan film (The methylene blue /pullulan film lost coloration upon exposure to AOS under high humidity conditions) [1-10]

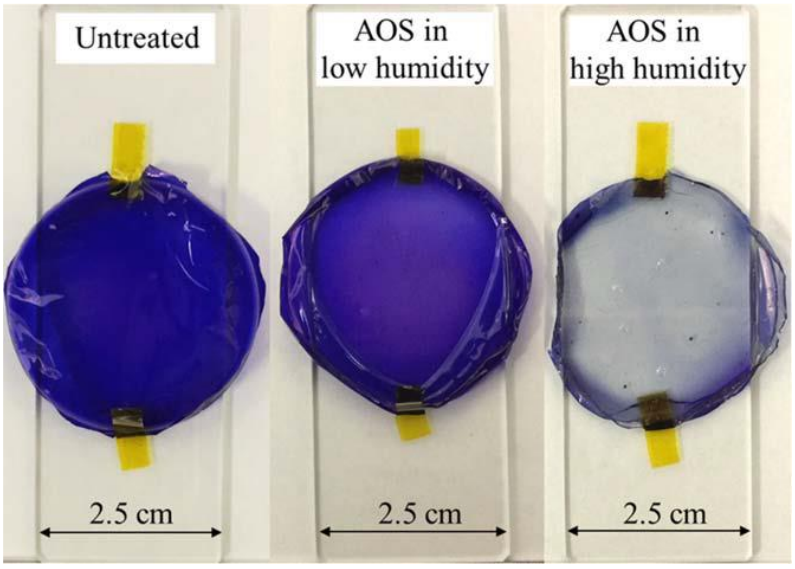

Fig 1-2 The methylene blue /sodium alginate film (The methylene blue /sodium alginate film lost coloration upon exposure to AOS under high humidity conditions) [1-11]

1-2 Current Research

In this paper, to clarify this indicator is a composite thin film based on methylene blue and water-soluble polymers such as pullulan or sodium alginate. It is well known also a decolorization mechanism that only occurs under a large amount of hydroxyl radical (OH*) condition, which has the strongest oxidative ability among AOS is presented. We investigated an index for AOS detection by elucidating the decolorization phenomenon that occurs between AOS and composite membranes by molecular orbital calculations were performed to clarify the molecular interactions between methylene blue, pullulan, sodium alginate, and AOS.

Calculations were performed using molecular orbital as a tool for predict the atomic orbitals of the system. MB and polymer structures were obtained using GaussView 5.0.9 software, which creates an input file for Gaussian 09 and outputs the calculation result as an image [1-12]. Calculations were performed using Gaussian 09 [1-13), (1-14)]. First, the semiempirical methods with PM6 and the HF methods with 3-21G and 6-31G(d) basis set calculations were performed to optimize the structures. Then, Gaussian 09 program was used to analyze molecular interactions, while molecular orbital calculations were used to predict the theoretical interaction positions as well as find the affinity binding energy orders of MB and polymer. The interactions between the filled orbitals of one reagent and the filled orbitals of another are inherently energy-raising, countered by a small attractive force from the interactions between the filled and unfilled orbitals, which are inherently energy-lowering. Both forces diminish exponentially with distance, but they come into play at short distances and are not the only interactions between nonpolar molecules. The resultant attractive force is known as a dispersion force, or more commonly, van der Waals (vdW) attraction. All chemists are familiar with the idea that atoms of a given element may be regarded as hard spheres whose radius, the vdW radius, is a characteristic of that element. A common reason for using the vdW radius is to compare nonbonded contact distances by subtracting the relevant radii from the distance observed in new crystal structures [1-15), (1-16)].

Moreover, the computational method, the MB/sodium alginate and MB/pullulan of complex structures can be evaluated by some chemical reactions descriptors such as LUMO energy (eV), HOMO

energy (eV), energy gap (eV), ionization potential (IP), electron affinity (EA), global hardness, chemical potential, softness, electrophilicity, and electronegativity. The decolorization of the film is caused by the degradation reaction of MB upon AOS exposure were also discussed. These investigations may also apply to evaluate uniform thin film indicators based on MB-dyed water-soluble polymers to elucidate the decolorization mechanism upon exposure to AOS.

As mentioned above, AOS with high oxidation that allows the film to decolorize. Polymer is readily oxidized in the presence of ozone; it was found that the degradation behavior relied heavily on the degree of oxidation [1-17]. Therefore, this can be used to develop thin-film indicators for AOS detection. O_3 is needed due to its very high oxidative ability, and similar studies using ozone suggested the decolorization of polymers [1-18], [1-19].

These observations apply to all the polymers studied, pullulan and sodium alginate. On comparing the rates of HOMO and LUMO energy value, however, it is observed that they vary from polymer to polymer, depending on the reactivity of the compound as defined by the stability of structure at specific points in the polymer chain.

In the computational method, the MB/sodium alginate and MB/pullulan of complex structures can be evaluated by some chemical reactions descriptors such as LUMO energy (eV), HOMO energy (eV), energy gap (eV), ionization potential (IP), electron affinity (EA), global hardness, chemical potential, softness, electrophilicity, and electronegativity. The decolorization of the film is caused by the degradation reaction of MB upon AOS exposure were also discussed. These investigations may also apply to evaluate uniform thin film indicators based on MB-dyed water-soluble polymers to elucidate the decolorization mechanism upon exposure to AOS.

The results offer insight into possible interaction modes allowing the decolorization of MB caused by OH*. The result of MO analysis suggested that the possibility of the formation between the OH group (in pullulan with sulfur, carbon, and nitrogen atoms in methylene blue) and the energy of the complex was lower than the calculated results for individual molecules. And the results indicated that stable methylene blue/sodium alginate complex structures possess intermolecular interactions between

the carboxylates (–COO-) of sodium alginate and sulfur, carbon, and nitrogen atoms in methylene blue. However, the indicators comprising sodium alginate or pullulan mixed with methylene blue cannot be decolorized in ozone exposure. In addition, chemical reactions of OH radical attack on methylene blue /pullulan and methylene blue/sodium alginate are investigated by using DFT calculations at B3LYP / 6-31G (d) level of theory. As a result, it was clarified that OH* has a significant effect on methylene blue /pullulan and methylene blue /sodium alginate complex structure of the decolorization mechanism.

1-3 Molecular orbital theory

What is molecular orbital theory

The molecular orbital theory provides a precise description of the molecular electronic structure only for one-electron molecules, but for many-electron molecules, it provides a sufficiently good approximate description to be generally useful. The full analytical calculation of the molecular orbitals for most systems of interest may be reduced to a purely mathematical problem, the digital computer programs that have been prepared to carry out these calculations have been mostly the result of extensive work by highly coordinated research groups [1-20]. The objective of any theory of molecular structure is to provide some insight into the various physical laws based on the chemical molecules. In terms of the more fundamental universal physical laws, in principle, such theories can aim at a precise quantitative description of the structure of molecules and their chemical properties, since the underlying physical laws are now well understood in terms of quantum theory based on the Schroedinger equation [1-21]. However, in practice mathematical and computational complexities make this goal difficult to attain, and one must usually resort to approximate methods.

1-4 Computational Chemistry

1-4-1 Approximate molecular orbital theory

Approximate molecular orbital theories [1-22] are based on pattern developed within the mathematical framework of molecular orbital theory, but with a few simplifications introduced in the computational procedure. Often experimental data on atoms and prototype molecular systems are used to estimate values for quantities entering the calculations as parameters, and for this reason, the procedures are widely known as semiempirical methods.

1-4-2 GaussView program and Gaussian 09 program

GaussView[1-23),(1-24),(1-25] is a graphical user interface developed to help you create input files to pass to Gaussian and to graphically analyze the output produced by Gaussian. GaussView elevated visualization capabilities make it quick and easy to draw even very large molecules. The drawn molecular structure can be rotated, moved, and enlarged with just a mouse operation. Also, GaussView makes it easy to set up various Gaussian calculations. If your computer has Gaussian installed on the same machine as GaussView, a researcher can start Gaussian directly from GaussView and start the calculation. The results of Gaussian calculations using GaussView's various graphics techniques. Gaussian calculation results that can be displayed graphically include:

- Structure-optimized molecular structure.
- Various molecular orbitals.
- Calculated electron density surfaces of various densities.
- Electrostatic potential surface.
- Surface of magnetic properties.
- Surface contour display.
- Atomic charge and dipole moment.
- Reference mode animation corresponding to vibration frequency.
- IR, Raman, NMR, VCD and other spectra.
- Stereochemical information of molecules.

- Animation of structural optimization, IRC reaction path tracing, potential energy surface scanning, ADMP and BOMD orbits. In 2-variable scanning, it can be displayed as a 3D plot.
- Total energy changes and plots of each data obtained in the above calculations (structural optimization, IRC, etc.).

Gaussian is an ab initio molecular orbital calculation software developed and provided by Gaussian, Inc. in the United States. The purpose is to analyze the electronic structure of a substance, and it is possible to model molecules under various conditions and analyze their physical properties in quantum mechanics.

1-4-3 Ab initio method

This type of computation is based only on theoretical principles, using no experimental data. The numerous methods have the same basic approach but differ in the mathematical approximations used. These are the most popular type of models, even though the calculations take a long time.

1-4-4 Hartree-Fock (HF)

HF is the basic ab initio model. It uses the approximation that Coulombic electron-electron repulsion can be averaged, instead of considering explicit repulsion interactions (central field approximation). There are two ways to compute molecular orbitals using HF: UHF (unrestricted) or RHF (restricted). UHF uses a separate orbital for each electron, even if they are paired (used for ions, excited states, radicals, etc.). RHF uses the same orbital spatial function for electrons in the same pair (good for species with paired electrons, no spin contamination). The major drawback of the HF method is the exclusion of electron correlation. The following models start with an HF calculation and then correct for electron repulsion.

1-4-5 Semiempirical method

Semiempirical methods use a certain number of experimental data throughout the calculation. For example, bond lengths of a specific type will have a fixed value independently of the system. This dramatically speeds up computational time, but in general, is not very accurate. Usually, semiempirical methods are used for very big systems, since they can handle large amounts of calculation.

1-4-6 PM6

The semi-empirical method has been improved in the order of AM1 (1985) → PM3 (1989) → PM5 (2002) → PM6 (2007) → PM7 (2012) by devising integral calculations and parameters. Here, PM is an abbreviation for parameter method, and experimental values are used as statistical parameters instead of integral calculations. On top of that, a method is most often used to model organic molecules.

1-4-7 Density functional theory

DFT methods are becoming more popular because the results obtained are comparable to the ones obtained using ab initio methods. The DFT differs from methods based on HF calculations in the way that it is the electron density that is used to compute the energy instead of a wave function.

1-4-8 B3LYP

This is the most popular DFT model. This method is called to be a hybrid, because it is uses corrections for both gradient and exchange correlations.

1-4-9 Basis sets

Most methods require a basis set be specified; if no basis set keyword is included in the route section, then the STO-3G basis will be used. The following basis sets are stored internally in the Gaussian program, listed below by their corresponding Gaussian keyword:

• 3-21G

• 6-31G

• 6-311G

Adding Polarization and Diffuse Functions Single first polarization functions can also be requested using the usual * or ** notation. Note that (d, p) and ** are synonymous-6-31G** is equivalent to 6-31G(d, p), for example-and that the 3-21G* basis set has polarization functions on second row atoms only. The + and ++ diffuse functions are available with some basis sets, as are multiple polarization functions. The keyword syntax is best illustrated by example: 6-31+G(3df,2p) designates the 6-31G basis set supplemented by diffuse functions, 3 sets of d functions and one set of functions on heavy atoms and supplemented by 2 sets of p functions on hydrogens. A basis set is a set of wave functions that describes the shape of atomic orbitals (AOs). The molecular orbitals (MOs) are computed using the selected theoretical model by linearly combining the AOs (LCAO). Not all theoretical models require the user to choose a basis set to work with. For example, PMn (n=3...,6) models use an internal basis set, while ab initio or density functional theory requires a basis set specification. The level of approximation of your calculation is directly related to the basis set used. The choice to make is a trade-off between the accuracy of results and CPU time.

Adding a single polarization function to 6-311G (i.e. 6-311G(d)) will result in one d function for first and second row atoms and one f function for first transition row atoms, since d functions are already present for the valence electrons in the latter. Similarly, adding a diffuse function to the 6-311G basis set will produce one s, one p, and one d diffuse functions for third-row atoms.

1-4-10 Type of calculation

1-4-10-1 Geometry optimization (Opt)

Geometry optimization is a name for the procedure that attempts to find the configuration of the minimum energy of the molecule. The procedure calculates the wave function and the energy at a starting geometry and then proceeds to search for a new geometry of lower energy. This is repeated until the lowest energy geometry is found.

The desired fitting basis set is specified as a two-component of the model chemistry, as in this example:

```
%chk=(file name).chk

# opt hf/6-31g(d) (method/ basis sets) geom=connectivity

Title Card Required

0 1

Component (1)  0.00    0.00    0.00

Component (2)  0.00    0.00    0.00
```

0 1 is the molecule specification section specifies the net electric charge (a signed integer) and the spin multiplicity (usually a positive integer). Thus, for a neutral molecule in a singlet state, the entry 0 1 is appropriate. For a radical anion, -1 2 would be used. Multiple charge/spin pairs may/must be included for some calculation types.

1-4-10-2 Energy

This procedure simply calculates the energy, wave function, and other requested properties at a single fixed geometry. It is usually done first at the beginning of a study on a new molecule to check out the nature of its wave function.

The desired fitting basis set is specified as a two-component of the model chemistry, as in this example:

```
%chk=(file name).chk

# hf/6-31g(d) (method/ basis sets) geom=connectivity

Title Card Required

0 1

Component (1)  0.00  0.00  0.00

Component (2)  0.00  0.00  0.00
```

1-4-10-3 Counterpoise

The Counterpoise keyword requires an integer value that specifies the number of fragments or monomers in the molecular environment. This feature also requires an integer value to be added to the end of the atom designation to indicate which fragment monomer each atom belongs to.

BSSE is an abbreviation for "Basis Set Superposition Error". BSSE is the error that one molecule overestimates the stabilization energy when calculating the complex of molecules by using the basis function of the other molecule to supplement the degrees of freedom of the electron.

The following input is an example of a counterpoise calculation:

```
%chk=(file name).chk

# hf/6-31g(d) (method/ basis sets) geom=connectivity Counterpoise=2

0 1

Component (1) (Fragment=1)          0.00    0.00    0.00

Component (1) (Fragment=2)          0.00    0.00    2.98
```

1-4-11 UV-Vis and electronic transition

Most molecules have bound higher energy excited electronic states in addition to the ground electronic state E0. These states may be thought of as arising from the promotion of one of the electrons from the occupied orbital in the ground state to a vacant higher energy orbital. The excitation of an electron from the occupied orbital to a higher-energy orbital occurs when a photon with the energy that matches the difference between the two states that interact with the molecule. The classical Franck-Condon principle states that because the rearrangement of electrons is much faster than the motion of nuclei, the nuclear configuration does not change significantly during the energy absorption process. Thus, the absorption spectrum of molecules is characterized by vertical excitation energies.

TD: This Time-Dependent calculation is based on a DFT computational method. TD-DFT obtains the wave functions of MOs that oscillate between the ground state and the first excited states.

The desired fitting basis set is specified as a one-component of the model chemistry, as in this example:

```
%chk=(file name).chk

# td hf/6-31g(d) (method/ basis sets) geom=connectivity

Title Card Required

0 1

Component (1)
```

Singlets: solve only for singlet excited states. Only effective for closed-shell systems, for which it is the default.

1-4-12 Information achieves from calculation

- Atomic coordinates of optimized molecule
- Optimized parameters: atomic distances and angles
- HOMO/LUMO (hartree)
- Single Point energy
- Thermochemistry
    - Temperature
    - Pressure
    - Isotopes used
    - Molecular mass
    - Thermal energy: E (Thermal)
    - Constant volume molar heat capacity (CV)
    - Entropy (S)
    - Free Energy (sum of electronic and thermal Free Energies)
    - Enthalpy (sum of electronic and thermal Enthalpies)

- Ground to excited state transition
- Excitation energies and oscillator strengths
- Electronic Circular Dichroism (ECD)

1-5 Purpose of this study

In this study, we investigated an index for AOS detection by elucidating the decolorization phenomenon that occurs between AOS and composite membranes. To address this issue, the index for AOS detection using the decolorization phenomenon that occurs between AOS and composite membranes was explored at the atomic interaction level. To approach the goal, the quantum chemical calculation techniques were used to clarify the molecular interactions between AOS and a methylene blue/pullulan or methylene blue/sodium alginate composite thin film.

1. We investigated the intramolecular interaction between methylene blue and pullulan by using a methylene blue/pullulan composite thin film for detecting OH * with high oxidizing power.

2. The decolorization mechanism of methylene blue was investigated by using sodium alginate. This chapter also provide theoretical evidence for understanding how ozone causes decolorization of methylene blue and why the indicators made of sodium alginate or pullulan mixed with methylene blue are not decolorized by the ozone exposure.

3. Geometrical properties, highest unoccupied molecular orbital (HOMO), and the lowest unoccupied molecular orbital (LUMO) have been studied for better understanding of decolorization mechanism of OH* reaction with methylene blue and water-soluble polymers (pullulan and sodium alginate).

1-6 Organization of this paper

This paper consists of the following chapters:

Chapter 1 is an introduction. Consists of a part that describes the molecular orbital theory, computational chemistry, purpose of this study, and organization of this paper.

Chapter 2 is Interactions between Methylene Blue and Pullulan According to Molecular Orbital Calculations. In the previous studies, we aim to detect the presence of active oxygen species (AOS) and establish its technology for sterilization and surface modifications of polymer substrates. A colorimetric indicator based on methylene blue (MB)-dyed pullulan thin films for detection of hydroxyl radicals as a novel indicator to detect active oxygen species with improved oxidative ability was developed [(1-8)]. However, information concerning intermolecular interactions between MB and pullulan remains insufficient. To develop a target sensor for detecting OH* [(1-9)], which has the strongest oxidative ability among AOS, we investigated AOS reactions on MB-dyed, uniform pullulan thin films, revealing that MB decolorization of the thin films occurred only under high humidity conditions presumably caused by OH* [(1-8)]. In this study, we identified MB–pullulan interactions using molecular orbital (MO) calculations for used a truncated pullulan model represented by five glucose units to investigate the large and complex pullulan structure. The results identified MB–pullulan interactions at the HF/6-31G(d) level, revealing 10 MB–pullulan complex structures with full geometry optimization. Moreover, structural and energy analyses predicted the existence of the hydrogen-bonding interactions between pullulan hydroxyl groups and MB nitrogen, carbon, or sulfur atoms. The results of MO analysis suggested the formation of hydrogen bonds between S, C, and N atoms in the MB benzene ring with a pullulan OH group groups, resulting in lower electronic energy in the complex structure relative to that observed in the individual molecules.

Chapter 3 is Molecular interactions between methylene blue and sodium alginate studied by molecular orbital calculations. In the previous result [(1-8)]., an indicator of AOS made from uniform thin films was developed using MB-dyed SA, which can be generated under atmospheric conditions and have high reactivity. The aim of previous research was to detect AOS and establish AOS technology

for the sterilization and surface modification of polymer substrates. Decolorization occurred when the film was exposed to AOS with high humidity. This process allows us to reveal the intermolecular interactions between MB and SA since the molecular structure will appear digitally. In addition, it will deepen our understanding of the interactions between MB and SA as the decolorization reaction occurs due to AOS. The molecular orbital theory is used to describe the arrangement of electrons in chemical structures. It can also provide insights into the forces involved in the making and breaking of chemical bonds—the chemical reactions that are of high interest to organic chemists. The most rewarding approach to date has been using molecular orbital calculations to predict the atomic orbitals of the system. MB and SA structures were obtained using GaussView 5.0.9 software, which creates an input file for Gaussian 09 and outputs the calculation result as an image

Chapter 4 is reaction of hydroxyl radical (OH*) with methylene blue (MB) and polymer (pullulan and sodium alginate) account for chemical reactions and the decolorization mechanism. In previous study, we developed a colorimetric indicator based on methylene blue-dyed and polymer (pullulan and sodium alginate) thin films for detecting OH* as a novel indicator to detect active oxygen species with the improved oxidative ability. In the present work, Geometrical characteristics, HOMO-LUMO, and binding energy has been studied. Chemical reactions of OH* attack on MB/pullulan and MB/SA are investigated using the density functional theory (DFT) B3LYP method with 6-31G (d) basis sets. Accordingly, our DFT calculations elucidated that OH* has a significant effect on MB/pullulan and MB/SA complex structure of chemical reactions and the decolorization mechanism. Results suggested that OH* shows a strong decolorization mechanism of both complex structures. Furthermore, the binding energy and HOMO-LUMO energy results indicated that the estimation of MB/pullulan complex structures are more stable in comparison with MB/ sodium alginate complex structures.

Chapter 5 is summarizing the results obtained in Chapters 2, Chapters 3 and Chapters 4.

References

(1-1) S. Iwamori, N. Nishiyama, K. Oya. “A colorimetric indicator for detection of hydroxyl radicals in atmosphere using a methylene blue dye based on nafion film”. Polymer Degradation and Stability. 2016, 123, 131-136.

(1-2) K. Yoshino, H. Matsumoto, T. Iwasaki, S. Kinoshita, K. Noda and S. Iwamori, “Study on sterilization system using reactive oxygen species”, Journal of the Vacuum Society of Japan, Vol. 54 (2011), pp. 467-473.

(1-3) K. Hosoya, S. Yenchit, Y. Tadokoro, K. Oya, S. Iwamori. “Improved Singlet Oxygen Detection Sensitivity in Electron Spin Resonance Using a Spin-trap Agent Incorporated into a Water-soluble Polymer Film”. The Chemical Society of Japan. 2018, 47, 1191-1193.

(1-4) C. Bailly. “Active oxygen species and antioxidants in seed biology”. Seed Science Research. 2004, 14(2), 93-107.

(1-5) K. Oya, K. Hosoya, T. Suto, S. Iwamori. “Surface modification of polydimethylsiloxane by exposure of active oxygen and ultraviolet lights to improve cell adhesion”. The Japan Society of Mechanical Engineers. 2019, 85(871).

(1-6) H. Masaki, Y. Okano, H. Sakurai. “Generation of Active Oxygen Species from Advanced Glycation End-Products (AGE) under Ultraviolet Light A (UVA) Irradiation”. Biochemical and Biophysical Research Communications. 1997, 235(2), 306-310.

(1-7) A. R. Allison, I. J. Stanley. “Ozone Deterioration of Elastomeric Materials”. Analytical Chemistry. Vol 24, NO. 4, April 1952.

(1-8) S. Yenchit, Y. Tadokoro, S. Iwamori. “Measuring Active Oxygen Species Across a Nonwoven Fabric Using a Pullulan-mixed Methylene Blue Thin Film and Electron Spin Resonance”. The Institute of Electrical Engineers of Japan. 2019, 139(3), 54-60.

(1-9) S. Yenchit, Y. Tadokoro, Y. Oda, S. Iwamori. “Chemical stability of P thin film employing methylene blue dye for active oxygen species”. The 4th Japan-Korea International Symposium on Materials Science and Technology. 2017 (JKMST 2017), August 24-26, 2017.

(1-10) S.Yenchit , H. Yamanaka, P. Temeeprasertkij, Y. Oda, Y. Okamura,T. Inazu, S. Iwamori. “A Colorimetric Indicator Based on Methylene Blue-Dyed Pullulan Thin Films for the Detection of Hydroxyl Radicals”. Materials science and technology. 2020, pp. 109-113.

(1-11) S.Yenchit , H. Yamanaka, P. Temeeprasertkij, Y. Oda, O. Kanie, Y. Okamura,T. Inazu, S. Iwamori. “Chemical stability of a colorimetric indicator based on sodium alginate thin film and methylene blue dye upon active oxygen species exposure”. Japanese Journal of Applied Physics. 2020, Vol. 59, SDDF09.

(1-12) C. Tabti, N. Benhalima. “Molecular Structure, Vibrational Assignments and Non-Linear Optical Properties of 4,4’ Dimethylaminocyanobiphenyl (DMACB) by DFT and ≪i≫Ab Initio HF Calculations”. Advances in Materials Physics and Chemistry. 2015, Vol. 05, pp. 221-228.

(1-13) P. Temeeprasertkij, S. Yenchit, M. Iwaoka, S. Iwamori. “Interactions between Methylene Blue and Pullulan by Molecular Orbital Calculations”. 4th Japan-Thailand Joint Symposium on Advanced Nanomaterials and Devices for Electronics and Photonics (JT-AND 2020), DEI-20-018, Thailand.

(1-14) D. Nori-Shargh, M.M. Amini, S. Jameh-Bozorghi. “Ab Initio Study of Ring Flipping of the Overcrowded Peri-Substituted Naphthalenes”. Phosphorus, Sulfur, and Silicon and the Related Elements. 2003, Vol. 178, pp. 2529-2537.

(1-15) R.S. Rowland, R. Taylor. “Intermolecular Nonbonded Contact Distances in Organic Crystal Structures: Comparison with Distances Expected from van der Waals Radii”. Journal of Physical Chemistry. 1996, Vol. 100, pp. 7384-7391.

(1-16) P. Temeeprasertkij, S. Yenchit, M. Iwaoka, S. Iwamori. “Interactions between Methylene Blue and Pullulan According to Molecular Orbital Calculations”. IEEJ Transactions on Fundamentals and Materials. 2020, Vol. 140, pp. 529-533.

(1-17) C. Gao, M. Liu, J. Chen, X. Zhang. “Preparation and controlled degradation of oxidized sodium alginate hydrogel”. Polymer Degradation and Stability. (2009, 1405–1410.

(1-18) N. Nagasawa, H. Mitomo, F. Yoshii, T. Kume. “Radiation-Induced Degradation of Sodium Alginate”. Polymer Degradation and Stability. 2000, Vol. 69, pp. 279-285.

(1-19) H.C. Beachell, S.P. Nemphos. “Oxidative Degradation of Polymers in Presence of Ozone”. Advances in Chemistry. Ozone Chemistry and Technology Advances in Chemistry, American Chemical Society: Washington, DC. 1959, pp. 168-175.

(1-20) R.S. Mulliken and C.C.J. Roothaan, "Broken Bottlenecks and the Future of Molecular Quantum Mechanics", Proc. Natl. Acad. Sci. (U.S.), 45 (1959) 394-398.

(1-21) V. Christianto. “A Review of Schrödinger Equation & Classical Wave Equation”. Prespacetime Journal. 2014, pp. 400-413.

(1-22) Y.K. Pan. “Approximate molecular orbital theory”. Journal of Chemical Educafion. 1971, pp. Vol. 48, pp. A107-A132.

(1-23) Young, D. Computational Chemistry: A Practical Guide for Applying Techniques to Real World Problems; John Wiley & Sons, inc: USA, 2001.

(1-24) Jensen, F. Introduction to computational Chemistry, 2nd ed.; John Wiley & Sons, inc: England, 2007.

(1-25) GAUSSIAN 09W TUTORIAL AN INTRODUCTION TO COMPUTATIONAL CHEMISTRY USING G09W AND AVOGADRO SOFTWARE; Anna Tomb, (anna.tomberg@mail.mcgill.com).

Chapter 2

Interactions between Methylene Blue and Pullulan According to Molecular Orbital Calculations

[P. Temeeprasertkij, S. Yenchit, M. Iwaoka, S. Iwamori. “lnteractious between Methylene Blue and Pullulan According to Molecular Orbital Calculations”. IEEJ Transactions on Fundarncntals and Materials, 2020, Vol. 140 No.11, pp. 529-533.]

2-1 Background

In our previous study, we developed a colorimetric indicator based on methylene blue (MB)-dyed pullulan thin films for detection of hydroxyl radicals as a novel indicator to detect active oxygen species with improved oxidative ability; however, information concerning intermolecular interactions between MB and pullulan remain insufficient. In this study, we identified MB–pullulan interactions using molecular orbital (MO) calculations for used a truncated pullulan model represented by five glucose units to investigate the large and complex pullulan structure. Active oxygen species (AOS) play pivotal roles in the oxidation reactions of organic compounds. AOS, such as singlet oxygen (1O2), ozone (O3), and hydroxyl radicals (OH*), are of interest and value in surface modification, cleaning, and oxidation processes [(2-1)]. AOS is widely used to clean equipment in medical laboratories, including sterilization against Escherichia coli, and is considered more environmentally friendly than conventional methods used to clean packages in industrial environments. According to their solid oxidative properties, AOS can be generated by various techniques and applied to various industrial processes. Accordingly, there are a number of studies which recently developed an AOS indicator [(2-2), (2-3), (2-4), (2-5)].

Because methylene blue (MB), a redox dye used as a colorimetric oxygen indicator, can be decomposed by exposure to O3, thin films created using MB-dyed pullulan have been successfully established as indicators [(2-6)] However, in an effort to develop a target sensor for detecting OH*, which has the strongest oxidative ability among AOS, we investigated AOS reactions on MB-dyed, uniform pullulan thin films, revealing that MB decolorization of the thin films occurred only under high humidity conditions presumably caused by OH* [(2-7)].

MB-dyed pullulan films have been used as models to investigate MB decolorization [(2-8)]. For this process, it is crucial for MB to be stabilized by mixing with pullulan, where MB is one of the redox dyes that is used for colorimetric oxygen indicator. Pullulan also contains numerous OH groups, which are considered to form interactions with MB at N+/S+. Pullulan is a natural water-soluble polysaccharide with excellent film-forming properties. Pullulan has a large and complex structure that

makes it difficult to identify interactions with MB. Therefore, we used molecular orbital (MO) calculations to determine MB–pullulan interactions in the present study.

Determination of MO composition is frequently employed in quantum chemistry [2-9]. In the present study, we characterized the interaction parameters of possible intermolecular O–H···X (X= N, C, or S) hydrogen bonds and binding energies for the pullulan–MB complexes at HF/6-31G(d) to investigate changes in structural stability the structure as the energy level decreases [2-10]. The results identified MB–pullulan interactions at the HF/6-31G(d) level, revealing 10 MB–pullulan complex structures with full geometry optimization. Moreover, structural and energy analyses predicted the existence of the hydrogen-bonding interactions between pullulan hydroxyl groups and MB nitrogen, carbon, or sulfur atoms. The results of MO analysis suggested the formation of hydrogen bonds between S, C, and N atoms in the MB benzene ring with a pullulan OH group groups, resulting in a lower electronic energy in the complex structure relative to that observed in the individual molecules. To detect AOS with higher oxidative ability, it is necessary to stabilize MB by mixing it with pullulan, which has a high affinity for the dye, in order to form MB/pullulan composite films. The MB stabilization achieved from this composite enables MB decolorization in the presence of AOS. Additionally, in the present study, we aimed to elucidate the chemical reactions and the decolorization mechanism associated with exposure of the optimized MB–pullulan structures to OH*. The results offer insight into possible interaction modes allowing AOS detection under various conditions.

2-2 Purpose

It was confirmed that the mixture of MB and the water-soluble polymer was uses to form thin film did not react with AOS. However, hydroxyl radicals did, and the mechanism behind it was unknown. Therefore, to elucidate the decolorization mechanism upon exposure to OH* and apply it to industrial processes, my colleagues and I aimed to create a uniform thin film indicator based on MB and water-soluble polymers, pullulan. In addition, the decolorization mechanism was investigated by using Gaussview, Gaussian 09 programs. Then we analyze by using the calculation for atomic orbitals, which will be a good approximation to the molecular orbitals system.

2-3 Analytical Methods

MO calculations were performed at Tokai University (Tokyo, Japan) using Gaussview (v.5.0.9) and Gaussian 09 programs (https://gaussian.com/). Gaussview was used to create the molecular structures of MB–pullulan (Fig. 2-8), and Gaussian 09 was used to analyze molecular interactions. The pullulan molecule was represented by five glucose units and used to create the MB–pullulan complex structure. The respective MB, pullulan, and complex structures obtained from the Gaussview program were optimized at the Hartree–Fock 3-21G (HF/3-21G) level using MO calculations with the Gaussian 09 program [(2-11)]. For each complex structure, geometric parameters and bond energies were obtained from HF/3-21G ab initio calculations, with HF/3-21G basis sets used for the remaining atoms [(2-12)]. These calculations agreed well with our previous data. The geometries of the obtained structures with low electronic energy were further fully optimized at the HF/6-31G (d) and DFT calculations at B3LYP / 6-31G (d) level to obtain a set of 20 structures for the MB–pullulan complex.

2-4 Experiment

2-4-1 Procedure for submitting calculations

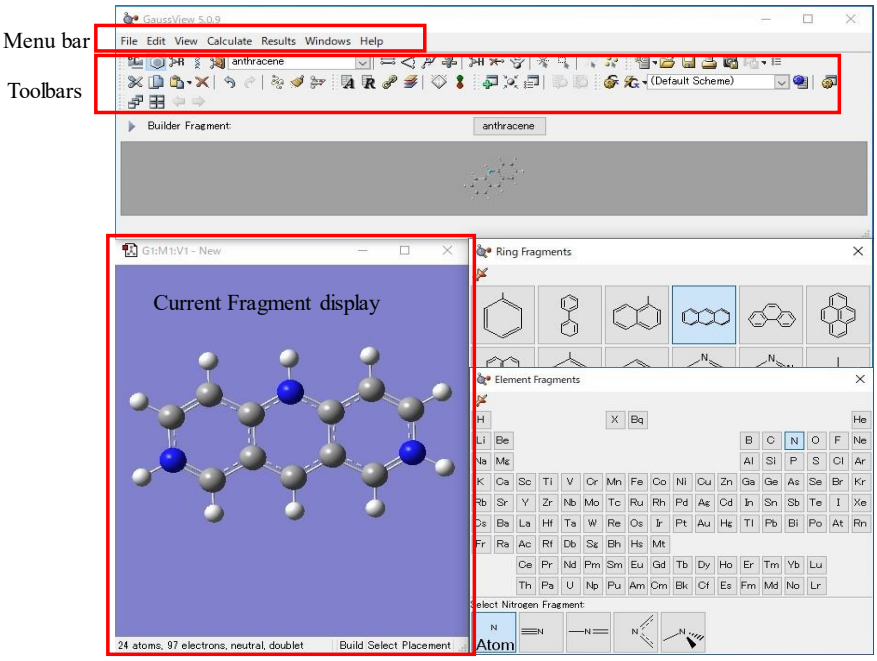

Fig 2-1 MB in which the user has just started to build a molecule

When we start by building the MB structure, we will see the main GaussView control panel. That consists of the menu bar, toolbars, and workspace, as shown in Fig. 2-1.

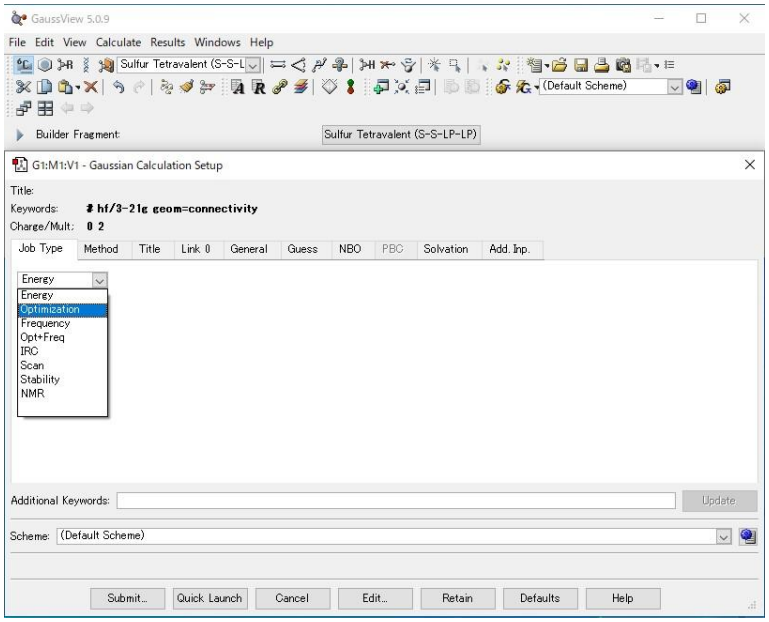

(a)

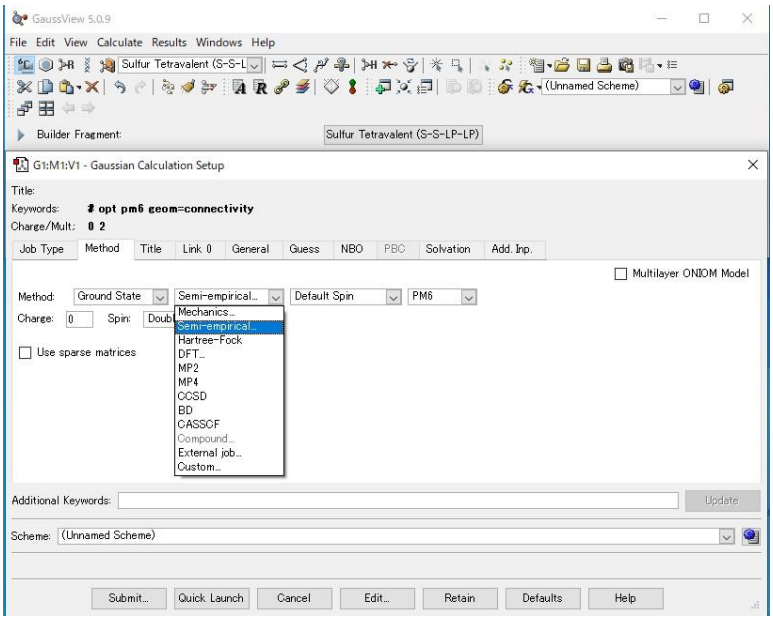

(b)

Fig 2-2 Gaussian Calculation setup

We must set up the program for computing to obtain a proper structure by setup "set the preferred Gaussian" at menu calculation and setup dialog settings, as shown in Fig. 2-2 (a). We start with setting job type by a set at Optimization in Method mode, as shown in Fig. 2-2 (b). In Method mode, we started with the Semiempirical method PM6 because this level of computation is entry-level,

making it faster to calculate. However, we need the accuracy of the calculation results. Therefore, we will increase the computational level to a higher level following at the Hartree–Fock method at the HF/3-21G level, HF/6-31G (d) and density functional theory (DFT) B3LYP/6-31G(d), respectively.

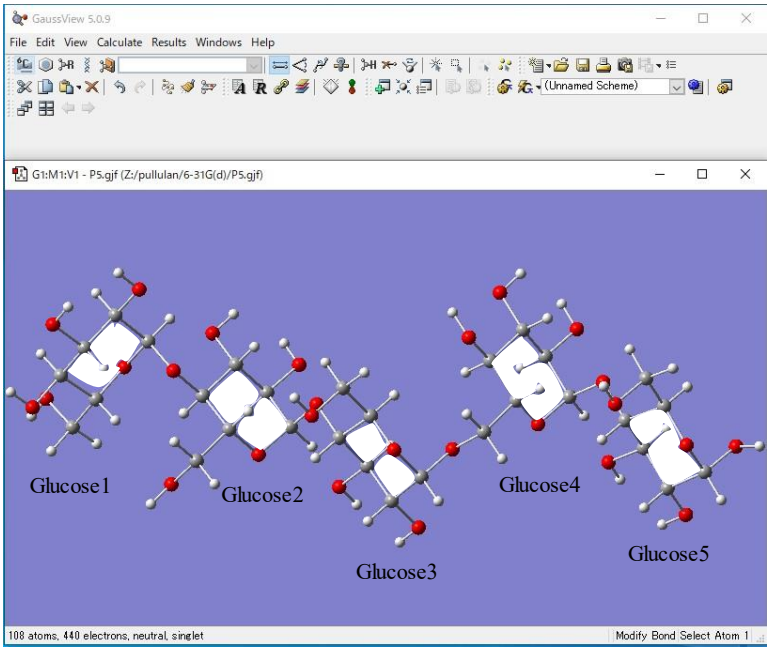

Fig 2-3 The structures of pullulan 5 glucose molecules

Although the accuracy and the computation time of calculation are in a trade-off relation depending on a molecular size, the size of the model should be kept in a reasonable range in the calculation. Therefore, the pullulan model was represented by five glucose units. The 3 glucoses units in maltotriose are connected by an α-1,4 glycosidic bond, whereas the consecutive maltotriose moieties are connected to each other by an α-1,6 glycosidic bond. Initially from previous experiments, we thought that the pullulan structure would cover MB. However, the pullulan 3 glucose structure was too short to see any changes. Therefore, we increase the number of glucoses in the pullulan structure. Since we don't want the structure to be very complicated, glucose increments are added one at a time. As a result, the 5 glucoses structure was the most suitable structure for this research. We start building the pullulan structure and follow the same steps as MB.

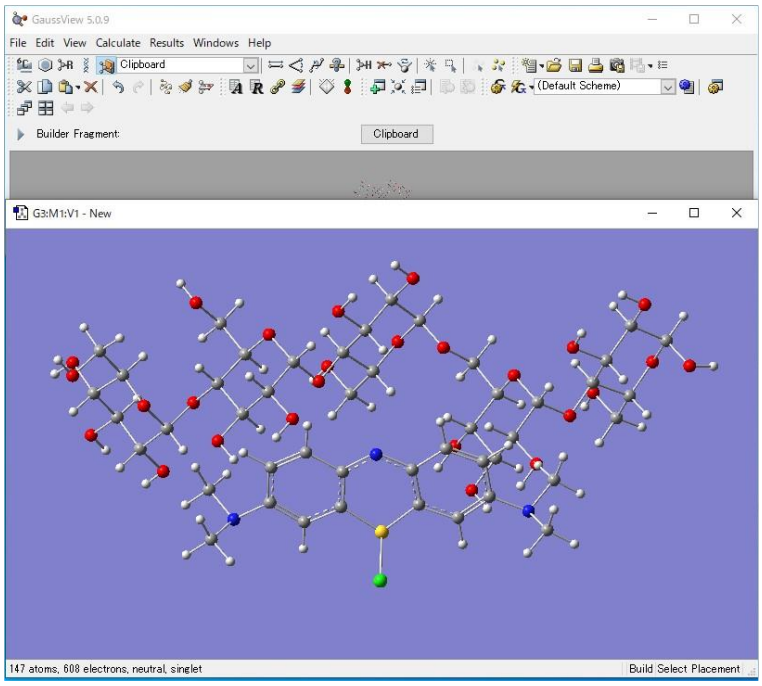

Fig 2-4 MB: Pullulan at 1:1

The Guassview program created 50-initial structures with the ratio of MB: Pullulan at 1:1. Initially, the Pullulan structure was set at the same position. As for MB, the structure was rotated for the position around the pullulan structure. Subsequently, these structures were sent to Gaussian 09 for geometry optimization at the calculation level of the semi-empirical PM6 method. The accuracy of semi-empirical PM6 is good for screening structure errors at the early stage. The PM6 method has been well-tuned with empirical parameters to predict roughly geometries [(2-13)]. Thus, the 50 stable structures were obtained as an initial set of MB–pullulan complex structures.

Since the semiempirical method is not very accurate to discuss the geometry of a molecular complex [(2-14)], the geometries of the resulting 50 structures were reoptimized using the ab initio Hartree–Fock method at the HF/3-21G level.

We selected some structures (from a total of 50) that provided the lowest energy calculated by the energy at the HF/3-21G level. Continued geometric optimization using this method allowed identification of the optimized intermolecular separation. Structures were generated according to the energy difference between the optimized complex for several trial values [(2-15)].

Further geometry optimization was employed at the HF/6–31G(d) level and DFT B3LYP/6-31G(d) for some structures. This process resulted in 20 stable structures, which could be used to identify the modes of interactions and the binding energies.

2-4-2 Assessment of the interaction modes

The van der Waals radii of atoms were employed as standards to identify the interaction modes between MB and pullulan. Van der Waals radii describe interatomic distances calculated using the sum of atomic radii, which differ between metals and non-metals (Table 1).

Table 1. Several definitions for van der Waals radii of atoms [2-16]

Author, year	Radii, Angstrom (Å)				
	H	N	C	O	S
Bondi, 1964	1.20	1.55	1.70	1.52	1.80
Pauling, 1939	1.20	1.50	1.70	1.40	1.85
Rowland, 1996	1.10	1.64	1.77	1.58	1.81
Zefirov, 1974	1.16	1.50	1.71	1.29	1.84
Gavezzotti, 1983–1999	1.17	1.50	1.70	1.40	1.85

In this study, we developed a method for obtaining molecular volumes based on the use of standard molecular geometries and atomic radii. To obtain bond distances with the stable structures, we calculated these geometries using the Pauling equation [2-17] to identify atomic radii [Eq. (1)]:

$$R = r_c + 0.8 \quad (1)$$

Where R is an atomic radius and is the van der Waals radii of an atom. Therefore, the sum of the radii of two atoms associated with interaction is calculated using Eq. (2):

$$\sum R = (R_X + R_Y) = \sum(r_{cx} + r_{cy}) + 1.6 \quad (2)$$

In this study, the comparison between the calculated atomic distance (D) and the sum of van der Waals radii ($\sum R$) was performed to judge the presence or absence of the atomic contact (i.e., the interaction) between MB and pullulan based on the criteria in Eq. (3):

$$D = \begin{cases} Interaction; \mathrm{D} < \sum R \\ No\ interaction; \mathrm{D} > \sum R \end{cases} \quad (3)$$

If the value of D is less than $\sum R$, this shows an interaction between two atoms. On the other hand, if the value of D is greater than $\sum R$, there is no interaction between two atoms, as shown in Fig. 2-5.

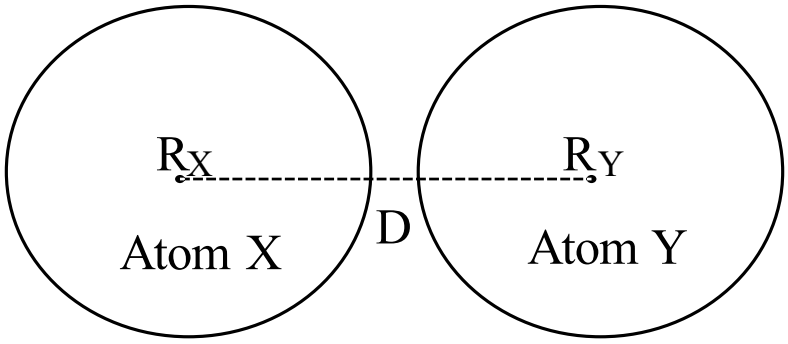

(a) No interaction between 2 molecules

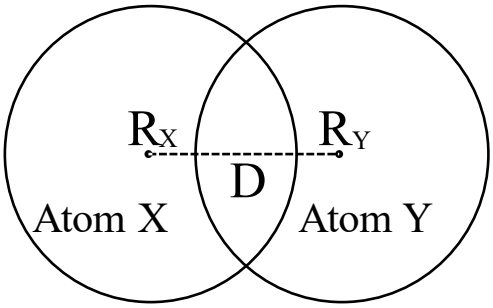

(b) Interaction between 2 molecules occurs

Fig 2-5 Molecular interactions according to the atomic distance between atoms X and Y [2-16].

2-4-3 Hydrogen bonds

Hydrogen bonding Interactions would be important in understanding the interaction modes and the energetics between MB and pullulan. Van-der-Waals Radii calculations to predict the location of atoms and to identify chemical interactions. It was using a chemical interaction position by finding the shortage of Van-der-Waals Radii. In general, the hydrogen bond is a fundamental element of the chemical structure and chemical reactivity [2-18]. Atoms are close to 180° it means they have strong interaction. It is primarily electrostatic and formed with strong and weak donors and acceptors illustrated in Fig. 2-6.

In this study, the hydrogen bonding angles (see Fig.2-6) were investigated to characterize the interaction between MB–pullulan. The typical angle of the hydrogen bond is the one that is closest to 180° [2-19]. We then analyzed the hydrogen bonds formed in the complex structure (OH---N, OH---C, and OH---S). We focused on the hydrogen bonding patterns of the obtained ten complex structures shown in tables 2-4. The geometrical parameters were obtained using the Gaussview program.

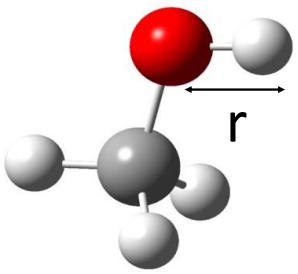

(a) Atomic radius

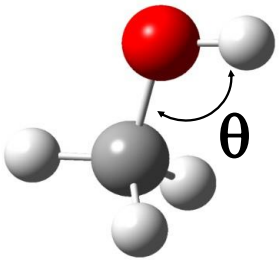

(b) Atomic angle

Fig 2-6 Model of hydrogen bonds [2-16]

The hydrogen bond is an intermolecular attraction caused by hydrogen atoms, forming covalent bonds with atoms that have high electronegativities which are F, O, and N, and covalent bonds. This bond is a terminal type that has a very strong polar condition. This is because the electron pair bond is pulled closer to the atom of an element with high electronegativity rather than hydrogen atoms and element atoms with high electronegativity. There are also lone electron pairs that attract each other between the lone electron pair and the hydrogen atom. These lone electron pairs have the high positive electrical power of another molecule to form hydrogen bonds. The example is shown in Fig. 2-6, where the formation of a hydrogen bond between hydrogen and oxygen atoms.

2-4-4 Binding energy

Amount of energy required to separate a particle from a system of particles or to disperse all the system particles. Binding energy is especially applicable to subatomic particles in atomic nuclei, to electrons bound to nuclei in atoms, and to atoms and ions bound together in crystals.

The binding energy (ΔEb) is the sum of intermolecular forces [2-20] as defined by Eq. (4):

$$\Delta Eb = [E(MB) + E(pullulan) - Ex] + BSSE \quad (4)$$

The binding energy is the sum of various atomic interactions, which should involve hydrogen bonds, van der Waals interaction, etc., between MB and pullulan.

2-5 Results

The molecular structures of Methylene Blue and Pullulan are created by using the Gauss view program. After obtaining the desired molecular structures, the Gaussian09 program analyzes the interaction position between Methylene Blue and pullulan and finds the interaction chemical structures. Find the common last structures from calculations PM6, HF3-21G, HF6-31G (d), and DFT B3LYP/6-31G(d) in Gaussian09. The chemical interaction position is obtained by finding the lowest distance of Van-der-Waals Radius from these common last structures.

2-5-1 The simulation concepts

The molecular structures of Methylene Blue and Pullulan are created by using the Gauss view program. After obtaining the desired molecular structures, the Gaussian09 program analyzes the interaction position between Methylene Blue and Pullulan and finds the interaction chemical structures. Find the common last structures from calculations PM6, HF3-21G, and HF6-31G (d) in Gaussian09. The chemical interaction position is obtained by finding the lowest Van-der-Waals Radius from these common last structures.

The simulation concept of final structure (from total of 50 structures) that provide the lowest energy which represent the stable structure. The results showed samples namely 1:1 of Methylene Blue and Pullulan.

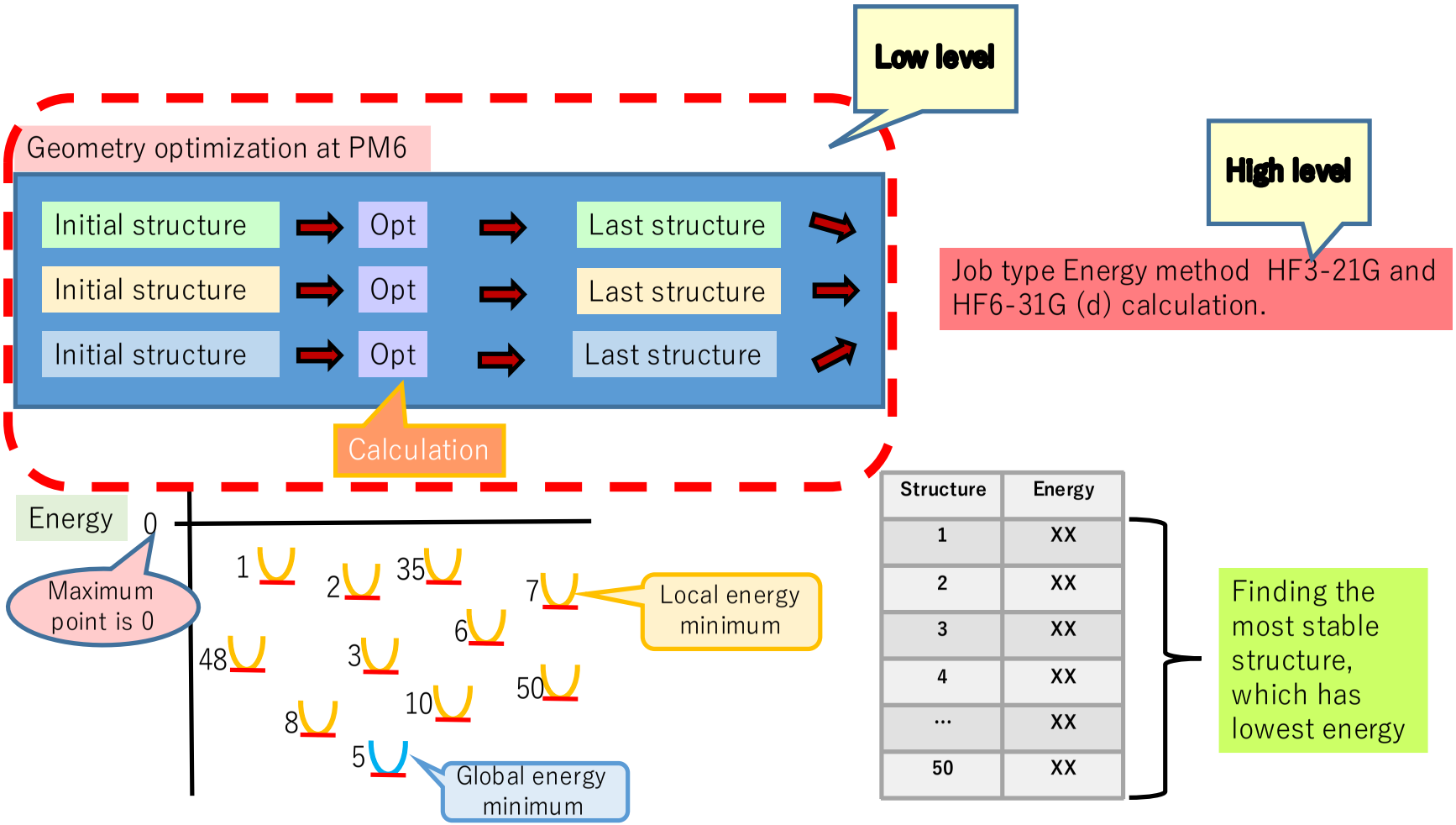

Fig 2-7 Simulation concept

2-5-2 Assessment of the possible intermolecular and binding energy

The complex structures included 147 atoms between the two molecules (Fig. 2-8), with atomic radii corresponding to isotropic (spherical) atoms. The lowest energy conformation for each complex structure obtained using the HF/6-31G (d) method and B3LYP/6-31G (d) method are presented in Tables 2 through 7. Initially, MB–pullulan structure models were created in Gaussview to observe the molecular structures, followed by Gaussian 09 to analyze interactions between MB–pullulan upon complex formation. The interaction positions were determined according to the shortage of interatomic distances relative to the sum of atomic radii. The complex structure was formed by placing MB and pullulan in different orientations relative to one another to create a complex structure. We obtained ten structures displaying low free energies and proceeded to determine the details concerning atomic interactions between MB and pullulan. Fig. 2-8 shows the MB–pullulan structure. The numbering of the atoms depends on the arrangement of atoms in the molecules. To create a complex structure, we arranged the molecules of both MB–pullulan differently. When pullulan atoms were placed adjacent to the MB molecule (with 39 atoms), the atom count for pullulan started from 40. Thus, the first nitrogen atom of MB counted at a lower number (N20/N21) as seen for MB/PL (16). On the other hand, when pullulan (with 107 atoms) was placed first, the atom count for MB started from 108, setting the position of the first nitrogen atom of MB in position N128/N129 as seen for MB/PL (1).

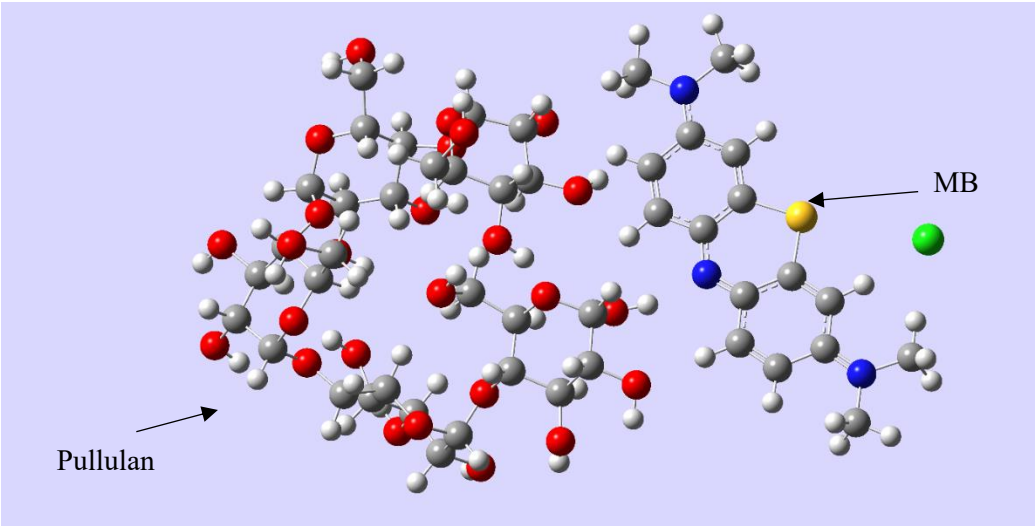

Fig 2-8 Structure of the MB–pullulan complex in a ball-and-stick representation generated by Gaussview [2-16]

In this study, the ratio between MB–pullulan was set at 1:1. We measured the close atomic contacts between MB and pullulan molecules after the ab initio calculation at HF/6-31G(d). As a result, three hydrogen bonds, i.e., OH--N, OH--C, OH--S hydrogen bonds, were specified for the MB–pullulan complexes. Tables 2 to Table 7 list the interaction patterns between the N, C, and S atoms, respectively, from the MB and the OH groups from the pullulan structures. The closer the distance of atoms, the stronger the interaction of the molecules is.

Table 2. Interaction parameters of the possible intermolecular OH---N hydrogen bonds for the MB/PL characterized at HF/6-31G(d).

Name of complex	N··O (Å)	N··H (Å)	Position	Angle (°)
MB/PL (1)	4.58	3.95	N129,O99,H106	43.50
MB/PL (6)	3.03	2.11	N130,O105,H108	13.00
MB/PL (14)	3.39	3.36	N128,O93,H100	80.31
MB/PL (16)	3.57	3.98	N21,O144,H147	108.95
MB/PL (20)	3.03	2.11	N130,O105,H108	13.00
MB/PL (21)	3.35	2.40	N22,O53,H54	4.49
MB/PL (25)	3.30	2.61	N22,O55,H56	37.62
MB/PL (27)	3.16	3.23	N21,O69,H76	85.93
MB/PL (28)	3.41	3.50	N22,O55,H56	87.91
MB/PL (29)	4.61	-	N129,O1	-
MB/PL (31)	3.63	3.33	N22,O120,H125	64.45
MB/PL (35)	3.37	2.43	N22,O53,H54	6.63
MB/PL (36)	3.30	2.62	N22,O55,H56	37.61
MB/PL (38)	3.30	2.62	N22,O55,H56	37.61
MB/PL (39)	3.37	2.43	N22,O53,H54	6.62
MB/PL (42)	3.29	2.60	N22,O55,H56	37.24
MB/PL (43)	3.84	4.10	N128,O84,H87	99.42
MB/PL (44)	3.46	3.12	N20,O120,H125	61.90
MB/PL (47)	3.60	2.81	N22,O53,H54	29.28

Considering the interaction parameters of complex structures from Table 2, atomic radii for the N---OH revealed that structure MB/PL (6) and MB/PL (20) displayed the shortest bond distance from the remaining structures. Therefore, it can be concluded that structure MB-PL (6) and MB/PL (20) are the structure with the strongest OH---N hydrogen bond. There is another structure, which would have a similar OH---N hydrogen bond. The other eight complex structures did not have OH---N hydrogen bond based on the atomic distances (according to Eq. (3)) and the angles (according to the large deviations from the ideal linear angle).

Table 3. Interaction parameters of the possible intermolecular OH---C hydrogen bonds for the MB/PL characterized at HF/6-31G(d).

Name of complex	C··O (Å)	C··H (Å)	Position	Angle (°)
MB/PL (1)	3.39	3.37	C111,O105,H108	80.59
MB/PL (6)	3.40	2.96	C121,O105,H108	55.29
MB/PL (14)	3.47	3.73	C143,O21,H22	99.05
MB/PL (16)	3.35	3.70	C35,O138,H145	103.87
MB/PL (20)	3.40	2.96	C121,O105,H108	55.29
MB/PL (21)	3.57	2.96	C13,O53,H54	43.76
MB/PL (25)	3.28	3.55	C31,O138,H145	99.11
MB/PL (27)	3.06	3.53	C12,O69,H76	112.29
MB/PL (28)	3.25	3.53	C7,O55,H56	99.04
MB/PL (29)	3.36	4.09	C139,O40,H43	135.40
MB/PL (31)	3.37	3.07	C3,O120,H125	63.96
MB/PL (35)	3.57	2.99	C13,O53,H54	45.53
MB/PL (36)	3.28	3.55	C31,O138,H145	99.15
MB/PL (38)	3.28	3.55	C35,O138,H145	99.15
MB/PL (39)	3.57	2.99	C13,O53,H54	45.53
MB/PL (42)	3.20	3.49	C31,O138,H145	100.13
MB/PL (43)	3.43	3.75	C131,O84,H87	102.27
MB/PL (44)	3.36	3.25	C13,O55,H56	73.98
MB/PL (47)	3.46	4.17	C5,O55,H56	133.35

At HF/6-31G (d) level, band interaction parameters of the possible intermolecular of OH⋯C hydrogen bonds C--O(Å) and C--H(Å) were calculated by using Eq. (3), the radii result of the interaction bond between C and HO were shown in Table 3. The results of the calculated structure of MB-PL (27) shows the shortest distance of O⋯C from among of structures. All the complex structures have molecular interactions.

Table 4. Interaction parameters of the possible intermolecular OH---S hydrogen bonds for the MB/PL characterized at HF/6-31G(d).

Name of complex	S··O (Å)	S··H (Å)	Position	Angle (°)
MB/PL (1)	3.64	4.02	S127,O105,H108	106.51
MB/PL (6)	6.13	5.23	S127,O105,H108	16.53
MB/PL (14)	4.20	3.96	S127,O12,H13	69.13
MB/PL (16)	4.08	3.86	S19,O55,H56	70.25
MB/PL (20)	6.13	5.23	S127,O105,H108	16.53
MB/PL (21)	6.16	5.26	S19,O53,H54	15.46
MB/PL (25)	5.45	5.18	S19,O55,H56	68.69
MB/PL (27)	3.77	3.75	S19,O55,H56	81.42
MB/PL (28)	3.45	4.23	S19,O55,H56	141.33
MB/PL (29)	3.90	3.71	S127,O30,H37	71.58
MB/PL (31)	3.46	3.64	S19,O120,H125	93.46
MB/PL (35)	6.23	5.32	S19,O53,H54	15.59
MB/PL (36)	5.45	5.18	S19,O55,H56	68.71
MB/PL (38)	5.45	5.18	S19,O55,H56	68.71
MB/PL (39)	6.22	5.31	S19,O53,H54	15.60
MB/PL (42)	5.51	5.22	S19,O55,H56	67.39
MB/PL (43)	3.49	3.13	S127,O105,H108	60.42
MB/PL (44)	3.82	3.67	S19,O123,H126	73.95
MB/PL (47)	6.42	5.78	S19,O53,H54	44.63

Table 4 presents interaction parameters of the possible intermolecular OH---S hydrogen bonds from calculation at HF/6-31G (d) level by using S--O(Å) and S--H(Å) shows the radii results of the interaction bond between S and HO are summarized in Table 4. It can be concluded that structure MB/PL (28) is the strongest structure with the strongest OH---S hydrogen bond, although the OH---S angle is close to 180º. However, of these all of complex structures, there is another complex structure that has no interaction. As a result, the calculation distance of this structure is greater than $\sum R$, according to Eq. (3)

Table 5. Interaction parameters of the possible intermolecular OH---N hydrogen bonds for the MB/PL characterized at B3LYP/6-31G(d).

Name of complex	N··O (Å)	N··H (Å)	Position	Angle (°)
MB/PL (1)	3.47	3.35	N128,O30,H37	75.31
MB/PL (6)	2.82	1.83	N130,O105,H108	2.09
MB/PL (14)	3.21	3.27	N128,O93,H100	85.16
MB/PL (16)	3.34	4.01	N21,O138,H145	127.85
MB/PL (20)	2.82	1.83	N130,O105,H108	2.09
MB/PL (21)	2.95	1.98	N22,O53,H54	6.54
MB/PL (25)	2.99	2.11	N22,O69,H76	21.84
MB/PL (27)	2.94	1.97	N22,O144,H147	7.13
MB/PL (28)	3.30	3.38	N22,O55,H56	85.77
MB/PL (29)	4.52	-	N129,O1	-
MB/PL (31)	3.08	2.14	N22,O69,H76	13.23
MB/PL (35)	2.98	2.00	N22,O53,H54	7.11
MB/PL (36)	2.99	2.11	N22,O69,H76	21.82
MB/PL (38)	2.99	2.11	N22,O69,H76	21.82
MB/PL (39)	2.97	1.99	N22,O53,H54	7.16
MB/PL (42)	2.98	2.10	N22,O69,H76	21.60
MB/PL (43)	3.44	3.83	N128,O84,H87	106.14
MB/PL (44)	3.30	2.94	N20,O120,H125	60.64
MB/PL (47)	3.18	2.34	N22,O53,H54	26.51

Table 5 presents interaction parameters of the possible intermolecular OH---S hydrogen bonds from calculation at B3LYP/6-31G(d) level by using N--O(Å) and N--H(Å) shows the radii results of the interaction bond between N (from MB) and HO (from pullulan). MB-PL (6) and MB-PL (20) shows the shortest distance of N···O is 2.82 Å where the result is less than the result of HF/6-31G (d) level. Meanwhile, the results of B3LYP/6-31G(d) level suggest stronger the interaction of the molecules occur.

Table 6. Interaction parameters of the possible intermolecular OH---C hydrogen bonds for the MB/PL characterized at B3LYP/6-31G(d).

Name of complex	C··O (Å)	C··H (Å)	Position	Angle (°)
MB/PL (1)	3.25	3.28	C111,O105,H108	82.62
MB/PL (6)	3.33	2.56	C113,O14,H15	32.02
MB/PL (14)	3.33	3.57	C143,O21,H22	96.40
MB/PL (16)	3.14	3.13	C2,O55,H56	80.07
MB/PL (20)	3.33	2.56	C113,O14,H15	32.02
MB/PL (21)	3.34	2.81	C13,O53,H54	50.15
MB/PL (25)	3.16	2.88	C5,O69,H76	64.93
MB/PL (27)	2.98	3.12	C11,O69,H76	88.70
MB/PL (28)	3.17	3.80	C8,O55,H56	123.24
MB/PL (29)	3.32	4.14	C139,O40,H43	142.82
MB/PL (31)	3.26	3.02	C3,O120,H125	67.20
MB/PL (35)	3.33	2.81	C13,O53,H54	50.73
MB/PL (36)	3.16	2.88	C5,O69,H76	64.93
MB/PL (38)	3.16	2.88	C5,O69,H76	64.93
MB/PL (39)	3.33	2.81	C13,O53,H54	50.80
MB/PL (42)	3.16	2.89	C5,O69,H76	65.03
MB/PL (43)	3.26	3.34	C135,O84,H87	86.53
MB/PL (44)	3.18	3.05	C13,O55,H56	73.10
MB/PL (47)	3.24	4.07	C5,O55,H56	143.71

The interaction parameters of the possible intermolecular of OH···C hydrogen bonds C--O(Å) and C--H(Å) from calculation at B3LYP/6-31G(d) level show in table 6. The result indicates than MB/PL (27) is the strongest structure with the strongest C---OH hydrogen bond. MB-PL (27) shows the shortest distance of C···O is 2.98 Å and C···H is 3.12 Å.

Table 7. Interaction parameters of the possible intermolecular OH---S hydrogen bonds for the MB–pullulan complex characterized at B3LYP/6-31G(d).

Name of complex	S··O (Å)	S··H (Å)	Position	Angle (°)
MB/PL (1)	3.45	3.91	S127,O105,H108	110.42
MB/PL (6)	5.99	5.00	S127,O105,H108	3.07
MB/PL (14)	3.95	3.67	S127,O12,H13	66.67
MB/PL (16)	3.65	3.06	S19,O53,H54	46.28
MB/PL (20)	5.99	5.00	S127,O105,H108	3.07
MB/PL (21)	5.98	5.05	S19,O53,H54	18.07
MB/PL (25)	5.22	4.90	S19,O55,H56	65.34
MB/PL (27)	3.61	3.66	S19,O55,H56	85.26
MB/PL (28)	3.28	4.10	S19,O55,H56	142.65
MB/PL (29)	3.53	3.45	S127,O30,H37	76.83
MB/PL (31)	3.36	3.62	S19,O120,H125	97.61
MB/PL (35)	6.00	5.07	S19,O53,H54	18.60
MB/PL (36)	5.23	4.90	S19,O55,H56	65.29
MB/PL (38)	5.23	4.90	S19,O55,H56	65.29
MB/PL (39)	5.97	5.05	S19,O53,H54	19.53
MB/PL (42)	5.23	4.90	S19,O55,H56	65.03
MB/PL (43)	3.38	3.07	S19,O105,H108	63.71
MB/PL (44)	3.59	3.43	S19,O123,H126	72.91
MB/PL (47)	6.01	5.36	S19,O53,H54	45.01

The interaction parameters of the possible intermolecular OH---S hydrogen bonds from calculation at B3LYP/6-31G(d) level by using S--O(Å) and S--H(Å) shows the radii results of the interaction bond between S and HO are summarized in Table 7. MB-PL (28) shows the shortest distance of S···O is 3.28 Å and S···H is 4.10 Å.

As for the calculations at different levels. the results show the difference in results. It is can clearly see in Tables 2-7. At higher levels of computation, the shortest distance of atom, which results in show strength in interaction position between MB and pullulan.

Table 8. Binding energies (ΔEb) for the MB–pullulan complexes characterized at HF/6-31G(d).

Structure Name	Binding energy (kcal/mol)	Relative energy (kcal/mol)	BSSE (kcal/mol)
MB/PL (16)	-51.06	0	6.90
MB/PL (1)	-41.57	9.49	7.53
MB/PL (29)	-35.41	15.65	3.14
MB/PL (14)	-31.75	19.31	5.65
MB/PL (43)	-29.9	21.16	4.39
MB/PL (28)	-22.11	28.95	4.39
MB/PL (31)	-20.37	30.69	8.16
MB/PL (44)	-15.49	35.57	7.53
MB/PL (6)	-4.53	46.53	4.39
MB/PL (20)	-4.53	46.53	4.39
MB/PL (47)	-4.29	46.77	3.14
MB/PL (36)	-3.99	47.07	4.39
MB/PL (42)	-3.86	47.2	4.39
MB/PL (21)	-3.54	47.52	2.51
MB/PL (39)	-3.25	47.81	2.51
MB/PL (35)	3.13	54.19	2.51

The calculated binding energies of the MB–pullulan complexes are shown in Table 8. Structure name MB/PL (16) showed the highest binding energy (-51.06 kcal/mol) via the calculation. The relative energy between highest binding energy and lowest binding energy is -54.19 kcal/mol.

2-6 Discussions

The results of MO analysis suggested the formation of hydrogen bonds between S, C, and N atoms in the MB benzene ring with a pullulan OH group groups, resulting in lower electronic energy in the complex structure relative to that observed in the individual molecules. The results show that:

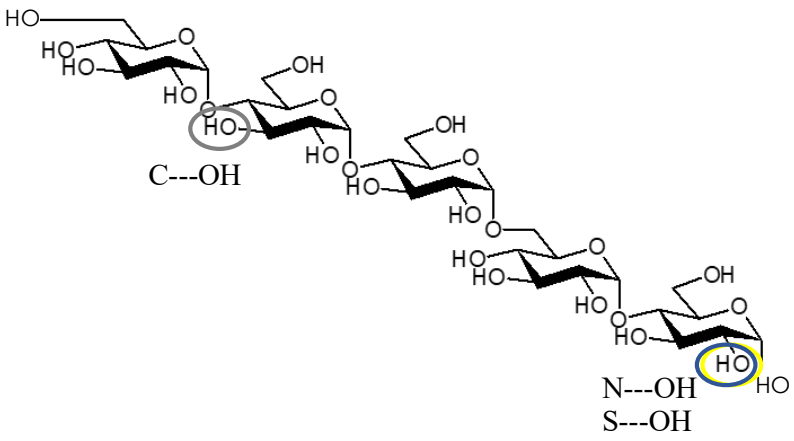

Interaction position of MB

Fig 2-9 Sites of atomic interactions in the pullulan 5 glucose molecules at HF 6-31G (d) [2-16]

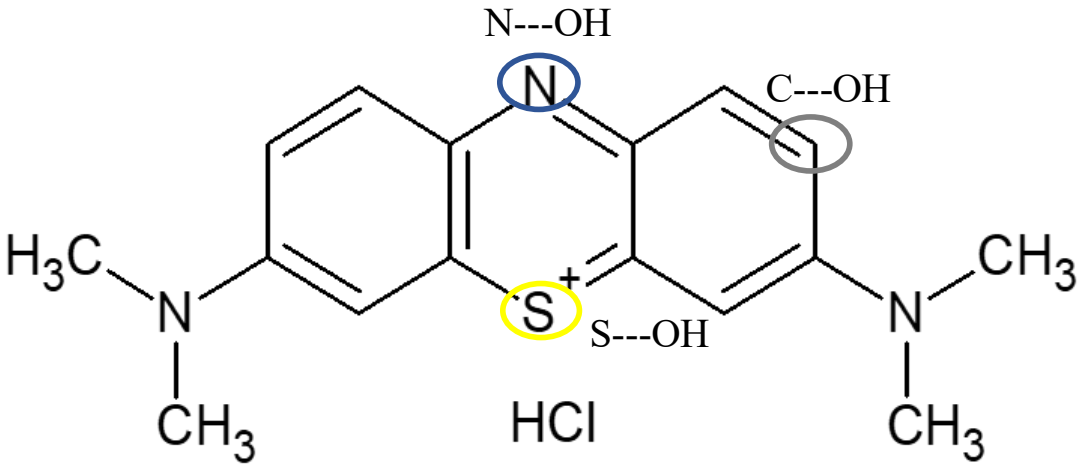

Interaction position of MB

Fig 2-10 Sites of atomic interactions in the MB benzene ring at HF 6-31G (d) [2-16]

Moreover, we are considering that the positions of pullulan and MB after mixed are very close, and MB molecular was covered by pullulan in a weak interaction between MB and pullulan. For clarity, of the optimization of MB/PL complex structure at HF/6-31G(d) as shown is below.

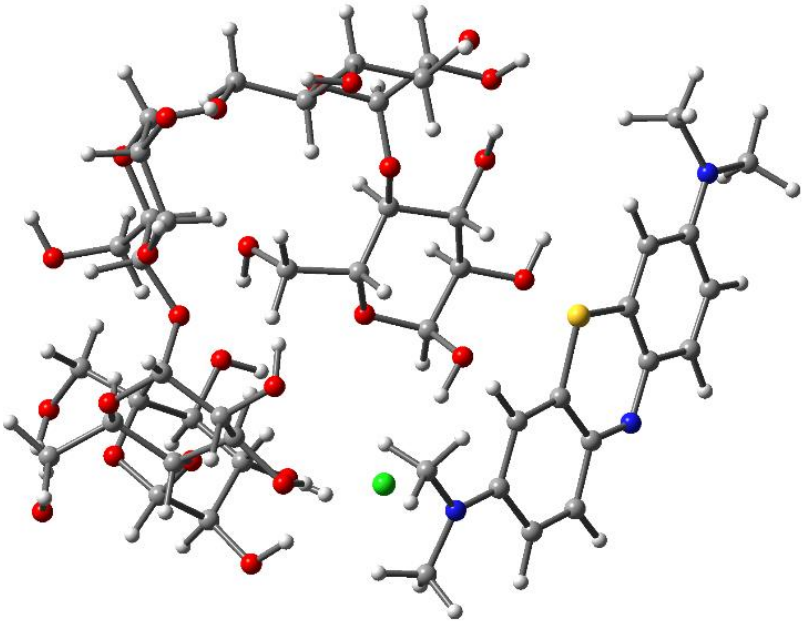

MB/PL (1)

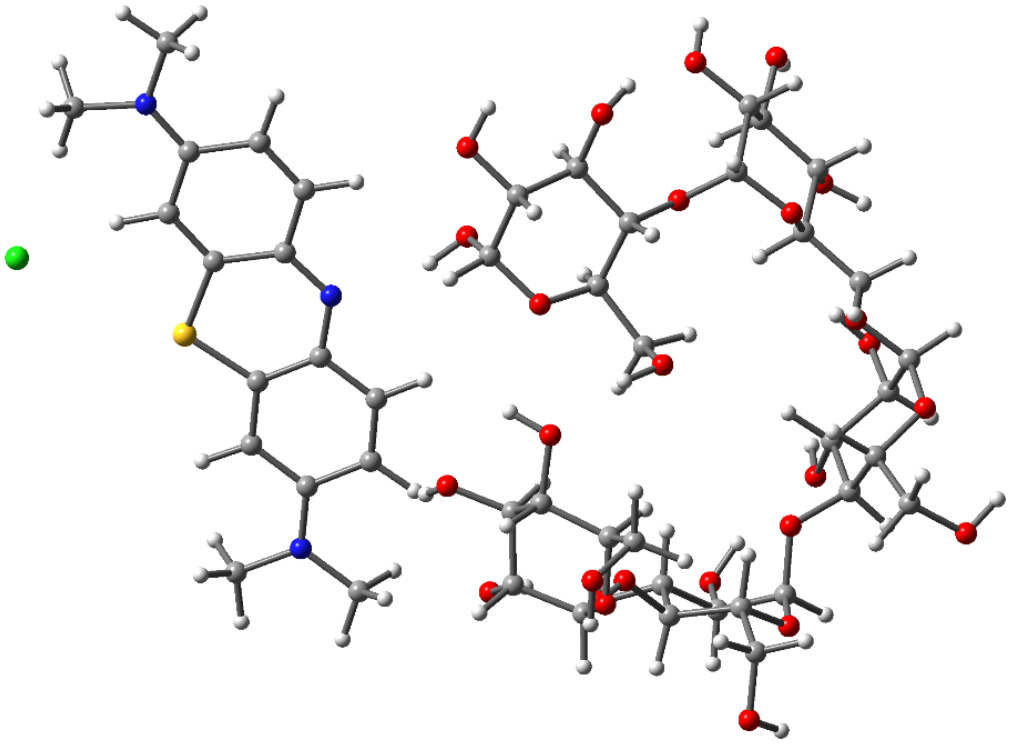

MB/PL (6)

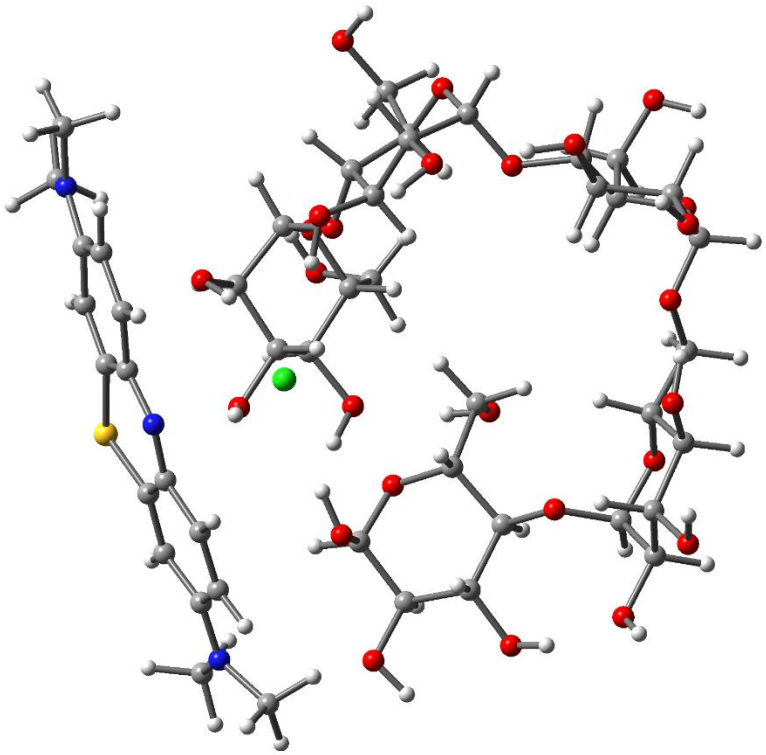

MB/PL (16)

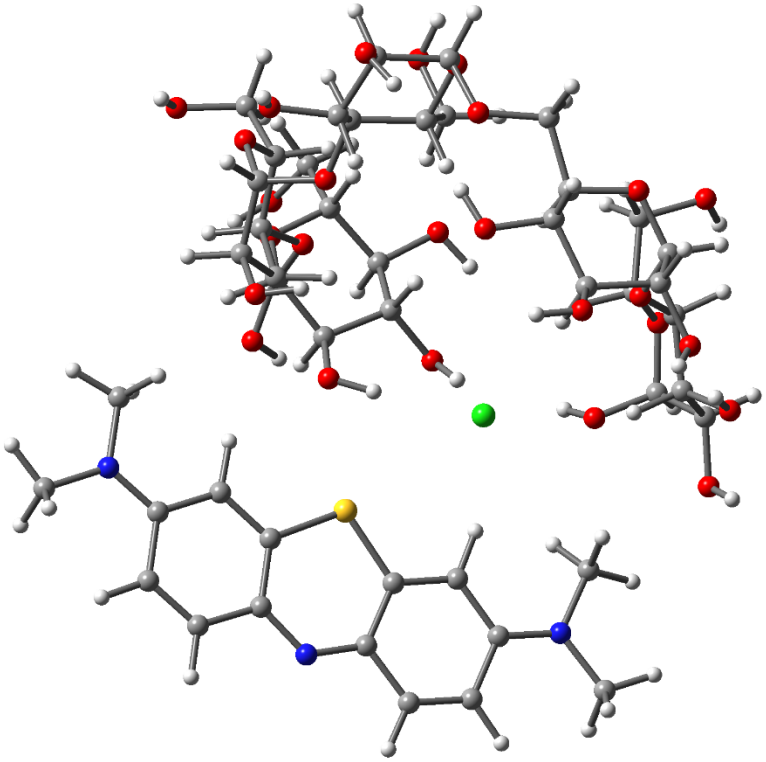

MB/PL (20)

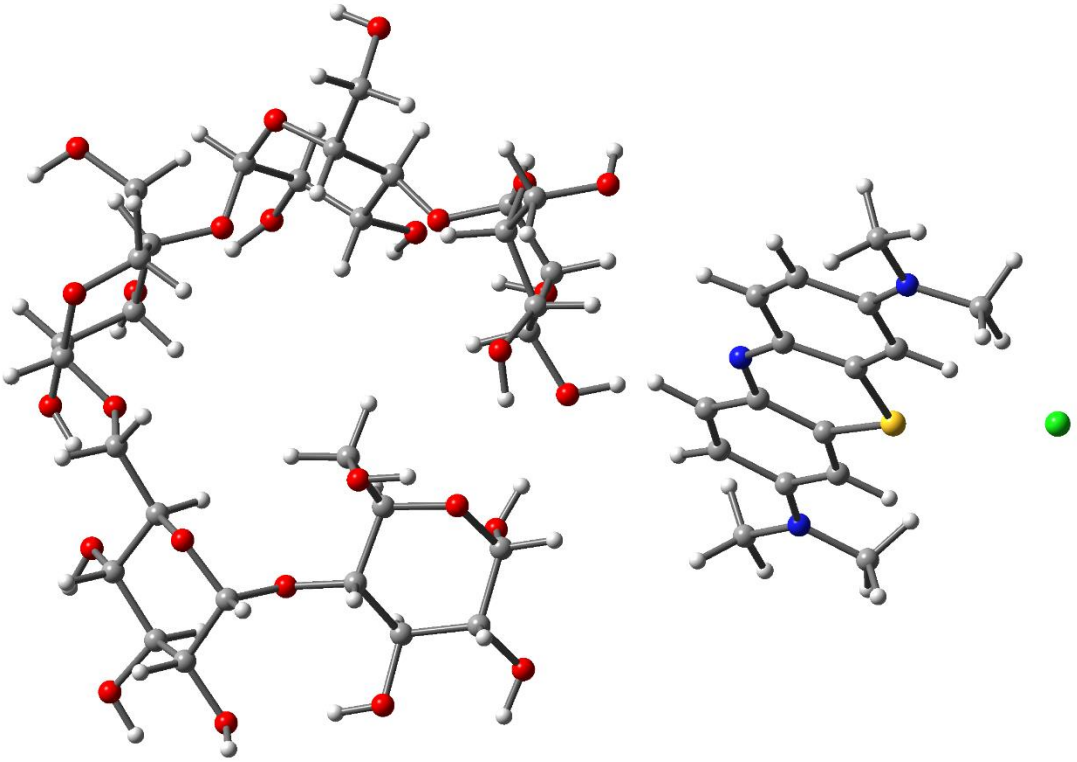

MB/PL (21)

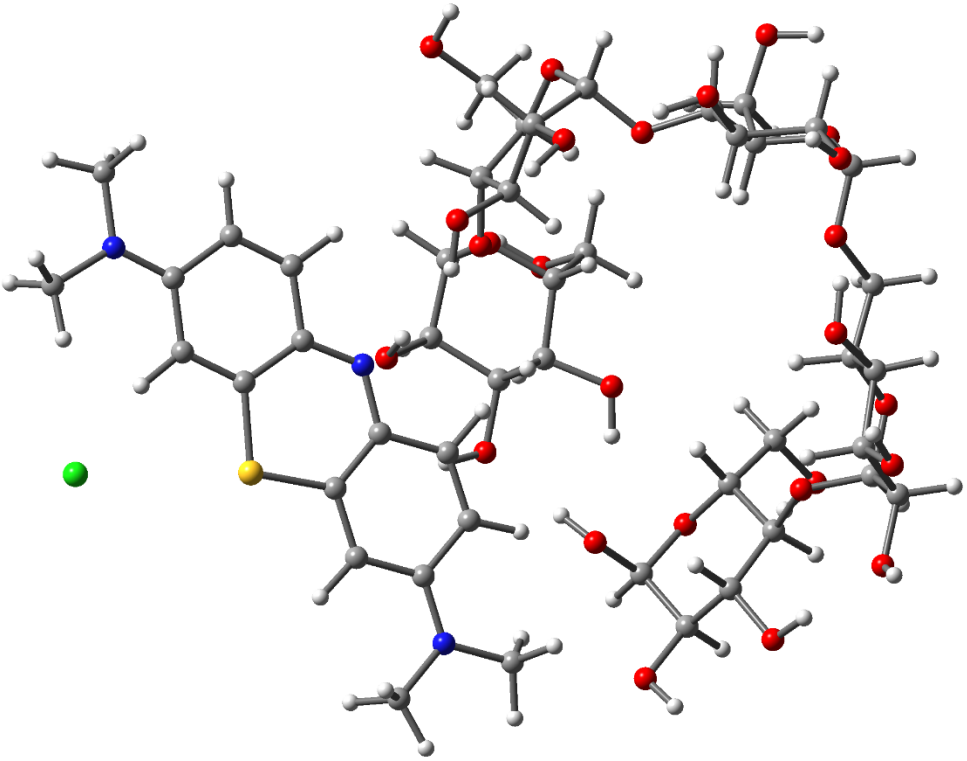

MB/PL (25)

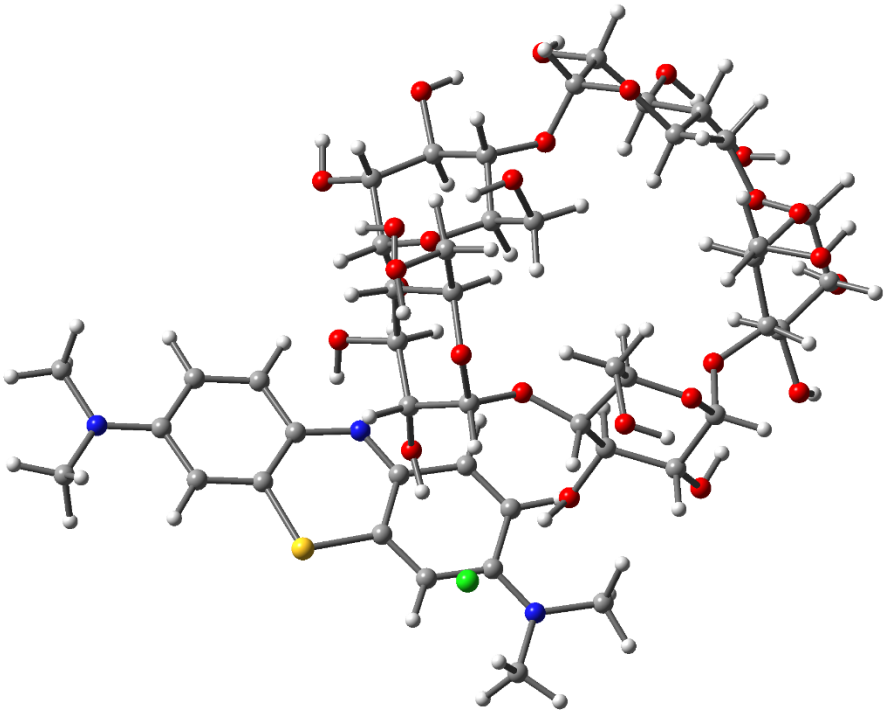

MB/PL (27)

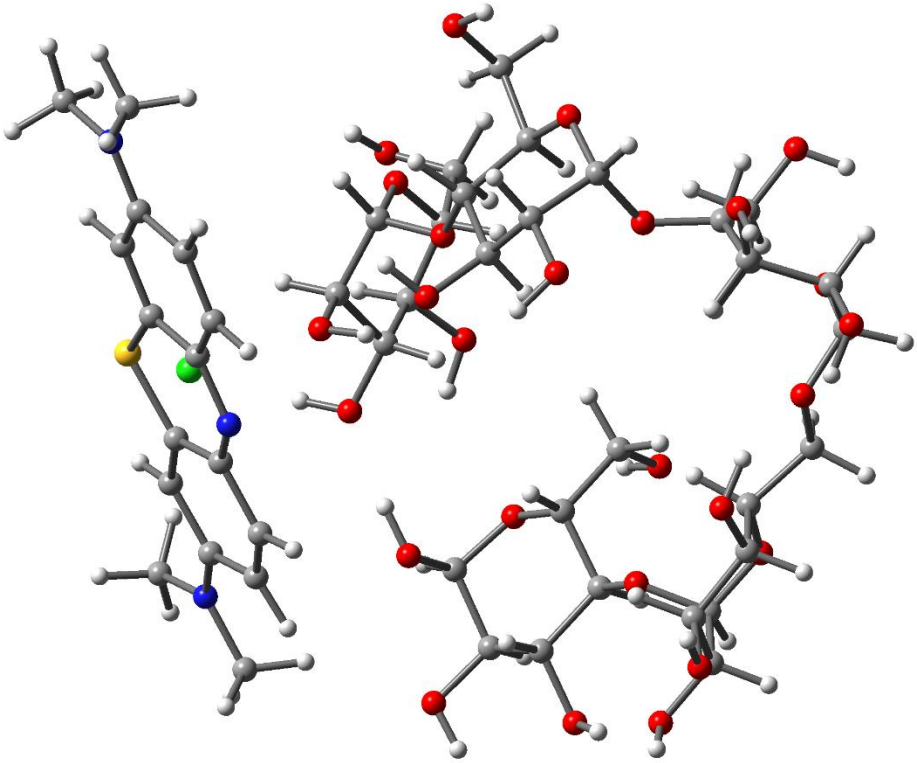

MB/PL (28)

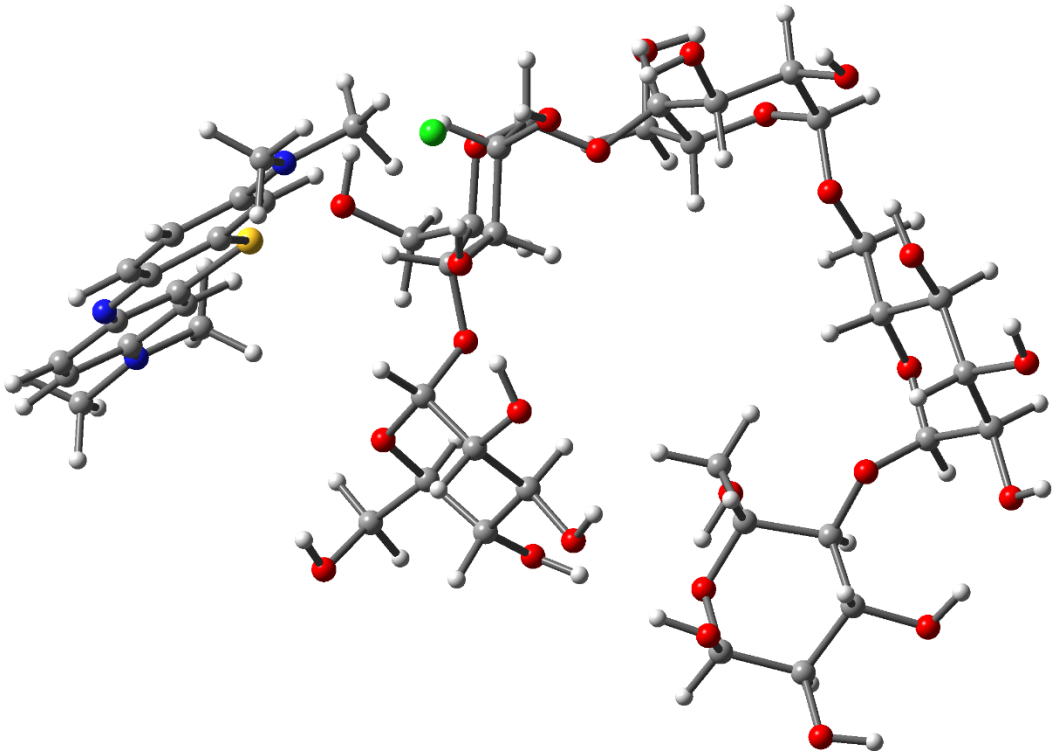

MB/PL (29)

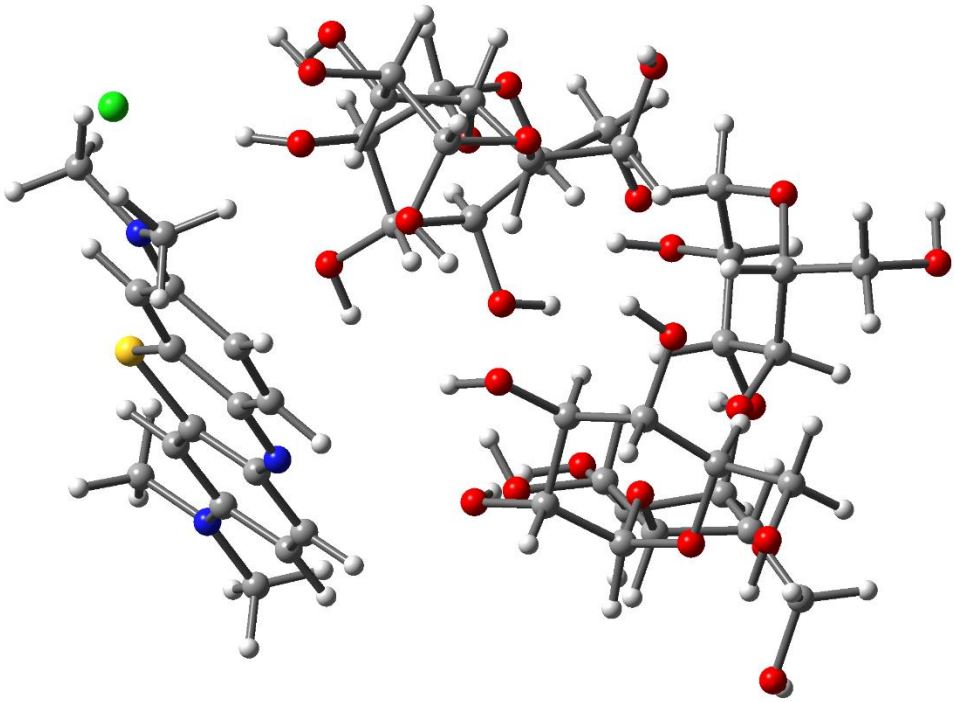

MB/PL (31)

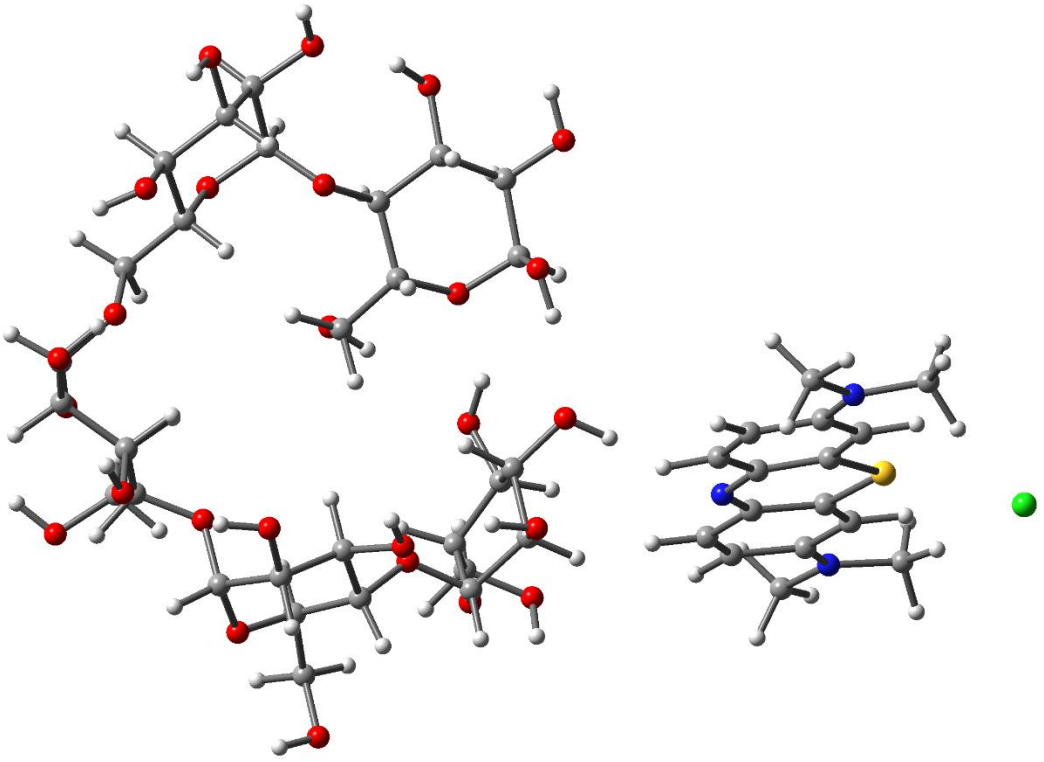

MB/PL (35)

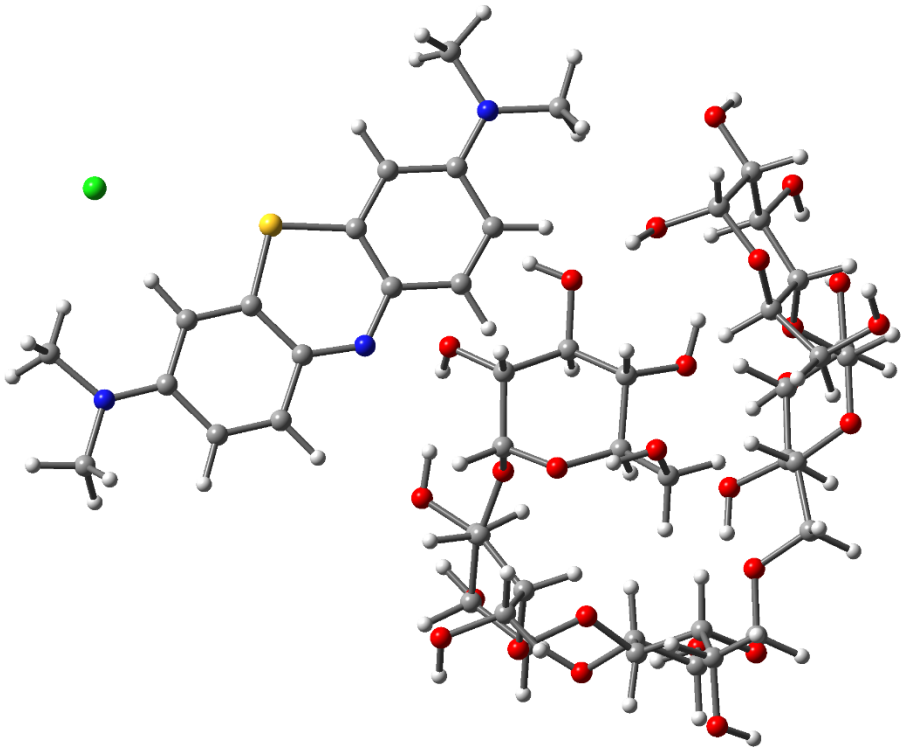

MB/PL (36)

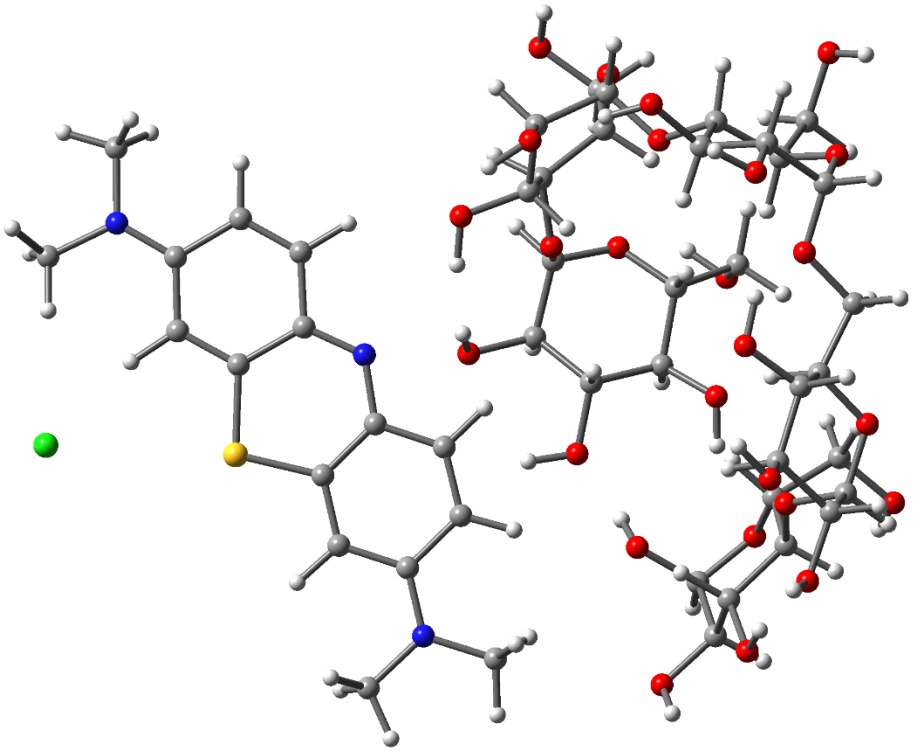

MB/PL (38)

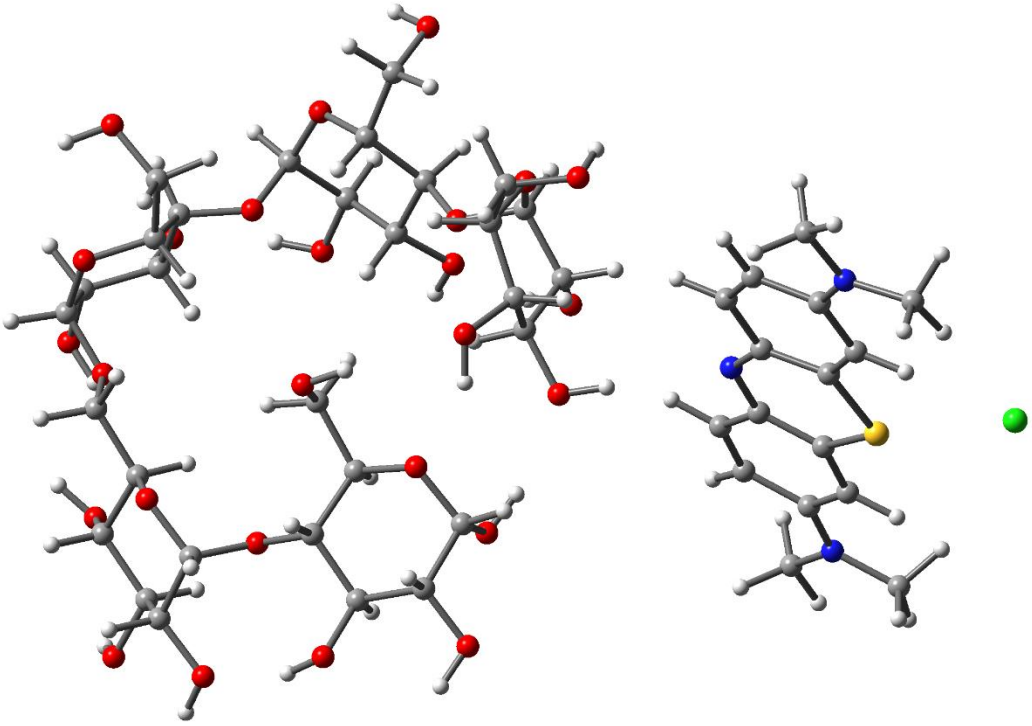

MB/PL (39)

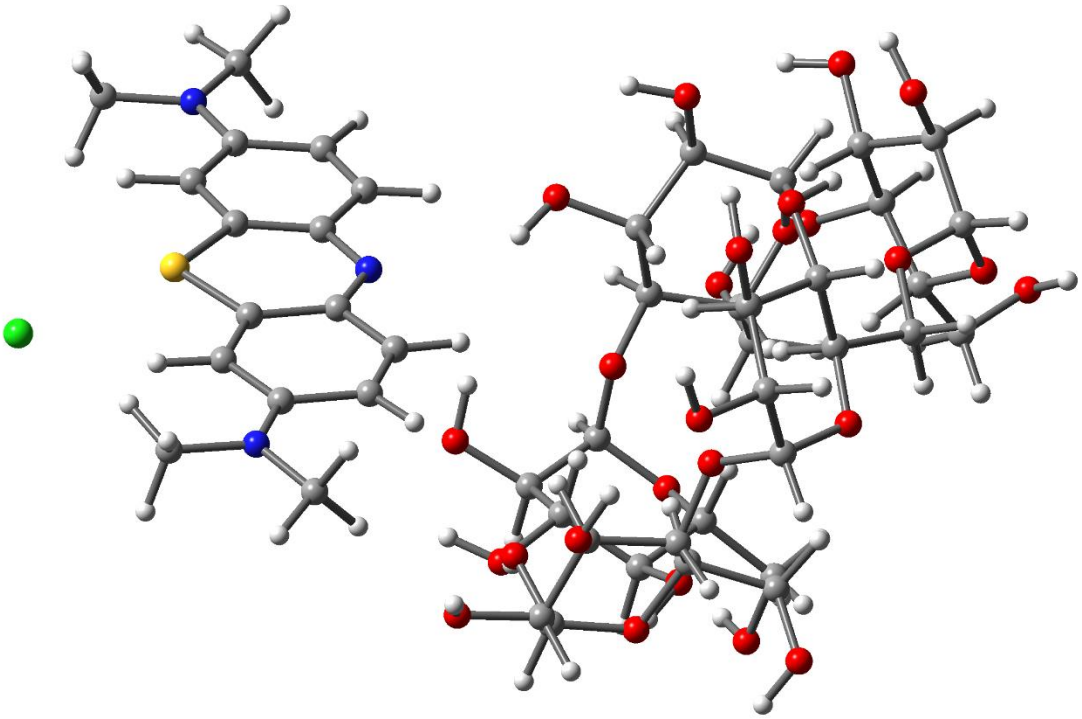

MB/PL (42)

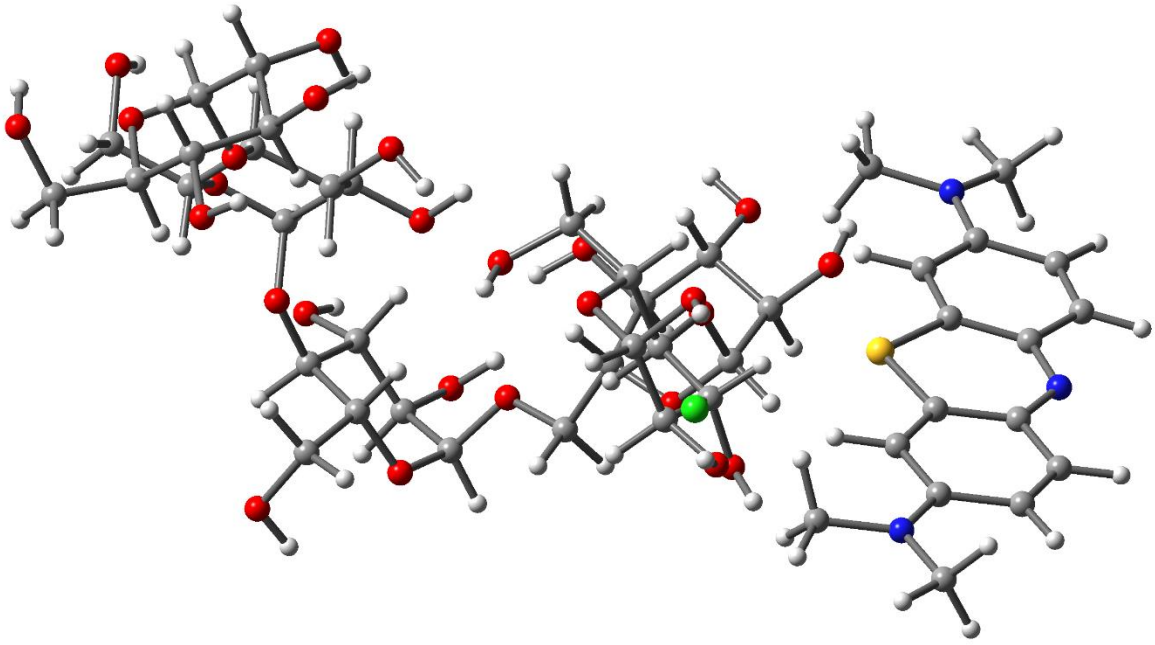

MB/PL (43)

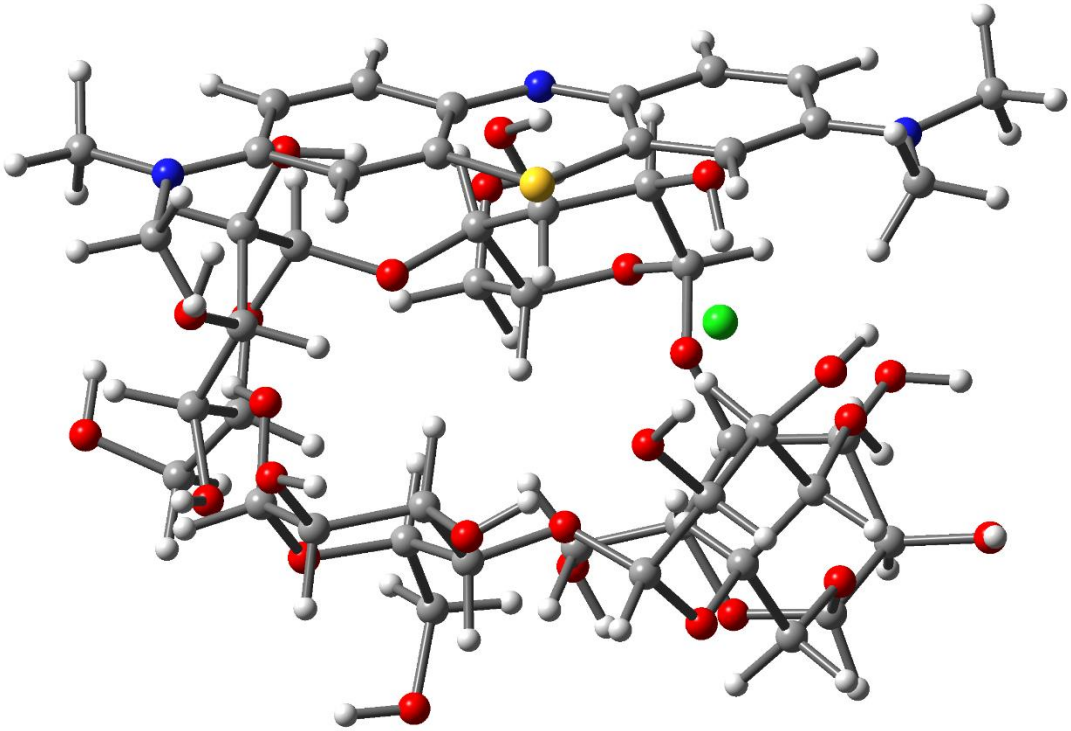

MB/PL (44)

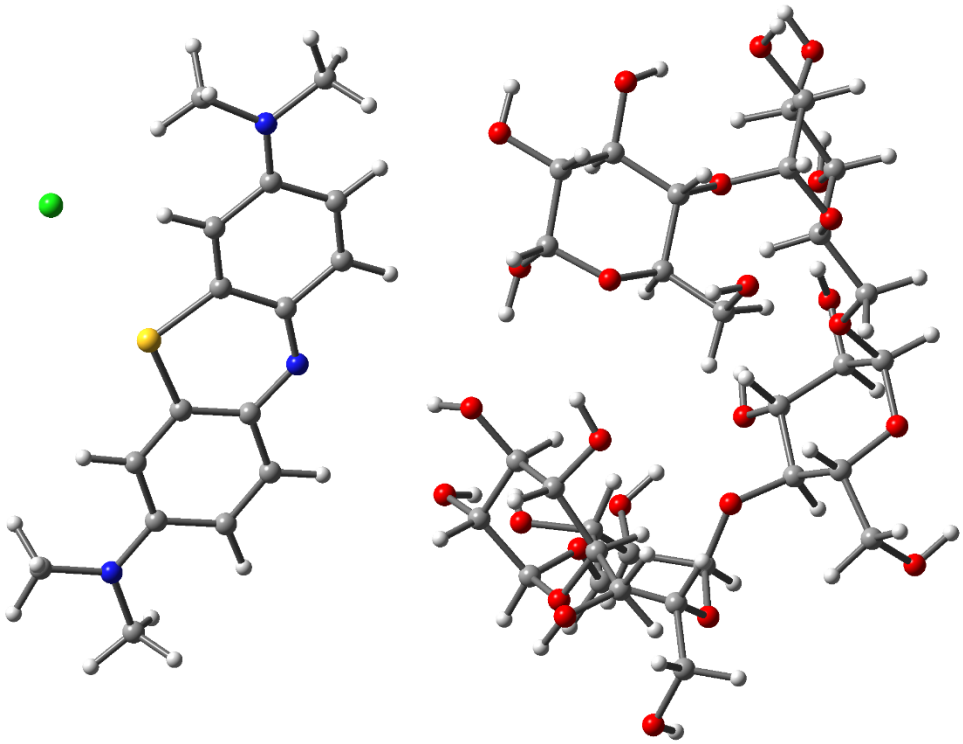

MB/PL (47)

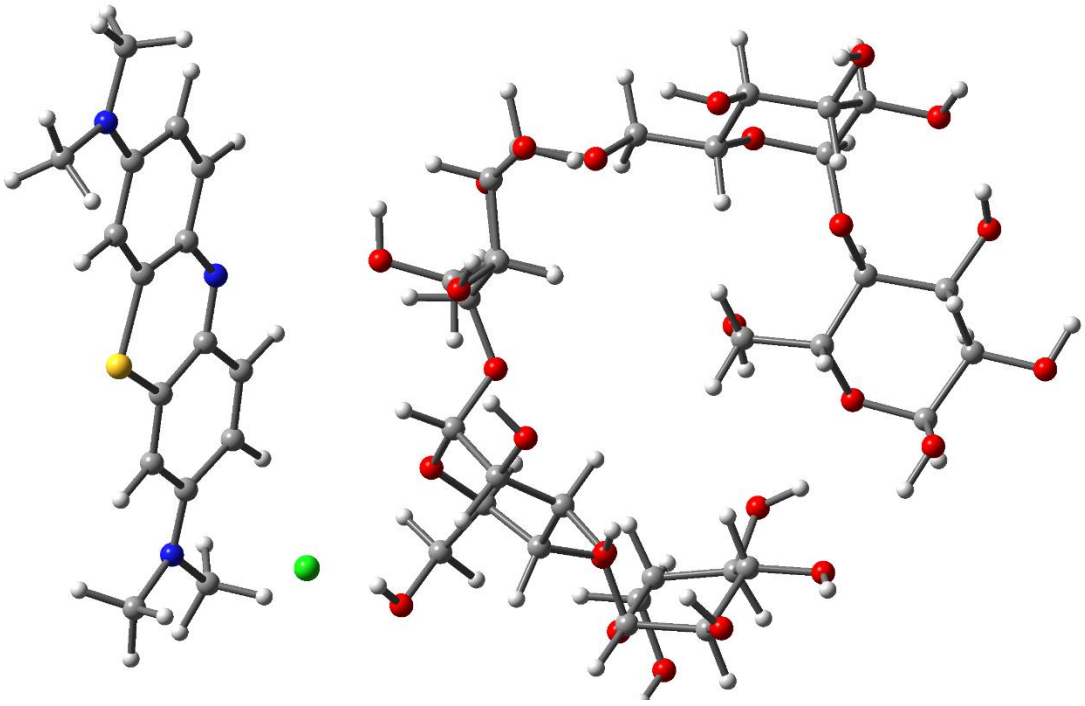

MB/PL (50)

Fig 2-11 The optimization of MB/PL complex structure at HF/6-31G(d)

The results for the binding energy of the complex structures show that the energy level from the experiment results to find the binding energy of the complex structure between MB and pullulan compared to single calculations of MB and single calculations pullulan are different. The binding energy result of the complex structure between MB and pullulan has decreased and less than single calculations. This result presents when the energy level goes down, the structure becomes more stable, and the two molecules interact together.

The 3D figure shows structure MB/PL (16) was the most stable. This allows the change to be identified from its original structure. When calculating the structure of MB and pullulan, particularly pullulan was clearly changed. The figure shows that the pullulan structure is contorted to form a cluster or circle. As for the MB, some structures are slightly bent.

2-7 Conclusions

In conclusion, by the MO calculation at the HF/6-31G(d) level, we have succeeded in analyzing the interaction patterns of the MB–pullulan complex, which undergoes decolorization upon insight into possible interaction modes allowing AOS detection under various conditions. The MO analysis suggested the formation of hydrogen bonds between N, C, and S atoms in the MB benzene ring and pullulan OH group groups. Further analysis of interactions between the N, C, and S atoms in MB revealed benzene rings (Fig. 2-9 and Fig.2-10) proximal to the OH group in pullulan.

In contrast, another N and C associated with amine groups were located farther from this OH group. These results indicated that the pullulan structure did not undergo self-binding in the presence of MB but rather formed bonds with MB, as shown in Fig. 2-10. The calculations determined the shortest bond distances among the ten complex structures displaying the lowest free energies, resulting in identifying interactions promoting high affinity between the two molecules.

References

(2-1) S. Iwamori, N. Nishiyama, K. Oya. “A colorimetric indicator for detection of hydroxyl radicals in atmosphere using a methylene blue dye based on nafion film”. Polymer Degradation and Stability. 2016, 123, 131-136.

(2-2) K. Hosoya, S. Yenchit, Y. Tadokoro, K. Oya, S. Iwamori. “Improved Singlet Oxygen Detection Sensitivity in Electron Spin Resonance Using a Spin-trap Agent Incorporated into a Water-soluble Polymer Film”. The Chemical Society of Japan. 2018, 47, 1191-1193.

(2-3) C. Bailly. “Active oxygen species and antioxidants in seed biology”. Seed Science Research. 2004, 14(2), 93-107.

(2-4) K. Oya, K. Hosoya, T. Suto, S. Iwamori. “Surface modification of polydimethylsiloxane by exposure of active oxygen and ultraviolet lights to improve cell adhesion”. The Japan Society of Mechanical Engineers. 2019, 85(871).

(2-5) H. Masaki, Y. Okano, H. Sakurai. “Generation of Active Oxygen Species from Advanced Glycation End-Products (AGE) under Ultraviolet Light A (UVA) Irradiation”. Biochemical and Biophysical Research Communications. 1997, 235(2), 306-310.

(2-6) K. Yoshino, H. Matsumoto, T. Iwasaki, S. Kinoshita, K. Noda, K. Oya, S. Iwamori, “Investigation of a Sterilization System Using Active Oxygen Species Generated by Ultraviolet Irradiation”. Biocont. Sci. 2015, 20(1), 11-18.

(2-7) S. Yenchit, Y. Tadokoro, S. Iwamori. “Measuring Active Oxygen Species Across a Nonwoven Fabric Using a Pullulan-mixed Methylene Blue Thin Film and Electron Spin Resonance”. The Institute of Electrical Engineers of Japan. 2019, 139(3), 54-60.

(2-8) S. Yenchit, Y. Tadokoro, Y. Oda, S. Iwamori. “Chemical stability of P thin film employing methylene blue dye for active oxygen species”. The 4th Japan-Korea International Symposium on Materials Science and Technology. 2017 (JKMST 2017), August 24-26, 2017.

(2-9) F. Chen, T. Lu. “Calculations of Molecular Orbital Composition”. ACTA CHIMICA SINICA. 2011, 2393-240

(2-10) S. S. Batsanov. “van der Waals Radii of Elements”. Inorganic Materials. 2001, 37(9), 871-885.

(2-11) M. Karakaya. “Complexation Energies and Electronic-Structural Properties of Adamantane Derivatives: A DFT Study”. ADYUJSCI. 2019, 9(2), 290-302.

(2-12) P. Temeeprasertkij, S. Yenchit, M. Iwaoka, S. Iwamori. “Interactions between Methylene Blue and Pullulan by Molecular Orbital Calculations”. 4th Japan-Thailand Joint Symposium on Advanced Nanomaterials and Devices for Electronics and Photonics (JT-AND 2020), DEI-20-018, Thailand.

(2-13) N.I. Dodoff “A DFT/ECP-Small Basis Set Modelling of Cisplatin: Molecular Structure and Vibrational Spectrum”. Computational Molecular Bioscience. 2012, 2, 35-44.

(2-14) J.J. P. Stewart. “Optimization of parameters for semiempirical methods V: Modification of NDDO approximations and application to 70 elements”. Springer-Verlag. 2007, 13, 1173-1213.

(2-15) N. DiCesarea, M. Belletetea, M. Leclercb, G. Durochera. “HF/3-21G*ab initio calculations on methoxy-substituted bithiophenes”. Journal of Molecular Structure (Theochem). 1999, 467, 259–273.

(2-16) P. Temeeprasertkij, S. Yenchit, M. Iwaoka, S. Iwamori. “lnteractious between Methylene Blue and Pullulan According to Molecular Orbital Calculations”. IEEJ Transactions on Fundarncntals and Materials, 2020, 140 No.11, 529-533.

(2-17) E. R. Johnson, A.D. Becke. “A post-Hartree–Fock model of intermolecular interactions”. The Journal of Chemical Physics, 2005, 123, 024101.

(2-18) S.S. Batsanov “Calculation of van der Waals radii of atoms from bond distances”. Journal of Molecular Structure (Theochem), 1999, 468(1-2), 151-159.

(2-19) K. Morokuma, K. Kitaura. “Energy decomposition analysis of molecular interactions”. Springer Science+Business Media New York, 1981, 215-242.

(2-20) M. Oftadeh, S. Srlahvarzi, M. Keshavarz. “Intermolecular Interactions between TNAZ and H2O: a DFT Study”. Central European Journal of Energetic Materials. 2013, 10(2), 289-300.

Chapter 3

Molecular interactions between methylene blue and sodium alginate studied by molecular orbital calculations

[P. Temeeprasertkij, S. Yenchit, M. Iwaoka, S. Iwamori. “Molecular Interactions between Methylene Blue and Sodium Alginate Studied by Molecular Orbital Calculation”. Molecules, 2021, Vol.26, pp. 7029.]

3-1 Background

Interactions between sodium alginate (SA) and methylene blue (MB) have long been studied. In particular, the chemical stability of the colorimetric indicator based on SA thin film and MB dye has been investigated upon active oxygen species (AOS) exposure [3-1]. Indeed, the MB/SA film indicators were found to be useful for detecting hydroxyl radicals (OH*) in the atmosphere. To detect OH* with higher oxidative abilities, it is necessary to stabilize MB by mixing with a polymer matrix so that AOS other than OH* cannot react MB directly. SA, which has a high affinity to MB, was selected for this purpose as it stabilizes MB in its filmy matrix so that the attack of AOS to MB can be prevented. SA has attracted the attention of researchers in recent decades as it is a water-soluble polysaccharide biopolymer that is extracted from brown seaweed [3-2), (3-3]. SA, a linear binary copolymer made of β-D-mannuronic acid and α-L-guluronic acid (G), exhibits excellent film-forming ability, good moisture absorption and permeability, and high viscosity in aqueous solutions. It has been widely used in biomedical applications and for fabricating new materials [3-4), (3-5), (3-6]. Such biocomposite films are not only safe and environment friendly but also biocompatible, compensating for common inorganic materials employed for practical applications.

In the previous result [3-1], an indicator of AOS made from uniform thin films was developed using MB-dyed SA, which can be generated under atmospheric conditions. The aim of previous research was to selectively detect OH* among various AOS and establish AOS technology for the sterilization and surface modification of polymer substrates. Indeed, decolorization occurred when the film was exposed to OH* with high humidity, but the other AOS did not decolorize the film under the identical conditions. To clarify of the molecular interaction between MB and SA, the experiments using a microplate reader were performed. The results suggested that both MB and SA share an ionic bond, as evidenced by the peak shift (Comparison between MB and MB in the mixture of MB and SA) corresponding to the benzene ring of MB in the mixture of MB and SA, and SA strongly interacts MB to stabilize MB enough to prevent the interaction with atmospheric AOS other than highly reactive OH*. Meanwhile, earlier research suggested that SA and MB interact each other between the carboxylates (–

COO-) of SA and the nitrogen or sulfur atom of MB [3-1]. However, the details of the intermolecular interactions were not clear.

In this study, A decolorization reaction of the MB occurs due to excited singlet oxygen molecules / atoms and hydroxyl radicals (OH*) including ozone (O_3). On the other hand, an indicator containing MB mixed with SA or pullulan can be decolorized by exposures of OH *, which has the strongest oxidizing abilities, but the decolorization reaction does not occur by O_3 or excited singlet oxygen / molecules exposures.

Furthermore, we aimed to analyze the interaction patterns of the MB/SA complex by molecular orbital calculations to address the interaction modes and binding energies between MB and SA and the location of the interactions in both molecules. We have estimated the decolorization mechanism of methylene blue dyes employed water-soluble polymers due to OH* by the experimental results [3-1].

In addition, we attempted to explain the molecular reasons for the resistance of MB/SA film against decolorization in the exposure to O_3 by calculation for bimolecular and trimolecular complexes among MB, SA, and O_3 by molecular orbital calculation. Molecule of MB mixed with SA molecular orbitals was assessed by the HOMO estimates the gap between HOMO and LUMO, LUMO energy value, and the HOMO-LUMO gap considering the changing HOMO-LUMO energy gap. The energy band gap can be used to determine the efficiency of the electron transition between the HOMO and LUMO energy levels within a structure, whether the transition occurs quickly or not.

In this experiment results, all 10 complex structures were used for theoretical investigation. The vdW radius and binding energies according to optimized structures of the MB/SA complexes and interaction energies based on molecular orbital have been calculated. It was found that in MB/SA complex structures, the most stable binding site for MB is N atom, C atom, and S atom in analysis. As for SA, we also found that at molecular arrangement structure R1 and R2 of the SA optimal molecular structures were more likely to interact with R3 and R4.

Moreover, the degradation of colors, the MB/SA complex underwent decolorization upon possible interaction modes that allowed AOS detection. O_3 was used to observe the decolorization mechanism of MB dye based on the SA film. Thus, HOMO and LUMO energy values can explain the intramolecular charge transfer from the electron donor to the electron acceptor in the MB/SA complex. The decolorization of the film is caused by the degradation reaction of MB upon AOS exposure were also discussed. These investigations may also apply to evaluate uniform thin film indicators based on MB-dyed water-soluble polymers to elucidate the decolorization mechanism upon exposure to AOS.

3-2 Purpose

Therefore, in this paper, we would like to calculate and show that O_3 causes MB decolorizing, and that indicators containing MB mixed with SA or pullulan do not cause decolorizing by the O_3 exposures. We have estimated decolorization mechanism of methylene blue dyes employed water soluble polymers due to hydroxyl radicals by the experimental results, however it is insufficient to make clear the mechanism. Thus, we make clear the methylene blue dyes employed these polymers have a resistance for ozone by a computational by using GaussView, Gaussian 09 programs.

3-3 Calculation Methods

3-3-1 Materials

3-3-1-1 Methylene blue (MB)

MB is a synthetic cationic thiazine dye of an amorphous nature with the molecular formula C16H18ClN3S, as shown in Fig. 3-1. It is also called basic blue 9 [3-7), (3-8)], which makes a dark blue-green solution with water, where it dissociates into an MB cation and a chloride anion. This neutral ionic molecule was used for molecular orbital calculation.

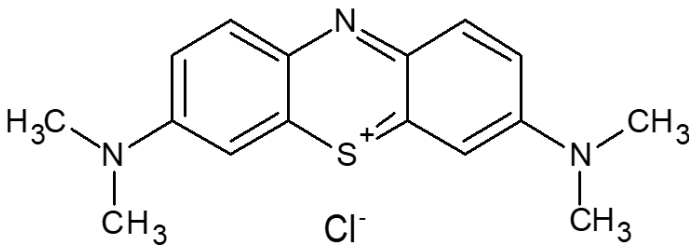

Fig 3-1 Structure of methylene blue (MB) [3-9]

3-3-1-2 Sodium alginate

SA structure from previous research [3-1]. Sodium alginate is a water-soluble polysaccharide biopolymer and exhibits excellent film-forming ability, good moisture absorption, permeability, and high viscosity. Furthermore, sodium alginate contains OH and COONa, which are also considered to interact with MB at N+/S+. SA is composed of β-D-mannuronic acid (M) and α-L-guluronic acid (G) linked by 1–4 glycosidic bonds with the molecular formula (C6H7NaO6)n [3-10]. In the calculation, this copolymer was simplified as a tetramer model as shown in Fig. 3-2.

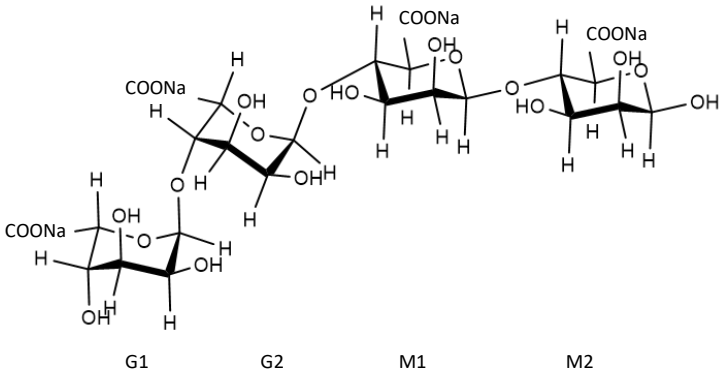

Fig 3-2 Structure of sodium alginate [3-9]

3-3-2 Methods

3-3-2-1 Computational details

All calculations were carried out using Gaussian 09 with GaussView 5.0.9 [3-11] as the interface. Molecular structures of MB and O_3 were fully optimized at the HF/6-31G(d) and B3LYP/6-31G(d) levels. For pullulan, the molecular structure reported in the literature [3-12] was employed. To obtain the stable conformations of SA, SA structure was created. Then we calculated at the HF/6-31G(d) and B3LYP/6-31G(d) levels until the last structure is remain and the energy is unchanged.

For a molecular complex between MB and SA, the fully optimized structures obtained for MB and SA as described above were employed in a ratio of 1:1. 20 initial structures were first created by locating SA at random around MB. The geometry for all the 20 complex structures was fully optimized at the HF6-31G(d) and then at the B3LYP6-31G(d) levels. Among the resulting complex structures, only 10 structures were employed for further analysis.

Single-point energy calculations were performed on the obtained structures at the B3LYP/6-31G(d) level to calculate the binding energies between MB and SA with consideration of the basis set superposition error (BSSE), which was estimated by the counterpoise method of Boys and Bernardi [3-13]. Similarly, molecular complex structures of MB—O_3, SA—O_3, pullulan—O_3, MB—pullulan, MB—SA—O_3, and MB—pullulan—O_3 were obtained.

3-3-2-2 Measurement of atomic distances

The bond lengths are taken from the vdW radii of the atoms. vdW radii can describe the calculation of interatomic distances using the sum of atomic radii, which differs for metals and nonmetals [3-14), (3-15), (3-16)]. There is concern about systematic analysis of nonbonded contacts among molecules, which may be affected by inaccuracies assumed by vdW radii. Therefore, the investigation was conducted to determine whether the Bondi vdW radii of common nonmetallic elements (C, N, O, S) are consistent (with vast numbers of nonbonded contact distances measured by crystallography). The vdW radius is estimated using equation (1):

$$\sum R = \sum(r_{A(vdW)} + r_{B(vdW)}) \quad (1)$$

At the $\sum R$ is the sum of the atomic radius of the complex structure (MB/SA), and $r_{A(vdW),B(vdW)}$ is the vdW.

Molecular interactions have critical roles in forming a stable MB/SA complex. However, existing methods typically allow us to probe vdW radii (e.g., bound or unbound) directly via geometry optimization, set at the B3LYP/6-31G(d) level of theory. This process enables identifying interactions and quantifying the vdW radii and binding energy.

3-3-2-3 Binding energy

The binding affinity of molecules is the sum of energy caused by thrust and the gravitational force between the nucleus and electron, as well as the action force between two electrons. The total energy of molecules can be obtained using the calculation of molecular structures. If the result presents a stable structure, the binding energy will negative. While the same molecule with the lowest total energy is more stable than the one with the highest energy. Binding energy is defined as the difference between the total energy of (MB-SA) and that of reactants (MB and SA). With the use of a finite basis set, BSSE occurs when atoms of interacting molecules approach one another. Counter poise method corrects this energy as shown in equation (2).

$$\text{The binding energy} = E(AB(\text{optimized}))-E(A(\text{optimized}))-E(B(\text{optimized}))+BSSE \quad (2)$$

where E(ABoptimized) and E(A(optimized), B(optimized)) are the total energy of products (MB-SA) and reactants (MB and SA). The BSSE is energies of the MB/SA complex structure. The binding energy is the change caused by BSSE.

3-3-2-4 Measurement of the decolorization mechanism of MB dye based on the SA film

To simulate AOS exposure, we used O_3, which is an AOS variant, although it may not have the same sterilization intensity as OH *. However, O_3 is a powerful oxidant and has many industrial and consumer applications related to oxidation. O_3 is an inorganic molecule with three O atoms, thus making it easier to react with other atoms because oxygen is a highly reactive element. We calculate this by using computationally predicting of HOMO and LUMO energy in MB dye based on the SA films.

3-4 Experiment

This research allows us to reveal the intermolecular interactions between MB and SA since the molecular structure will appear digitally. In addition, it will deepen our understanding of the interactions between MB and SA as the decolorization reaction occurs due to AOS. The molecular orbital theory is used to describe the arrangement of electrons in chemical structures [(3-17)]. It can also provide insights into the forces involved in the making and breaking of chemical bonds—the chemical reactions that are of high interest to organic chemists. The most rewarding approach to date has been using molecular orbital calculations to predict the atomic orbitals of the system. MB and SA structures were obtained using GaussView 5.0.9 software, which creates an input file for Gaussian 09 and outputs the calculation result as an image. Calculations were performed using Gaussian 09 [(3-18), (3-19), (3-20), (3-21)].

First, Molecular structures of MB, SA, O_3, and pullulan were fully optimized at the HF/6-31G(d) and B3LYP/6-31G(d) levels.

Second, bimolecular complexes which consist of MB−SA, MB−pullulan, MB−O_3, SA− O_3, and pullulan−O_3 were fully optimized at the HF/6-31G(d) and B3LYP/6-31G(d) levels and sent to further calculate multiple times in different structures. To analyze molecular interactions positions as well as find the binding energy orders of MB and SA. The interactions between the filled orbitals of one reagent and the filled orbitals of another are inherently energy-raising, countered by a small attractive force from the interactions between the filled and unfilled orbitals, which are inherently energy-lowering. Both forces diminish exponentially with distance, but they come into play at short distances and are not the only interactions between nonpolar molecules. The vdW radius is used to compare nonbonded contact distances by subtracting the relevant radii from the distance observed in new crystal structures [(3-22)].

Third, O_3 were added to the structure of MB−SA and MB−pullulan to create trimolecular complexes which is composition of MB−SA−O_3 and MB-pullulan−O_3 were fully optimized at the HF/6-31G(d) and B3LYP/6-31G(d) levels. Trimolecular is used to indicate decolorization mechanism of MB.

3-5 Results

Computational methods constitute one of the attractive and useful tools to obtain the optimal geometries and determine various aspects of molecules, such as the molecular structure, stability, and reactivity. The optimized molecular geometries of the structure were computed using quantum mechanical calculations by HF/6-31G(d) and B3LYP/6-31G(d). Then, we optimized and chosen energy lowered for the most stable structure. Bond lengths were later computed, which indicated the interaction positions between MB and SA. Whether the result of the absorption spectrum of molecules, the absorbances of the peaks between the TD-DFT spectra is show differences. These results indicate that an intermolecular force (interaction between molecules) occurred. As for the result of binding energy, the complex structure with the lowest energy indicates that the lower the energy is, the more stable the structure becomes. Next, the result of the decolorization mechanism of MB dye based on the SA film, which indicates that MB and the polymer (SA/pullulan) react with O_3.

Fig. 3-3 presents the 3D diagrams of molecular structures that we obtained from the calculation optimal of molecular structures and render using program Gaussian09. These include optimal molecular structures of MB, optimal molecular structures of SA, and optimal molecular structures of the MB/SA complex. The optimal molecular structures of MB present the Cl atom drifts apart from the position of the MB structure, while other atoms remain intact, as shown in Fig. 3-3(a) MB, Fig. 3-3(b) presents a visualization of the calculated optimal SA structure into a curve structure, but there are still connections not separated from each other. This structure has to change from the original structure of SA that be a straight line, as shown in Fig. 2. In Fig. 3-3(c) presents the optimal molecular structures of the MB/SA complex that N and O have interacted at position N20, O121 and the distance between N and O is 2.91 Å. In Fig. 3-3(d), this figure also has a distance of interaction between C and O is 2.95 Å at position C8, O60, which is the minimum distance from all calculations. Another result that we want to present is the S because we speculate that the N and S is a high potential for interaction because they are nonmetals with high electronegativity. In Fig. 3-3(e), we present the result of optimal molecular structures of the MB/SA complex that S and O interacted at the S19,O106 position and that the distance between S and O was equal to 3.20 Å. In addition, the interactions of the optimal molecular structures

of the MB/SA complex occur mainly at the position in the atomic distances of N, C, and S from MB between O from SA as shown in Table 1. As for binding energies (Table 2) is defined as the difference between the total energy of products (MB-SA) and that of reactants (MB and SA). Consequently, we obtained many structures displaying the lowest free energy of binding and proceeded to determine the details concerning atomic interactions between MB and SA [3-14].

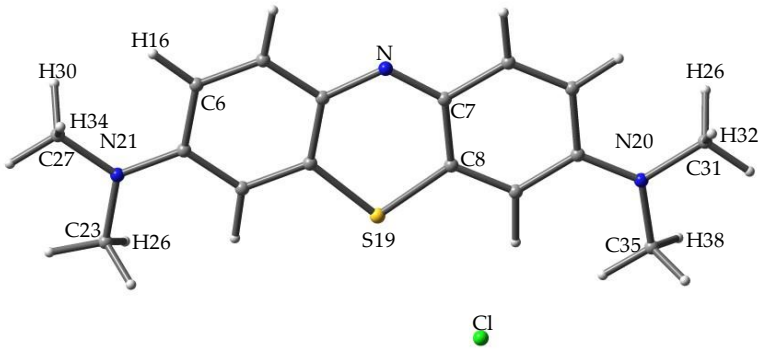

(a) [3-9]

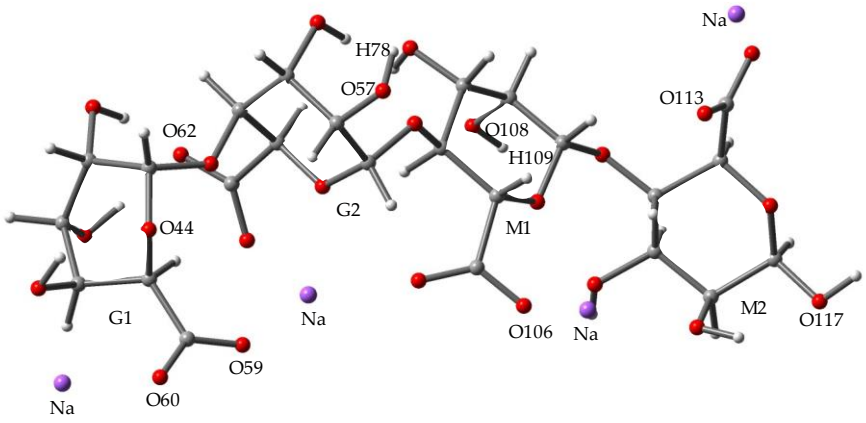

(b) [3-9]

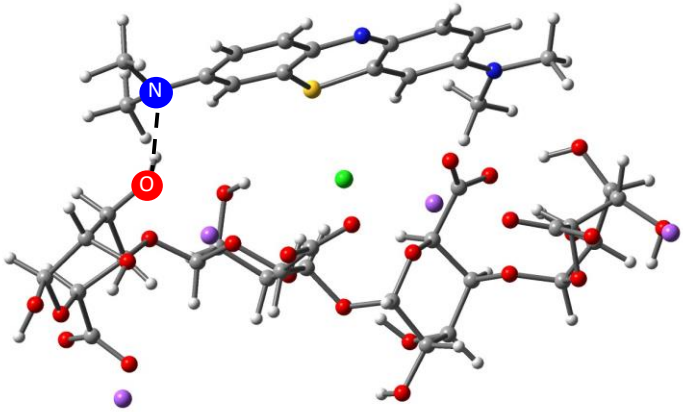

(c) MB/SA (19)

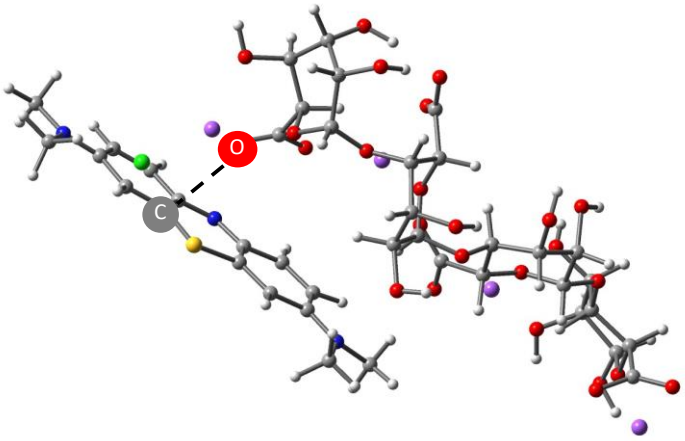

(d) MB/SA (6)

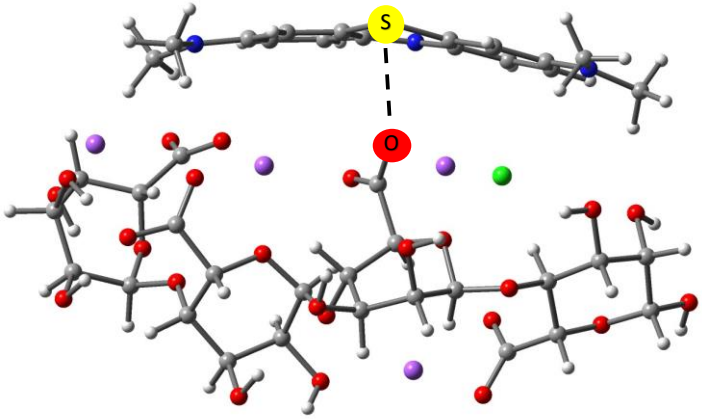

(e) MB/SA (20)

Fig 3-3 Optimal molecular structures (a) MB, (b) SA, and (c) N---O, (d) C---O, and (e) S---O the MB/SA complex at B3LYP/6-31G(d) level of theory.

3-5-1 Measurement of atomic distances

Table 1 The atomic distances between (N, C, and S from MB and O from SA) for the complex obtained at B3LYP/6-31G(d).

Structure Name	N---O (Å)	Position	C---O (Å)	Position	S---O (Å)	Position
MB/SA (1)	2.96	N20,O117	3.26	C35,059	3.71	S19,O113
MB/SA (2)	3.74	N20,O57,H78	3.53	C6,O106	3.23	S19,O60
MB/SA (3)	3.91	N22,O108,H109	3.24	C31,062	3.48	S19,O108
MB/SA (4)	3.51	N22,O60	3.46	C27,O106	3.27	S19,O60
MB/SA (5)	3.46	N22,O60	3.17	C7, O60	3.27	S19,O60
MB/SA (6)	3.51	N22,O60	2.95	C8, O60	3.26	S19,O60
MB/SA (7)	3.27	N21,O60	3.13	C35,O60	4.62	S19,O44
MB/SA (8)	3.51	N22,O60	2.96	C8, O60	3.27	S19,O60
MB/SA (9)	3.18	N22,O62	2.98	C7, O62	3.29	S19,O62
MB/SA (10)	3.73	N22,O62	2.96	C5, O60	3.94	S19,O57
MB/SA (11)	3.27	N21,O60	3.13	C35,O60	4.62	S19,O44
MB/SA (12)	3.53	N21,O59	3.32	C31, O59	3.69	S19,O113
MB/SA (13)	3.18	N20,O57	3.19	C30,O57	5.94	S19,O113
MB/SA (14)	4.19	N21,O60	3.56	C35,O60	3.11	S19,O63
MB/SA (15)	3.51	N21,O48	3.45	C32,O47	4.24	S19,O62
MB/SA (16)	3.44	N22,O57,H78	3.19	C35,O60	3.65	S19,O57
MB/SA (17)	3.51	N22,O60	2.95	C8,O60	3.26	S19,O60
MB/SA (18)	4.07	N20,O106	3.45	C23,O106	4.88	S19,O113
MB/SA (19)	2.91	N20,O121	3.57	C23,O121	3.59	S19,O108
MB/SA (20)	3.28	N21,O63	3.27	C31,O61	3.20	S19,O106

For geometry optimization, we decided to use the popular B3LYP functional. As it can be seen, the changes in geometry are relatively small. The parameters of complex structure (MB/SA) are given in Table1.

In this experiment, we create structures and perform calculations for optimized molecular structures, resulting in interaction and bond lengths. We use functional theory B3LYP/6-31G(d) to calculations the stable structure of MB, SA, and complex structure. The interaction between the two substances of N---O, C---O, and S---O when the atoms are close enough so that their atomic orbitals interact. the vdW radii are estimated using equation (1) [3-14]. We considered more than 20 structures in the interaction position. All structures are adjusted and calculated. Then, we select ten parameter structures from all structures displaying the lowest energy of binding, as shown in Table 1. This data presents the position and distance of N---O, C---O, and S---O. In each data presents an atom at short distances corresponding to an ionic bond. N--O's shortest distance is 2.96 Å at the position of N21, O58. The shortest distance of C--O is 3.18 Å at positions H32, C31, O58. The shortest distance of N --O is 3.20 Å at positions of S19, O78.

3-5-2 Binding energy measurement

Table 2 Binding energy (in kcal/mol) for the MB/SA complexes characterized at B3LYP/6-31G(d).

Structure Name	Complexation energy (kcal/mole)	Relative energy (kcal/mole)	BSSE (kcal/mole)
MB/SA (20)	-69.39	0	14.32
MB/SA (3)	-67.56	1.83	11.53
MB/SA (4)	-67.56	1.83	11.53
MB/SA (14)	-64.92	4.47	10.40
MB/SA (1)	-49.58	19.81	12.27
MB/SA (18)	-49.09	20.3	7.06
MB/SA (12)	-47.74	21.65	12.56
MB/SA (13)	-47.06	22.33	6.16
MB/SA (16)	-45.69	23.7	9.80
MB/SA (2)	-44.36	25.03	10.05

The binding energies [3-23), (3-24)] of complex structures are different from individual molecules. Ten structures were chosen from 20 initial structures calculated at HF/6-31G (d) and B3LYP6-31G (d), as shown in Table 2. We used the calculation values to support the geometry that the N, C, and S atoms of MB inter-act with the O atom of SA. Then, the result presents various stable complex structures with many designs, and there are also differences in binding energies. The binding of energy can be obtained from equation (2). However, when we considering binding energy, its value obtained with BSSE correction implemented during affects binding energy. In the cases of functional theory B3LYP/6-31G(d) to calculations, the structure MB/SA (20) presents the BSSE (14.32 kcal/mol) by the calculation. All the ten structures have relative energy larger than 25.03 kcal/mol.

3-5-3 Time-Dependent calculation

We successfully identified methylene blue and sodium alginate interactions at results of Time-Dependent calculation is based on a DFT computational method (TD-DFT). TD-DFT obtains the wave functions of MOs that oscillate between the ground state and the first excited states. We suggest that MB and sodium alginate share an ionic bond, as evidenced by the shifts in the peaks corresponding to the benzene ring of MB in the mixture of MB and sodium alginate.

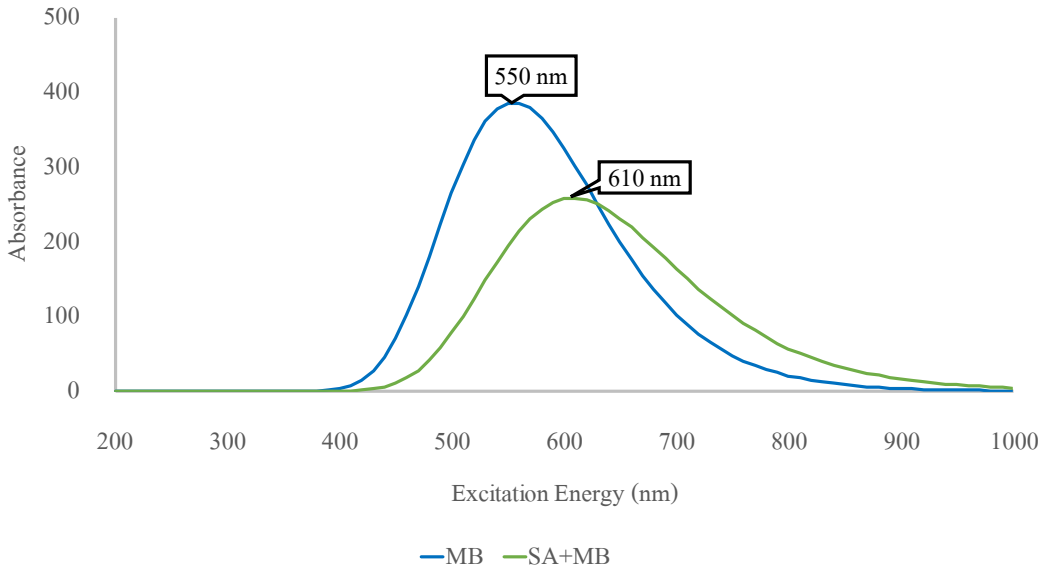

Fig 3-4 Absorbance TD-DFT of MB and MB/SA complex structures at a 1:1 ratio at B3LYP/6-31G(d) level of theory.

The Fig3-5 shows the absorbance from the TD-DFT of MB and a complex structure of MB/SA at a 1:1 ratio. The results report that the peak at 550 nm in the MB spectrum shifted to 610 nm in the complex structures of the MB and SA spectrum. The absorbances of the peaks between the TD-DFT spectra of 550 and 610 nm are show differences. These results indicate that an intermolecular force (interaction between molecules) occurred, thus suggesting that SA and MB undergo intermolecular interaction with one another at the –COO− (carboxylate salt) of SA and the N, C, and S position of MB. However, the prediction of the ultraviolet-visible absorption spectrum is still difficult, and the calculation accuracy is far inferior to the prediction of the real experiment spectrum.

3-5-4 Decolorization mechanism of MB dye based on the SA film

In a previous paper, we reported that to develop an indicator for AOS detection with enhanced oxidative ability, it is important to stabilize MB by combining it with SA. If MB is stabilized, it will prevent attacks from AOS [3-1]. From that, we assumed the SA acts as a protection layer for MB. In this research, we focused on finding the most stable structure of the MB/SA complex. The present work, as an extension of our earlier work [3-1], describes the DFT calculations implemented in the B3LYP/6-31G(d) level to get an insight into geometric and electronic structures. The molecular stability, namely O_3, O_3–SA, SA, pullulan, pullulan– O_3, MB– O_3, MB, MB/SA, and MB/SA/ O_3 were evaluated from the HOMO and LUMO energy values.

As mentioned above, AOS with high oxidation allows the film to decolorize. Therefore, we assumed that the MB-covered SA would be exposing MB to radical AOS. AOS such as singlet oxygen ($^1O_2$), O_3, and hydroxyl radicals (OH*) are of interest for surface modification, cleaning, and oxidation processes. From that, we can be used to develop thin-film indicators for AOS detection [3-25), (3-26), (3-27)]. Then, we experimented with calculating the HOMO–LUMO energy to evaluate the structures because the HOMO and LUMO are some of the best theories to explain a molecule's chemical stability [3-28), (3-29)]. The HOMO and LUMO energies of the structure provide information about energy distribution. When the higher the energy of HOMO, it more accessible to oxidization of the molecule. More than that, the more negative of the HOMO and LUMO energies will establish the stability of structures [3-30), (3-31)].

We present the 3D diagrams of the most optimized geometries by using DFT calculations, which were implemented in the B3LYP/6-31G(d) level, as shown in Fig. 3-4. We focus on a study uniform a thin film based on a water-soluble polymer with MB to describe the decolorization mechanism when exposed to AOS. In structure simulations, we focus to simulated two polymers, SA and pullulan. Both of these polymers have a similar positioning of O_3. We try to position O_3 as close to SA as possible in the simulation of complex structures because the experimental results of previous studies have shown that a powerful type of AOS

is required to react to the film for decolorization. From assumed above that SA would be a protective layer before the decolorization mechanism occurs.

We compared HOMO and LUMO energy values of the optimized structure per-formed to the following values: O_3, MB, SA, pullulan, MB/SA, and MB–pullulan shown in Table 3. The results obtained from the HOMO–LUMO energy calculation can be used to analyze the decolorization of the thin film [3-1]. To prove that both SA and pullulan act as a protective layer for MB, we must look at their HOMO value and compare it with the LUMO value of O_3. As you can see, the LUMO value of O_3 is -4.90 eV. If the HOMO value is above that, oxidation will occur. Therefore, MB oxidizes with O_3. On the other hand, SA and pullulan have lower HOMO values than the LUMO value of O_3. Thus, SA and pullulan cannot oxidize with O_3. Due to that matter, we combine SA and pullulan with MB, creating MB/SA and MB-pullulan. Nevertheless, when SA and pullulan are combined with MB, creating MB/SA and MB-pullulan complexes, we observed that the HOMO level of MB decreases to −5.73 and −5.57, respectively, strongly suggesting the prevention of MB from O_3 oxidation in the matrix of SA

Table 3 Comparing HOMO and LUMO energy values of the structures optimized at B3LYP/6-31G(d) [3-9]

Structure Name	HOMO (eV)	LUMO (eV)	HOMO-LUMO (eV)
O_3	-8.98	-4.90	-4.08
MB	-4.08	-2.99	-1.09
SA	-5.40	-2.05	-3.35
Pullulan	-6.73	0.81	-7.53
MB/SA	-5.73	-3.32	-2.41
MB/pullulan	-5.57	-3.48	-2.09

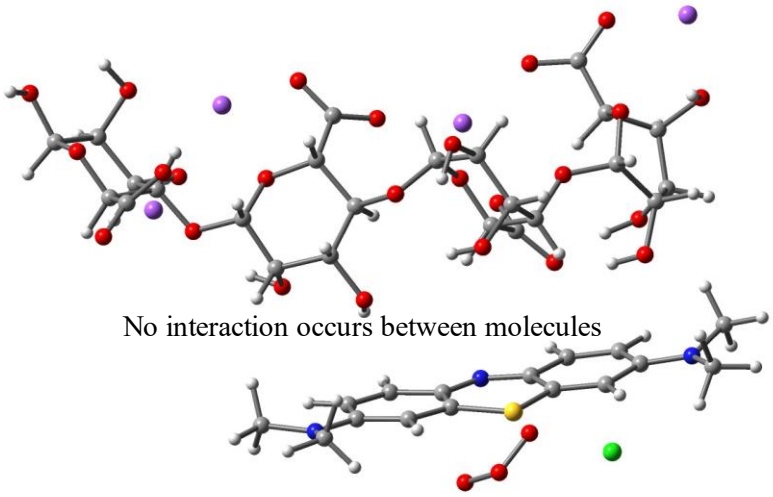

(a)

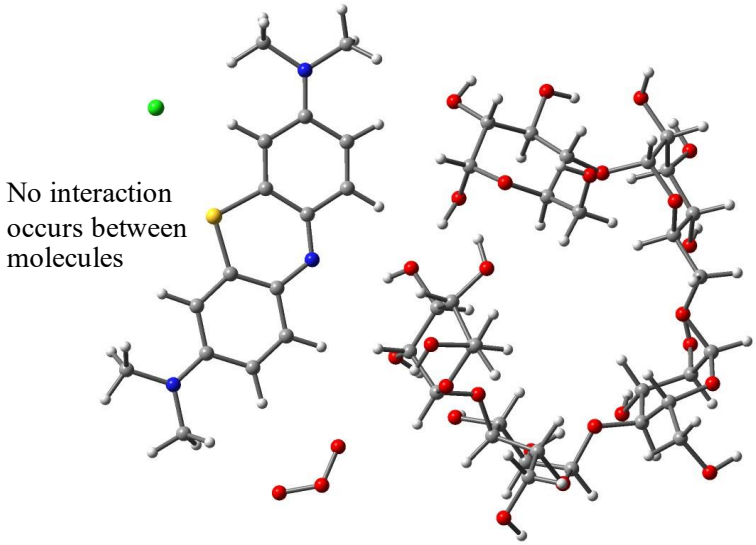

(b)

Fig 3-5 Optimal molecular structure of (a) MB/SA and O_3, (b) MB/pullulan and O_3 at B3LYP/6-31G(d) level of theory.

The 3D figure shows the most optimized geometries found using DFT calculations, which were implemented in the B3LYP/6-31(d) level (Fig. 3-5). The results obtained from the calculation can be used to analyze the decolorization of the thin film. However, the indicators comprising of sodium alginate or pullulan mixed with methylene blue cannot be decolorized in ozone exposure.

3-6 Discussion

In MB/SA complex structures, the most stable binding site for MB is N atom, C atom, and S atom in analysis. As for SA, we also found that at molecular arrangement structure R1 and R2 of the SA optimized molecular structures were more likely to interact with R3 and R4. The binding affinity of molecules is the sum of energy caused by thrust and the gravitational force between the nucleus and electron, and the action force between two electrons. The total energy of molecules can be obtained using the calculation of molecular structures. If the result presents a stable structure, the binding energy will be negative. At the same time, the same molecule with the lowest total energy is more stable than the one with the highest energy. Binding energy is defined as the difference between the total energy of (MB-SA) and that of reactants (MB and SA). Using a finite basis set, BSSE occurs when atoms of interacting molecules approach one another.

In addition, we attempted to explain the molecular reasons for the resistance of MB/SA film against decolorization in the exposure to O_3 by calculation for bimolecular and trimolecular complexes among MB, SA, and O_3 by molecular orbital calculation. The HOMO assessed molecule of MB mixed with SA molecular orbitals estimates the gap between HOMO and LUMO, LUMO energy value, and the HOMO-LUMO gap considering the changing HOMO-LUMO energy gap. The energy bandgap can be used to determine the efficiency of the electron transition between the HOMO and LUMO energy levels within a structure, whether the transition occurs quickly or not. The degradation of colors, the MB/SA complex underwent decolorization upon possible interaction modes that allowed AOS detection. O_3 was used to observe the decolorization mechanism of MB dye based on the SA film. Thus, HOMO and LUMO energy values can explain the intramolecular charge transfer from the electron donor to the electron acceptor in the MB/SA complex. The decolorization of the film is caused by the degradation reaction of MB upon AOS exposure was also discussed.

Pullulan is the most suitable for use as a protection layer against AOS attacks. However, pullulan still has the biggest gap (with/without O_3) compared with SA (with/without O_3), which means pullulan is more stable than the SA. From that, pullulan is hard to analyze because it is the most stable structure. Previous research [3-32), (3-33), (3-34] has mentioned elucidating the chemical reactions and the decolorization mechanism associated with exposure of the optimized MB–pullulan structures to OH*.

The results offer insight into possible interaction modes allowing AOS detection under various conditions. MB-dyed pullulan films have been used as models to investigate MB decolorization. Pullulan is a natural water-soluble polysaccharide with excellent film-forming properties but has a large and complex structure that makes it challenging to identify interactions with MB. We can confirm the strong affinity of the MB–polymer complex for AOS exposure from the bandgap calculation from the energies of HOMO and LUMO. Band gaps decrease while the LUMO energies increase upon interaction with O_3 by a polymer. This result also supports the mechanism of decolorization of MB/polymer com-plex towards O_3. Overall, we suggested the minimum and maximum values of HOMO and LUMO transition from the electron donor to the electron acceptor during the reaction between MB/SA and O_3. Furthermore, the HOMO–LUMO gaps of MB/pullulan/O_3 complex indicate that pullulan has the lowest oxidative ability more than MB/SA/O_3 complex. Therefore, SA is more suitable for computational analysis.

3-7 Conclusions

In this research, we have performed calculations at B3LYP/6-31G(d) levels of theory for the geometrical and energetic calculation of MB, SA, and MB/SA. Analysis of the molecular orbital (the MB/SA complexes were investigated by comparing vdW radii and binding energy) suggested forming bond lengths between N and C in the amine group of MB and O (-OOC-) of SA that happen. The impact of the binding energies showed that the complex structures (MB/SA) have different energies based on both calculations at the B3LYP/6-31G(d) level of theory. From that, these results supported previous results [3-1].

Consequently, When the binding energy at the B3LYP/6-31G(d) level has increased, the structure is more stable. The calculations experiment was achieved by stabilizing all ten complex structures and displaying the lowest free energies. The results in the identification of interactions that promote high affinity between MB and SA. The MB, SA, pullulan, MB/SA, and MB–pullulan to examine film decolorization's response decolorization mechanism of methylene blue dyes employed water-soluble polymers. As well as, clarifying the methylene blue dyes employed these polymers have a resistance for ozone by a calculation method by using GaussView and Gaussian09.

We can confirm the strong affinity of the MB–polymer complex for AOS exposure from the bandgap calculation from the energies of HOMO and LUMO. Band gaps decrease while the LUMO energies increase upon interaction with O_3 by a polymer. In this result, we suggested the minimum and maximum values of HOMO and LUMO transition from the electron donor to the electron acceptor during the reaction between MB/SA, and O_3. Furthermore, the HOMO–LUMO gaps of MB/pullulan/O_3 complex indicate that pullulan has the lowest oxidative ability more than MB/SA/O_3 complex. So, pullulan is more suitable for indicators of AOS that are made from uniform thin films than SA. The calculation for MB/O_3 and MB/SA or pullulan/O_3 complexes showed that O_3can decolorize MB; however, the indicators comprising SA or pullulan mixed with MB cannot be decolorized in O_3 exposure. Thus, the suitability of selecting SA or pullulan as a polymer matrix to develop AOS detectors was validated.

References

(3-1) S. Yenchit, H. Yamanaka, P. Temeeprasertkij, Y. Oda, O. Kanie, Y. Okamura, T. Inazu, S. Iwamori. “Chemical Stability of a Colorimetric Indicator Based on Sodium Alginate Thin Film and Methylene Blue Dye upon Active Oxygen Species Exposure”. Japanese Journal of Applied Physics. 2020, Vol. 59, p. SDDF09.

(3-2) Z. Wang, H. Yang, Z. Zhu. “Study on the Blends of Silk Fibroin and Sodium Alginate: Hydrogen Bond Formation, Structure and Properties”. Polymer. 2019, Vol. 163, pp. 144-153.

(3-3) W. Lan, L. He, Y. Liu. “Preparation and Properties of Sodium Carboxymethyl Cellulose/Sodium Alginate/Chitosan Composite Film”. Coatings. 2018, Vol. 8, p. 291.

(3-4) T. Harnsilawat, R. Pongsawatmanit, D.J. McClements. “Characterization of β-Lactoglobulin–Sodium Alginate Interactions in Aqueous Solutions: A Calorimetry, Light Scattering, Electrophoretic Mobility and Solubility Study”. Food Hydrocolloids. 2006, Vol. 20, pp. 577-585.

(3-5) P. Temeepresertkij, S. Yenchit, M. Iwaoka, S. Iwamori. “Interactions between Methylene Blue and Pullulan According to Molecular Orbital Calculations”. IEEJ Transactions on Fundamentals and Materials. Institute of Electrical Engineers of Japan. 2020, Vol. 140, pp. 529-533.

(3-6) Y. Yue, X. Wang, J. Han, L. Yu, J. Chen, Q. Wu, J. Jiang. “Effects of Nanocellulose on Sodium Alginate/Polyacrylamide Hydrogel: Mechanical Properties and Adsorption–Desorption Capacities”. Carbohydrate Polymers. 2019, Vol. 206, pp. 289-301.

(3-7) F. Raposo, M.A. De La Rubia, R. Borja. “Methylene Blue Number as Useful Indicator to Evaluate the Adsorptive Capacity of Granular Activated Carbon in Batch Mode: Influence of Adsorbate/Adsorbent Mass Ratio and Particle Size”. Journal of Hazardous Materials. 2009, Vol. 165, pp. 291-299.

(3-8) P. Temeeprasertkij, S. Yenchit, M. Iwaoka, S. Iwamori. “Interactions between Methylene Blue and Pullulan by Molecular Orbital Calculations”. 4th Japan-Thailand Joint Symposium on Advanced Nanomaterials and Devices for Electronics and Photonics (JT-AND 2020), DEI-20-018, Thailand.

(3-9) P. Temeeprasertkij, S. Yenchit, M. Iwaoka, S. Iwamori. “Molecular Interactions between Methylene Blue and Sodium Alginate Studied by Molecular Orbital Calculation”. Molecules, 2021, Vol.26, pp. 7029.

(3-10) C. Xiao, H. Liu, Y. Lu, L. Zhang. “Blend Films from Sodium Alginate and Gelatin Solutions”. Journal of Macromolecular Science, Part A. 2001, Vol. 38, pp. 317-328.

(3-11) G. Zhang, C.B. Musgrave. “Comparison of DFT Methods for Molecular Orbital Eigenvalue Calculations”. The Journal of Physical Chemistry. A. 2007, Vol. 111, 1554-1561.

(3-12) C. Tabti, N. Benhalima. “Molecular Structure, Vibrational Assignments and Non-Linear Optical Properties of 4,4’ Dimethylaminocyanobiphenyl (DMACB) by DFT and ≪i≫Ab Initio HF Calculations”. Advances in Materials Physics and Chemistry. 2015, Vol. 05, pp. 221-228.

(3-13) D. Nori-Shargh, M.M. Amini, S. Jameh-Bozorghi. “Ab Initio Study of Ring Flipping of the Overcrowded Peri-Substituted Naphthalenes”. Phosphorus, Sulfur, and Silicon and the Related Elements. 2003, Vol. 178, pp. 2529-2537.

(3-14) S.S. Batsanov. “Van Der Waals Radii of Elements”. Inorganic Materials. 2001, Vol. 37, pp. 871-885.

(3-15) S.S. Batsanov. “Calculation of Van Der Waals Radii of Atoms from Bond Distances”. Journal of Molecular Structure. 1999, Vol. 468, pp. 151-159.

(3-16) A. Bondi. “Van Der Waals Volumes and Radii”. The Journal of Physical Chemistry. 1964, Vol. 68, pp. 441-451.

(3-17) R.S. Rowland, R. Taylor. “Intermolecular Nonbonded Contact Distances in Organic Crystal Structures: Comparison with Distances Expected from van der Waals Radii”. Journal of Physical Chemistry. 1996, Vol. 100, pp. 7384-7391.

(3-18) S. Fu, A. Thacker, D.M. Sperger, R.L. Boni, I.S. Buckner, S. Velankar, E.J. Munson, L.H. Block. “Relevance of Rheological Properties of Sodium Alginate in Solution to Calcium Alginate Gel Properties”. AAPS PharmSciTech. American Association of Pharmaceutical Scientists. 2011, Vol. 12, pp. 453-460.

(3-19) A. Dreuw, M. Head-Gordon. “Single-Reference Ab Initio Methods for the Calculation of Excited States of Large Molecules”. Chemical Reviews. 2005, Vol. 105, pp. 4009-4037.

(3-20) E.R. Johnson, A.D. Becke. “A Post-Hartree–Fock Model of Intermolecular Interactions”. The Journal of Chemical Physics. 2005, Vol. 123, 24101, 16050735.

(3-21) E.R. Johnson, A.D. Becke. “A Post-Hartree–Fock Model of Intermolecular Interactions”. The Journal of Chemical Physics. 2005, Vol. 123, 24101, 16050735.

(3-22) Y.H. Zhao, M.H. Abraham, A.M. Zissimos. “Fast Calculation of Van Der Waals Volume as a Sum of Atomic and Bond Contributions and Its Application to Drug Compounds”. The Journal of Organic Chemistry. 2003, Vol. 68, pp. 7368-7373.

(3-23) K. Morokuma, K. Kitaura. “Energy Decomposition Analysis of Molecular Interactions”. Chemical Applications of Atomic and Molecular Electrostatic Potentials. 1981, pp. 215-242.

(3-24) V. Gapsys, S. Michielssens, J.H. Peters, B.L. de Groot, H. Leonov. ‘Calculation of Binding Free Energies’. Molecular Modeling of Protein S. Methods in Molecular Biology, Vol. 1215. pp. 173-209.

(3-25) S. Iwamori, N. Nishiyama, K. Oya. “A Colorimetric Indicator for Detection of Hydroxyl Radicals in Atmosphere Using a Methylene Blue Dye Based on Nafion Film”. Polymer Degradation and Stability. 2016, Vol. 123, pp. 131-136.

(3-26) K. Hosoya, S. Yenchit, Y. Tadokoro, K. Oya, S. Iwamori. “Improved Singlet Oxygen Detection Sensitivity in Electron Spin Resonance Using a Spin-Trap Agent Incorporated into a Water-Soluble Polymer Film”. Chemistry Letters. Chemical Society of Japan. 2018, Vol. 47, pp. 1191-1193.

(3-27) K. Oya, K. Hosoya, T. Suto, S. Iwamori. “Surface Modification of Polydimethylsiloxane by Exposure of Active Oxygen and Ultraviolet Lights to Improve Cell Adhesion”. Transactions of the JSME. Japan Society of Mechanical Engineers. 2019, Vol. 85, 18-00356.

(3-28) N. Nagasawa, H. Mitomo, F. Yoshii, T. Kume. “Radiation-Induced Degradation of Sodium Alginate”. Polymer Degradation and Stability. 2000, Vol. 69, pp. 279-285.

(3-29) H.C. Beachell, S.P. Nemphos. “Oxidative Degradation of Polymers in Presence of Ozone”. Advances in Chemistry. Ozone Chemistry and Technology Advances in Chemistry, American Chemical Society: Washington, DC. 1959, pp. 168-175.

(3-30) K. Fukui. “Role of Frontier Orbitals in Chemical Reactions”. Science. Nov. 19, 1982, Vol. 218, pp. 747-754.

(3-31) .K. Choudhary, A.K. Bhatt, D. Dash, N. Sharma. “DFT Calculations on Molecular Structures, HOMO–LUMO Study, Reactivity Descriptors and Spectral Analyses of Newly Synthesized Diorganotin(IV) 2-Chloridophenylacetohydroxamate Complexes”. Journal of Computational Chemistry. 2019, Vol. 40, pp. 2354-2363.

(3-32) S. Yenchit, Y. Tadokoro, S. Iwamori. “Measuring Active Oxygen Species across a Nonwoven Fabric Using a Pullulan-Mixed Methylene Blue Thin Film and Electron Spin Resonance”. IEEJ Transactions on Sensors and Micromachines. 2019, Vol. 139, pp. 54-60.

(3-33) P. Temeeprasertkij, S. Yenchit, M. Iwaoka, S. Iwamori. “Interactions between Methylene Blue and Pullulan According to Molecular Orbital Calculations”. IEEJ Transactions on Fundamentals and Materials. 2020, Vol. 140, pp. 529-533.

(3-34) S. Iwamori, N. Nishiyama, K. Oya. “A colorimetric indicator for detection of hydroxyl radicals in atmosphere using a methylene blue dye based on nafion film”. Polymer Degradation and Stability. 2016, 123, 131-136.

Chapter 4

Hydroxyl Radical Reaction with Methylene Blue and Polymer for the decolorization mechanism

4-1 Introduction

Hydroxyl radicals (OH radical), hydrogen peroxide (H_2O_2), and ozone (O_3) are active oxygen species (AOS) in the narrow sense [4-1), (4-2), (4-3)]. AOS is involved in various applications in numerous industrial processes owing to its extremely strong oxidative ability. It is well known that HO radicals are electrophilic in nature and react with electron sites of organic compounds by complex reaction mechanisms involving free radicals. Wherewith free radicals are usually unstable and highly reactive because the unpaired electrons tend to form pairs with other electrons [(4-5)].

A methylene blue of previous [(4-2)] studies has revealed the major reaction mechanisms of OH radicals in stabilizing methylene blue by mixing it with water-soluble polymers. Analyzed a methylene blue-dyed sodium alginate thin-film and methylene blue-dyed pullulan thin-film indicator to elucidate the chemical reactions occurring as well as the decolorization mechanism generated under the high-humidity condition. The results revealed that the AOS was exposed under low-humidity conditions and high-humidity conditions to the methylene blue-based water-soluble polymer film. The pigment on the thin film after AOS exposure in a high-humidity environment was markedly discolored and became transparent. However, the decolorization of the film after exposure to ozone and AOS under low-humidity conditions was hardly observed. Therefore, the decolorization of the film due to AOS exposure is related to the degradation reaction of methylene blue molecules caused by hydroxyl radicals. Moreover, methylene blue and water-soluble polymers results revealed that methylene blue and water-soluble polymers complex undergo decolorization upon insight into possible interaction modes, allowing AOS detection under various conditions. The molecular orbital analysis suggested the formation of hydrogen bonds between nitrogen, carbon, and sulfur atoms in the methylene blue benzene ring. On the side water-soluble polymers, OH group from pullulan and carboxylates salt (–COO-) from sodium alginate. The calculations determined the shortest bond distances among the various complex structures displaying the lowest free energies, resulting in the identification of interaction promoting high affinity between the two molecules.

The objective of this article is to apply computational methods to evaluate the decolorization mechanism ability between methylene blue /sodium alginate and methylene blue /pullulan of complex structures with OH radical, which has the strongest oxidative ability among AOS. In addition, we wanted to show that there is a difference in the decolorization mechanism between OH radical and another AOS species with a molecular model, in the previous paper [4-1], only ozone is simulated in advance.

In the present study, molecular orbital calculations reveal the details of the interaction between methylene blue and water-soluble polymers. We investigated the stable structures and their electronic properties for the complexes of methylene blue /sodium alginate and methylene blue/pullulan with ozone, H_2O_2, and OH radicals in a vacuum, respectively. With MB alone, bleaching reaction occurs due to excited singlet oxygen molecules/atoms and OH radicals including ozone (although there is a prior document in our laboratory, indicating that the indicators comprising sodium alginate or pullulan mixed with MB cannot be decolorized in ozone exposure). On the other hand, OH radicals, which have the strongest oxidizing power, can be decolorized by using an indicator containing methylene blue in sodium alginate or pullulan, but decolorization reaction does not occur in ozone or excited singlet oxygen or molecules. To highlight the difference in the mechanism of the attacking reaction of OH radicals to methylene blue /sodium alginate and methylene blue /pullulan, density functional theory (DFT) calculation has been analyzed to determine these chemical reactivity descriptor values of methylene blue, sodium alginate, pullulan, methylene blue /sodium alginate, and methylene blue /pullulan of molecules. Computational chemistry can be used to probe chemical reactivity and to analyze the changes in the electronic properties of the reactants, transition states, and products as a reaction proceeds. In the computational method, the methylene blue /sodium alginate and methylene blue /pullulan of complex structures can be evaluated by some chemical reactions descriptors such as LUMO energy (eV), HOMO energy (eV), energy gap (eV), global hardness, softness, and electro-negativity. Moreover, the degradation of colors, the methylene blue/sodium alginate complex underwent decolorization upon possible interaction modes that allowed AOS detection. The OH radicals were used to observe the decolorization

mechanism of MB dye based on the sodium alginate and pullulan. The decolorization of the film is caused by the degradation reaction of methylene blue upon AOS exposure was also discussed. These investigations may also apply to evaluate uniform thin film indicators based on methylene blue-dyed water-soluble polymers to elucidate the de-colorization mechanism upon exposure to AOS. Therefore, in this paper, we would like to clarify the molecular mechanism of decolorization of methylene blue in water-soluble polymers by OH radicals, which has the strongest oxidative ability among AOS.

4-2 Methods

In this paper, we carried out the DFT calculation [4-6),(4-7)] to provide theoretical supports for understanding how OH radical causes methylene blue to decolorize and to compare the stability of polymers (between pullulan and sodium alginate), which has the strongest oxidative ability that allow OH radical exposure.

Determination of the stable structure of methylene blue with polymer: Initial structures of methylene blue /sodium alginate and methylene blue /pullulan were chosen from the structure of a previous study. These calculations were done using the Gaussian 09 suite of programs. GaussView molecular modeling software was used to plot the molecular orbitals and draw the molecular structure. These structures were optimized in a vacuum and their charge distribution was analyzed by using DFT calculation as the exchange and correlation potentials and the B3LYP/6-31G(d) basis-set of ab initio MO program Gaussian09. Here we employed the DFT calculation due to its good performance for accurate and reliable calculation. Recently, computational techniques especially DFT calculation have been commendably applied to determine these various parameters of complex molecules.

To create a complex structure, the formation of the complex structure was undertaken by placing methylene blue and water-soluble polymers in different orientations relative to one another. To create a complex structure, we arranged the molecules of methylene blue and water-soluble polymers differently in terms of position. Different positions arrangement allows the energy of complex structures to be diverse.

4-3 Active oxygen species

AOS refers to oxygen-based species that are characterized by high oxidizing power and are generated by irradiating oxygen molecules with a specific wavelength of UV radiation. Such species include ozone (O3), excited singlet oxygen (1O2), hydroxyl radical (OH*), and excited singlet oxygen [O(1D)]. Among the types of AOS, OH* have high oxidizing power. The hydroxyl radical (OH*) is a powerful oxidant that is produced in a wide range of environments1. This radical degrades organic compounds, which makes it harmful if produced in excess and in close proximity to cells. Such oxidative stress reactions can have a range of adverse effects, and ·OH production may be accelerated by reactive nanoparticles, which reactions are of great practical significance.

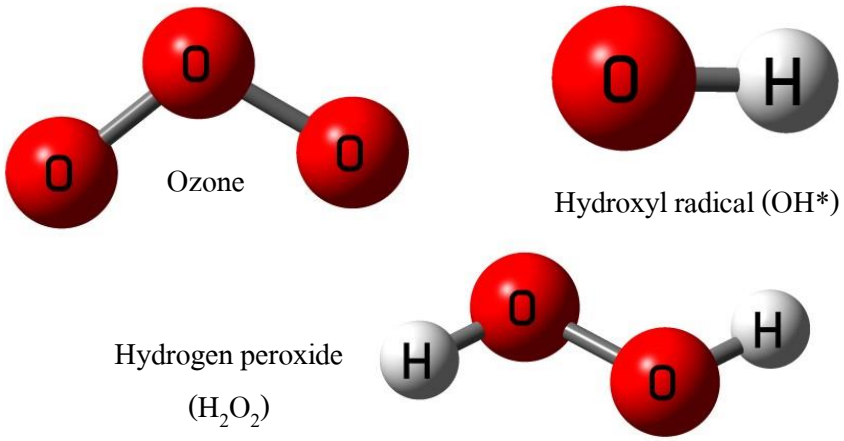

Fig.4-1. AOS structure at the B3LYP/6-31G(d) level of theory

4-4 Results and Discussion

The various parameters LUMO energy (eV), HOMO energy (eV), energy gap (eV), hardness, softness, and electronegativity associated with decolorization mechanisms have been calculated for the methylene blue pullulan and methylene blue /sodium alginate complex structures. Spin density distribution is an important quantum property in the estimation of methylene blue, pullulan, and sodium alginate structures.

We first placed the methylene blue structure close to the polymer (pullulan and sodium alginate) structure and optimized the structures in a vacuum by use of the calculations. We perform the binding energy and force calculations using density functional theory at the B3LYP/6-31G(d) level. The total binding energy of the optimized methylene blue /pullulan complex structures are listed in Fig4-1., indicating that the structure is shown optimized methylene blue /pullulan complex structure is at least -54.19 kcal/mol more stable than the other structures. As for Fig4- 2, the total binding energy of the optimized methylene blue /sodium alginate complex structures. The optimized structure of methylene blue /sodium alginate in the gas phase contains -69.39 kcal/mole less energy than the other structures. We can predicate that the binding energy results indicated that the estimation of methylene blue /pullulan complex structures is more stable in comparison with methylene blue/sodium alginate complex structures.

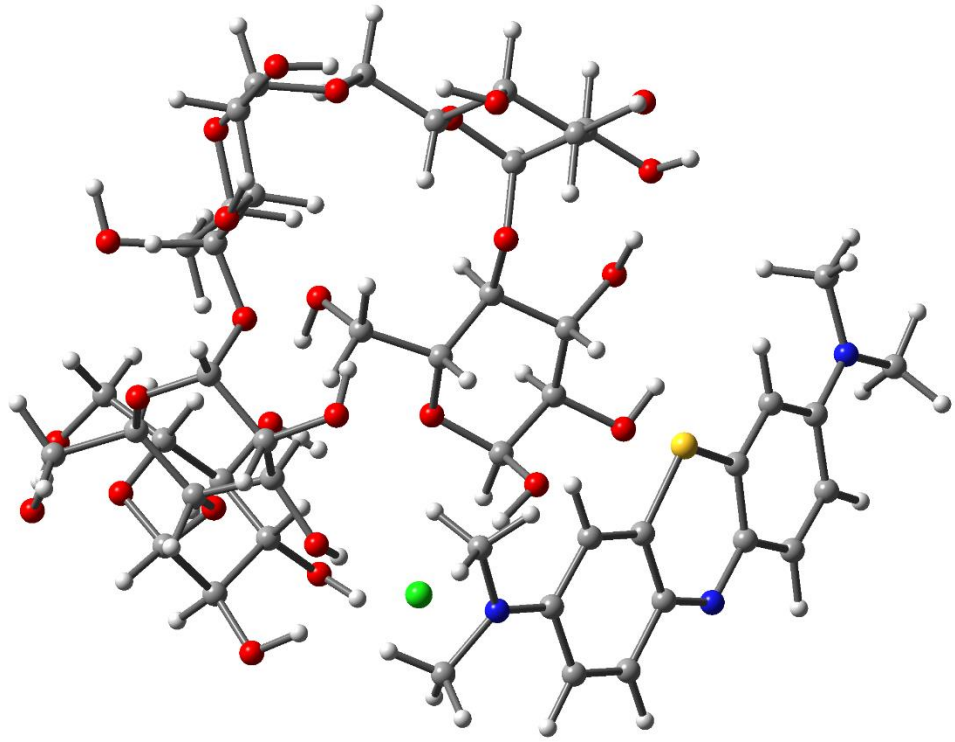

methylene blue /pullulan 1

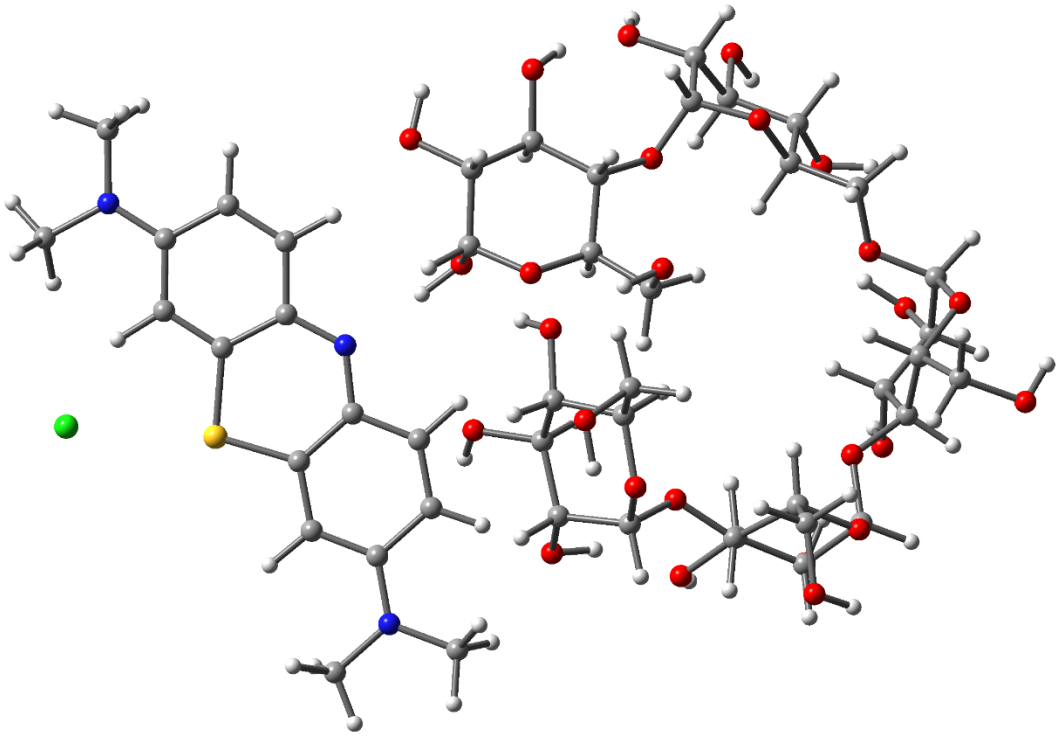

methylene blue /pullulan 6

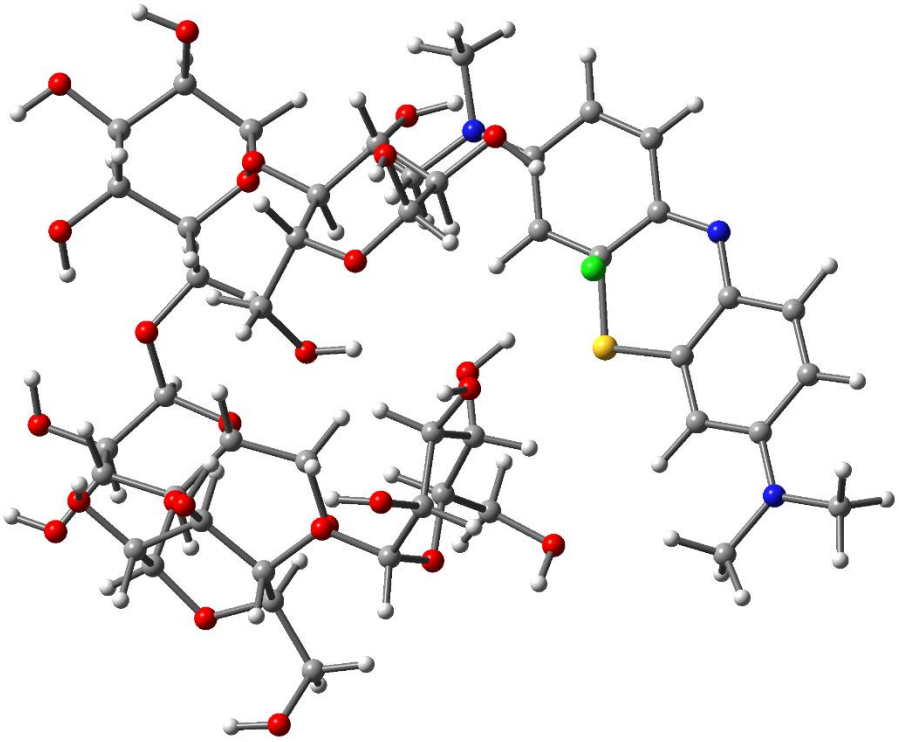

methylene blue /pullulan 14

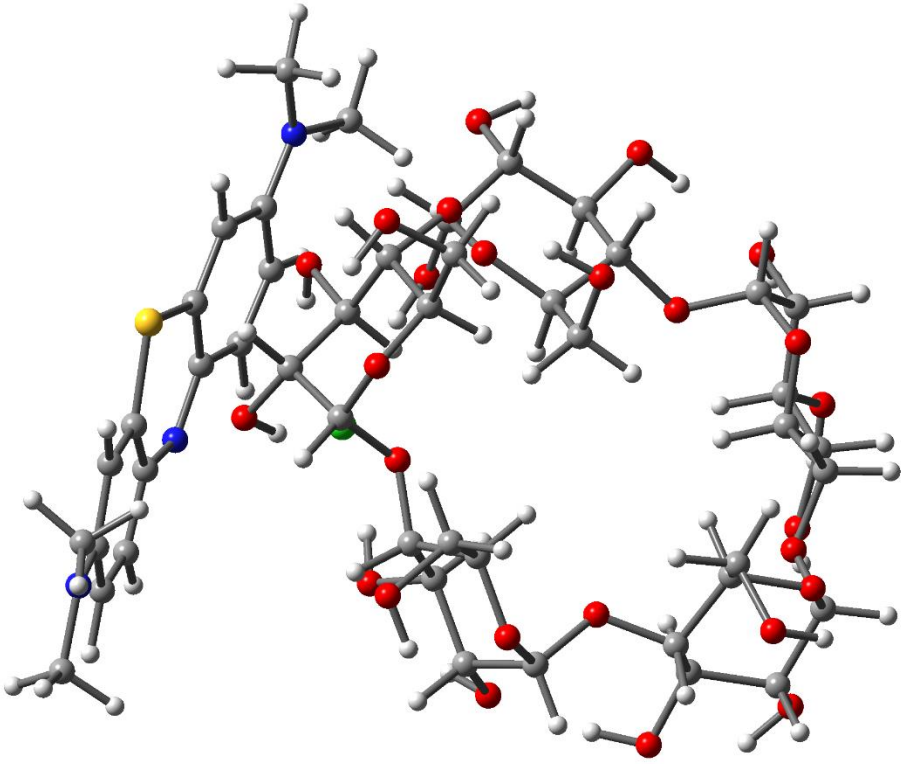

methylene blue /pullulan 16

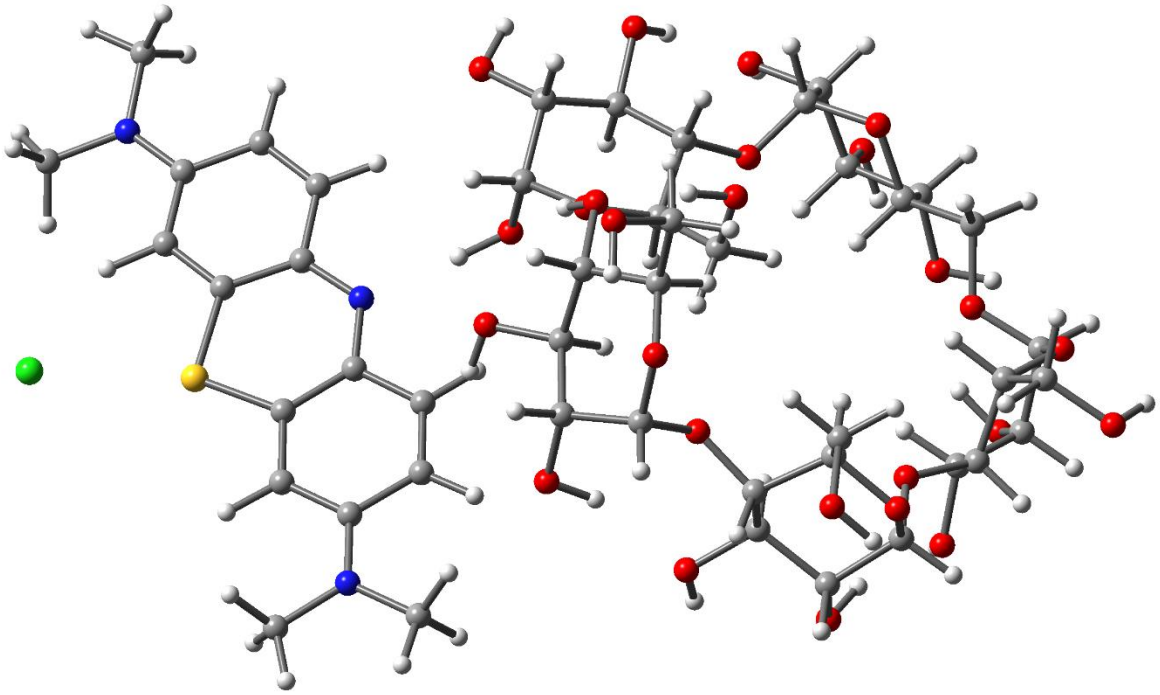

methylene blue /pullulan 20

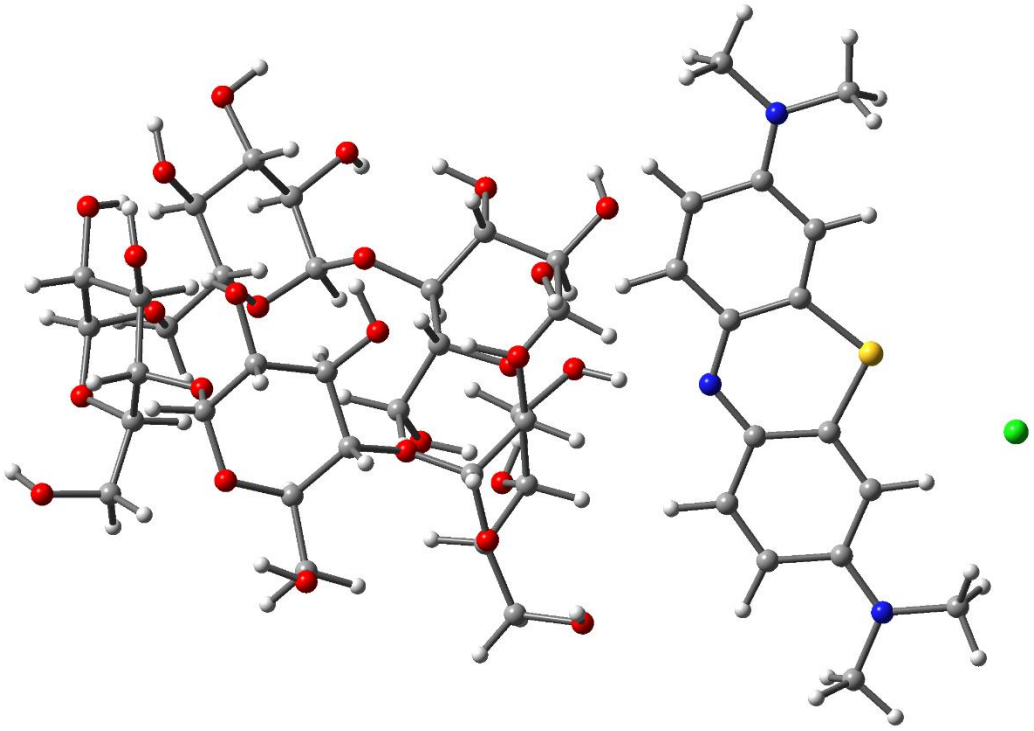

methylene blue /pullulan 21

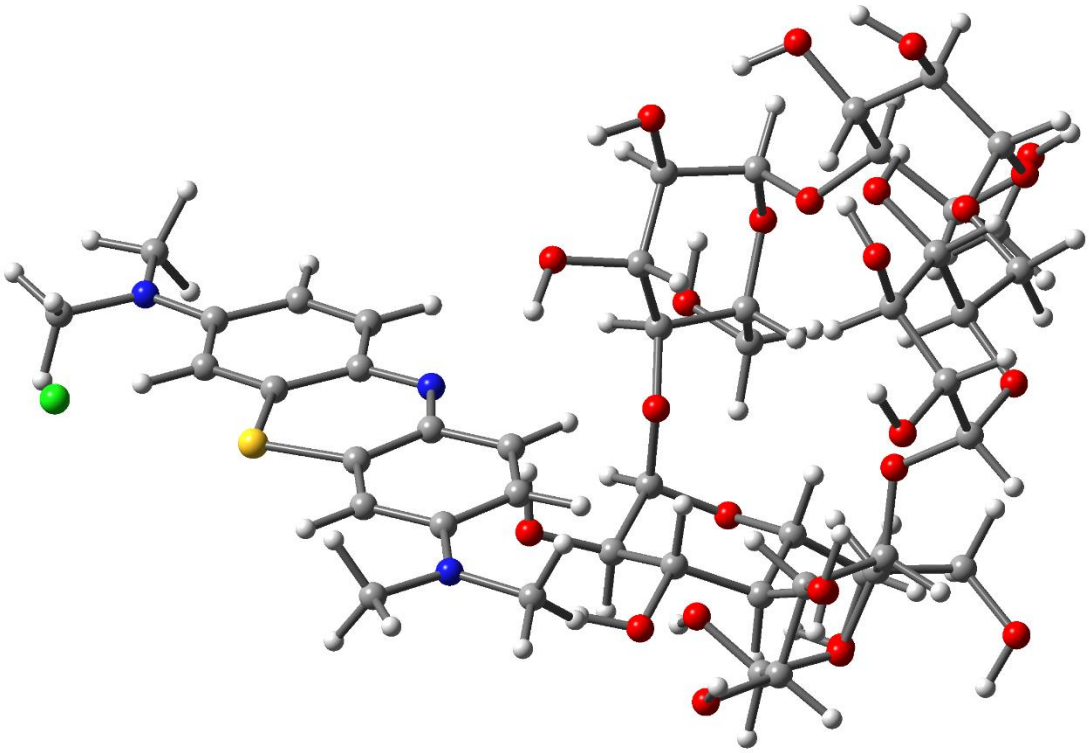

methylene blue /pullulan 25

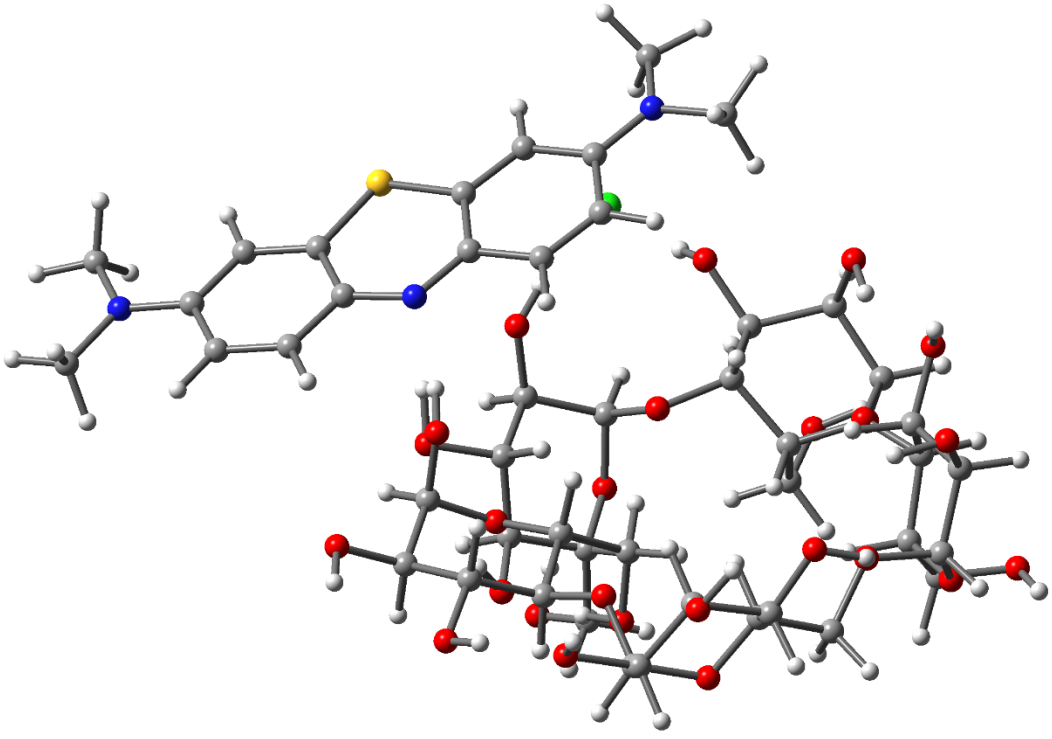

methylene blue /pullulan 27

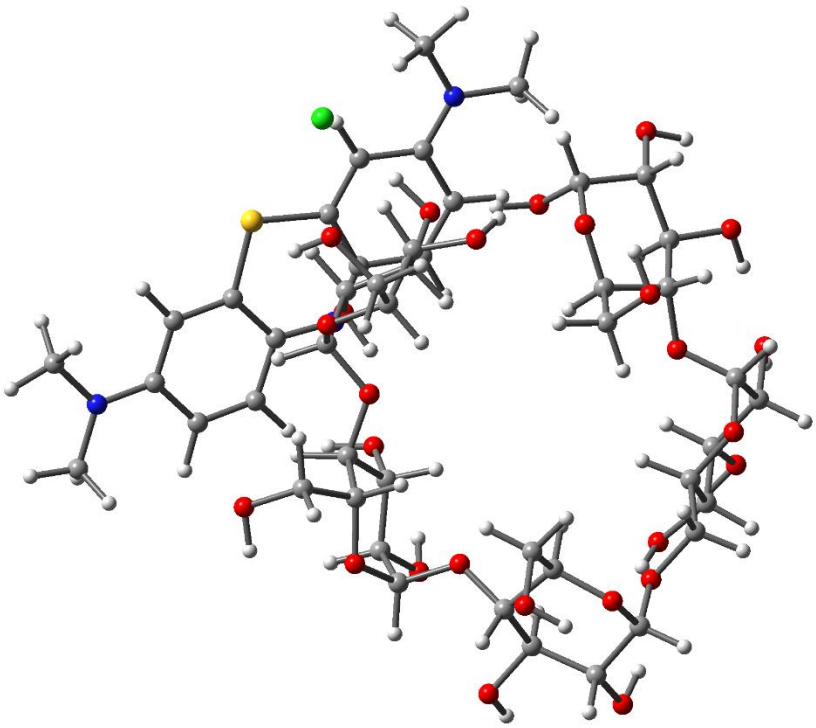

methylene blue /pullulan 28

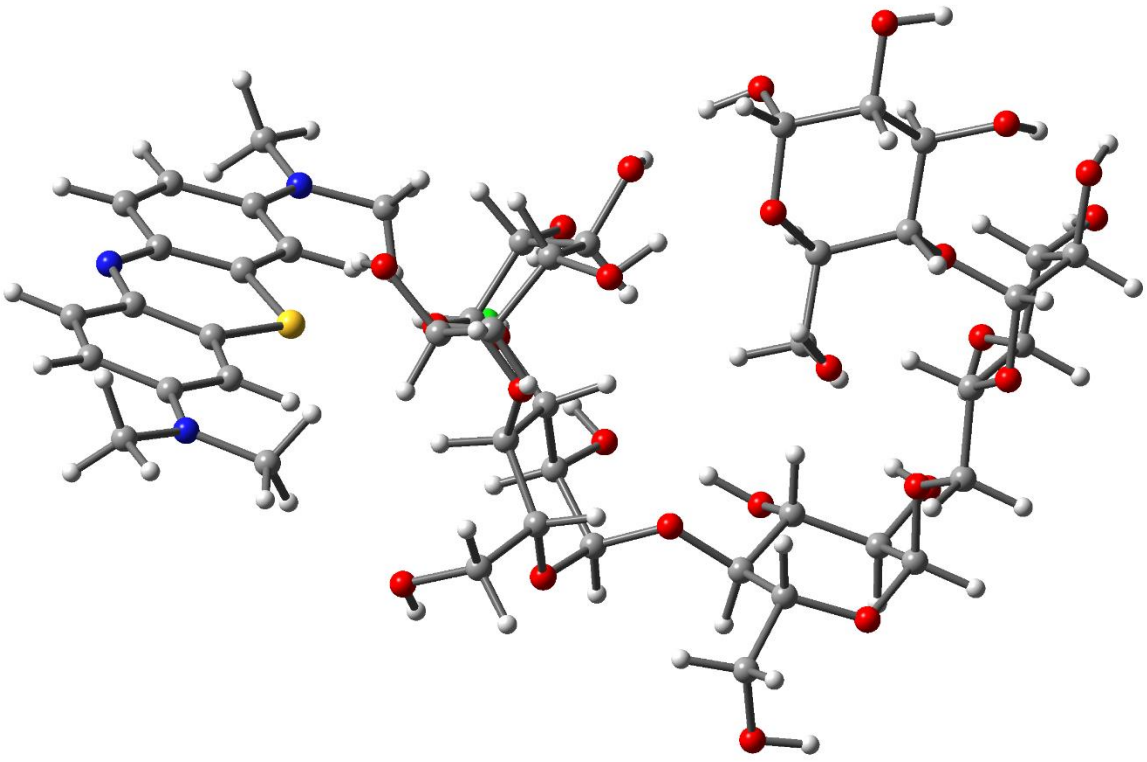

methylene blue /pullulan 29

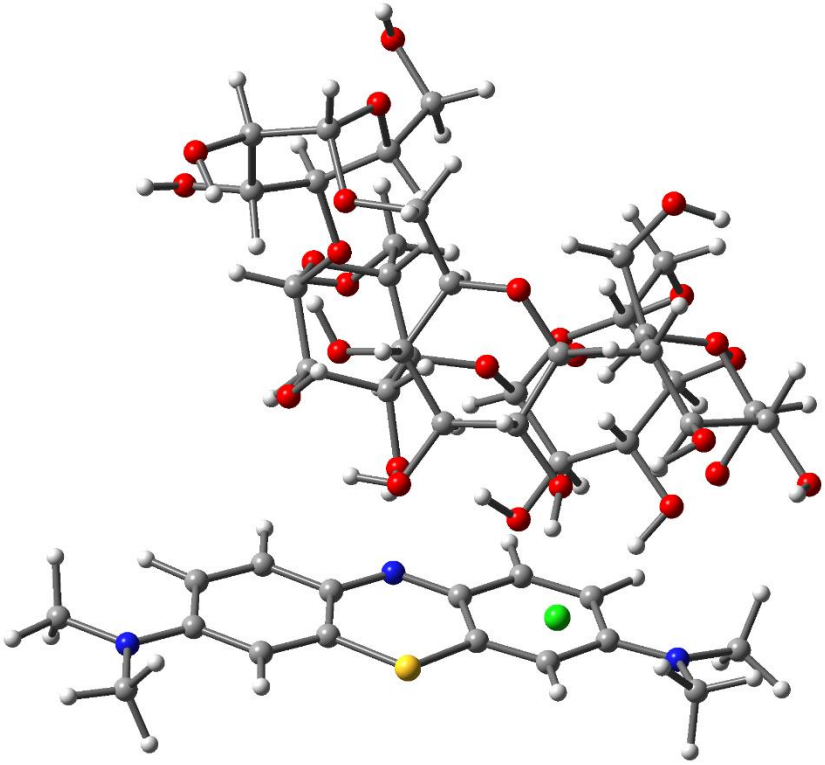

methylene blue /pullulan 31

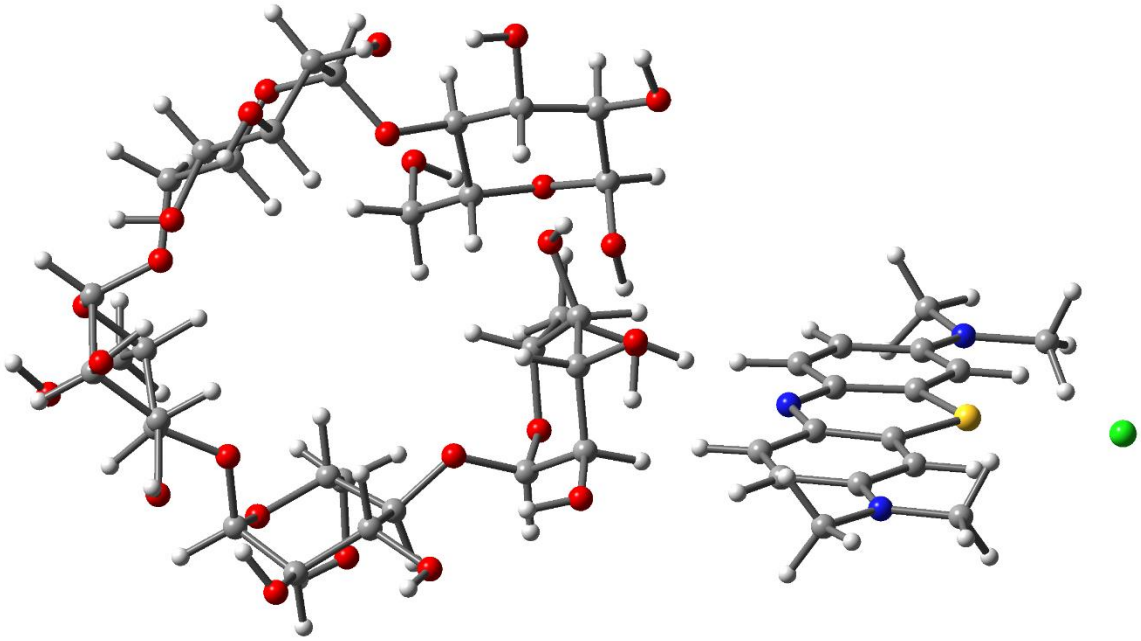

methylene blue /pullulan 35

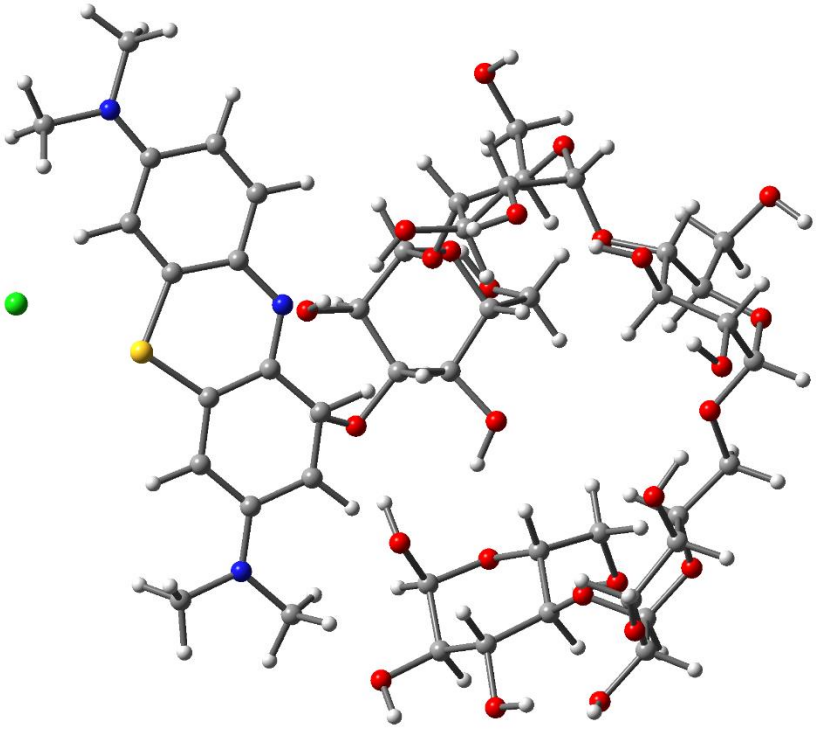

methylene blue /pullulan 36

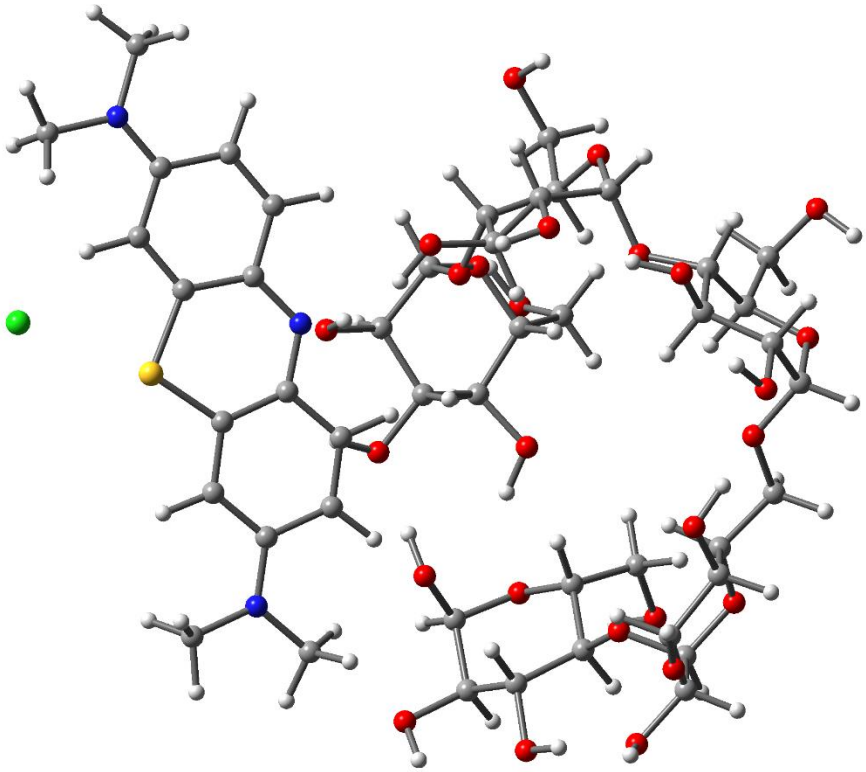

methylene blue /pullulan 38

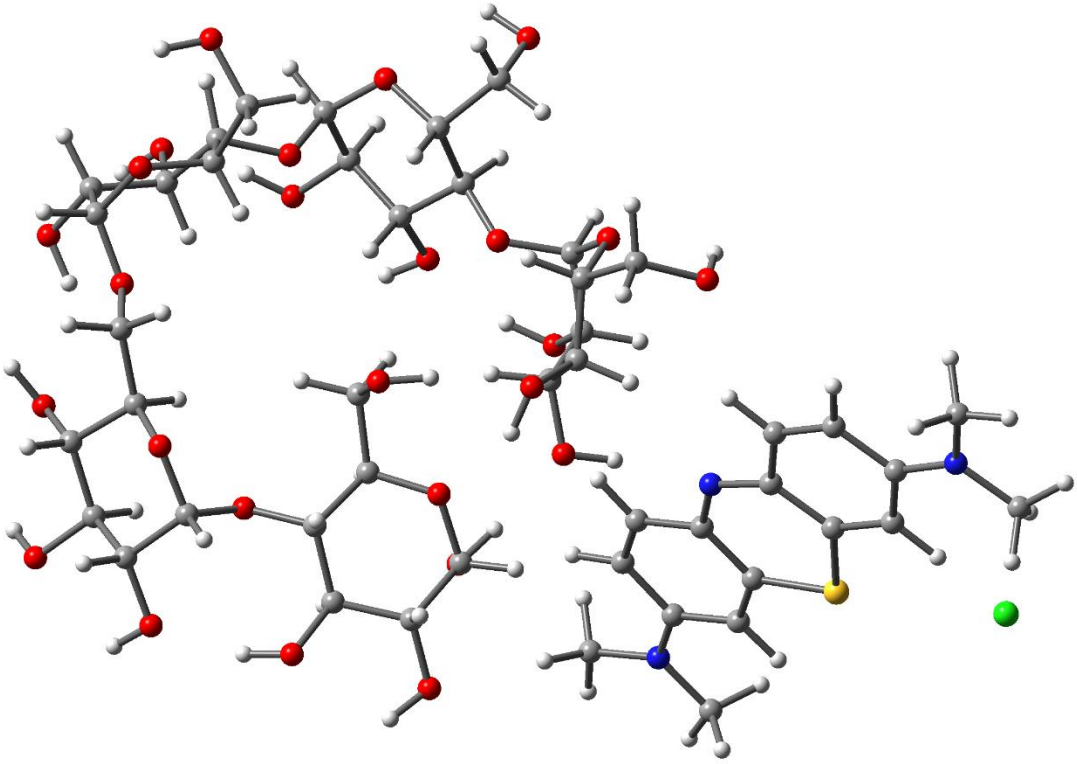

methylene blue /pullulan 39

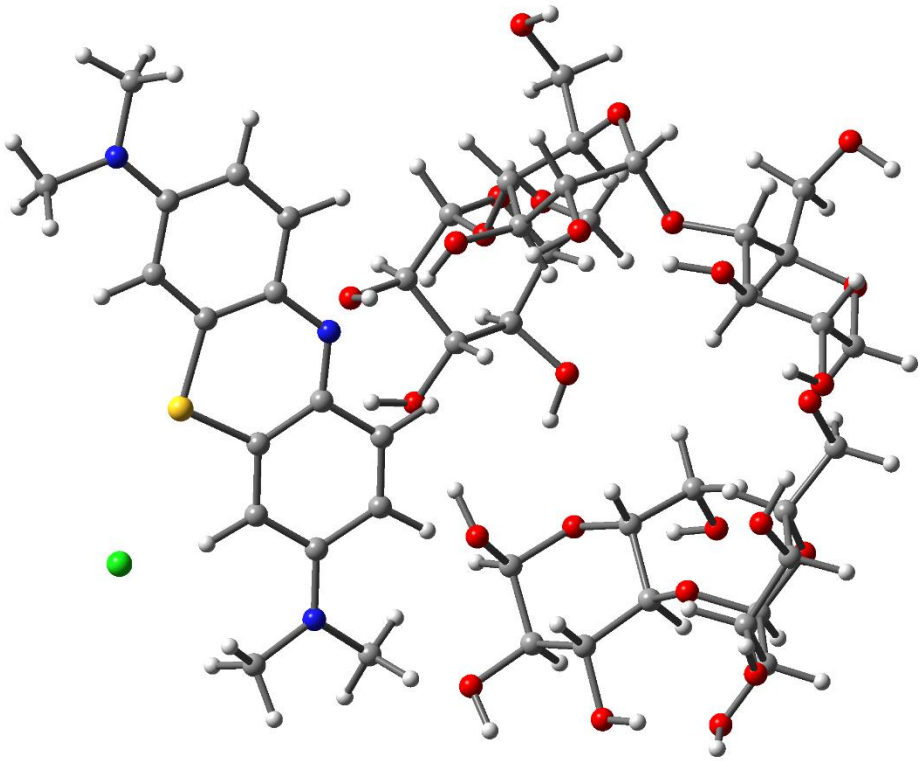

methylene blue /pullulan 42

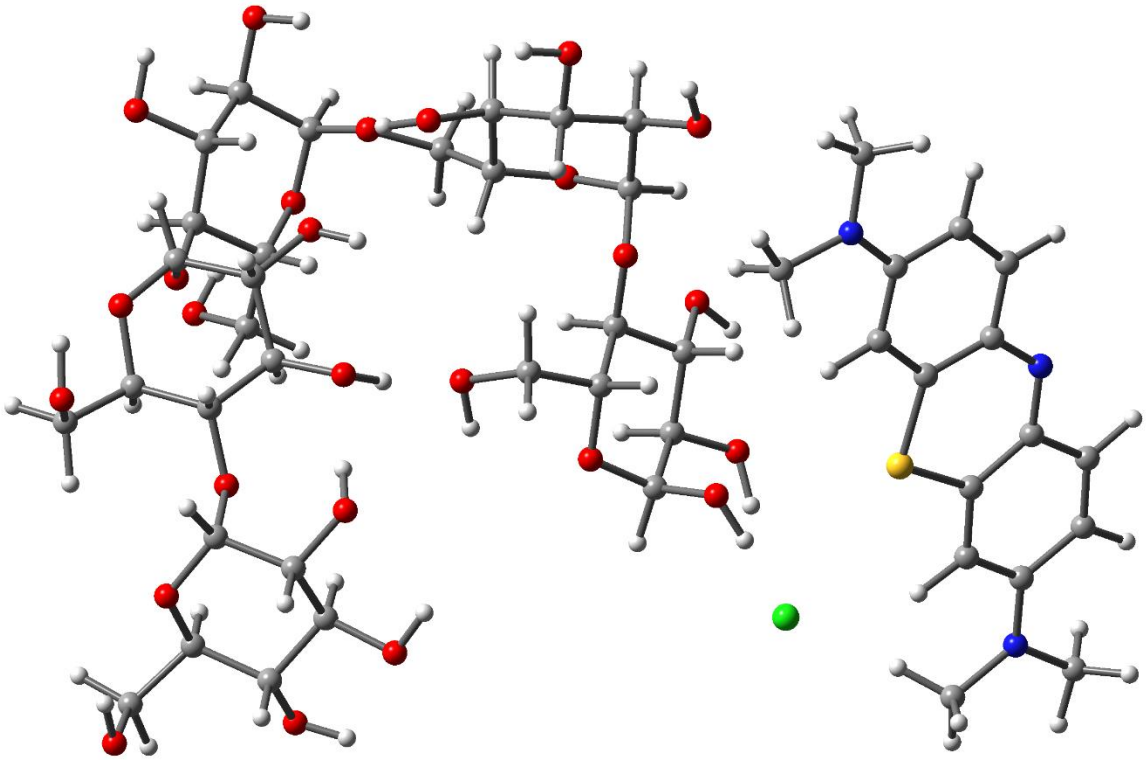

methylene blue /pullulan 43

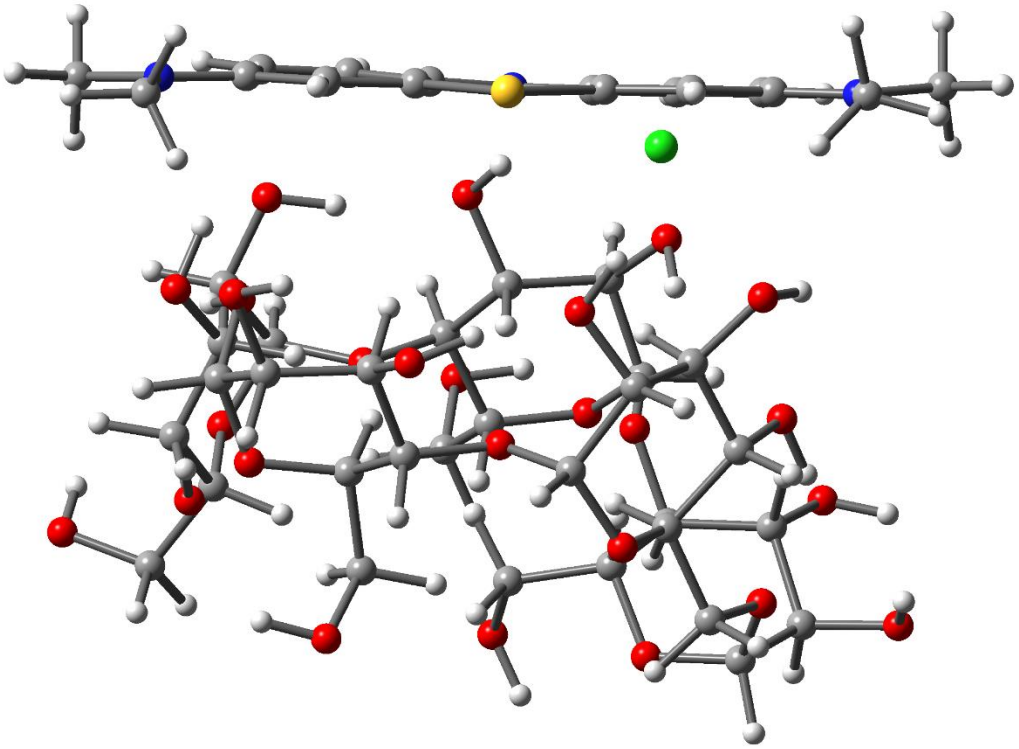

methylene blue /pullulan 44

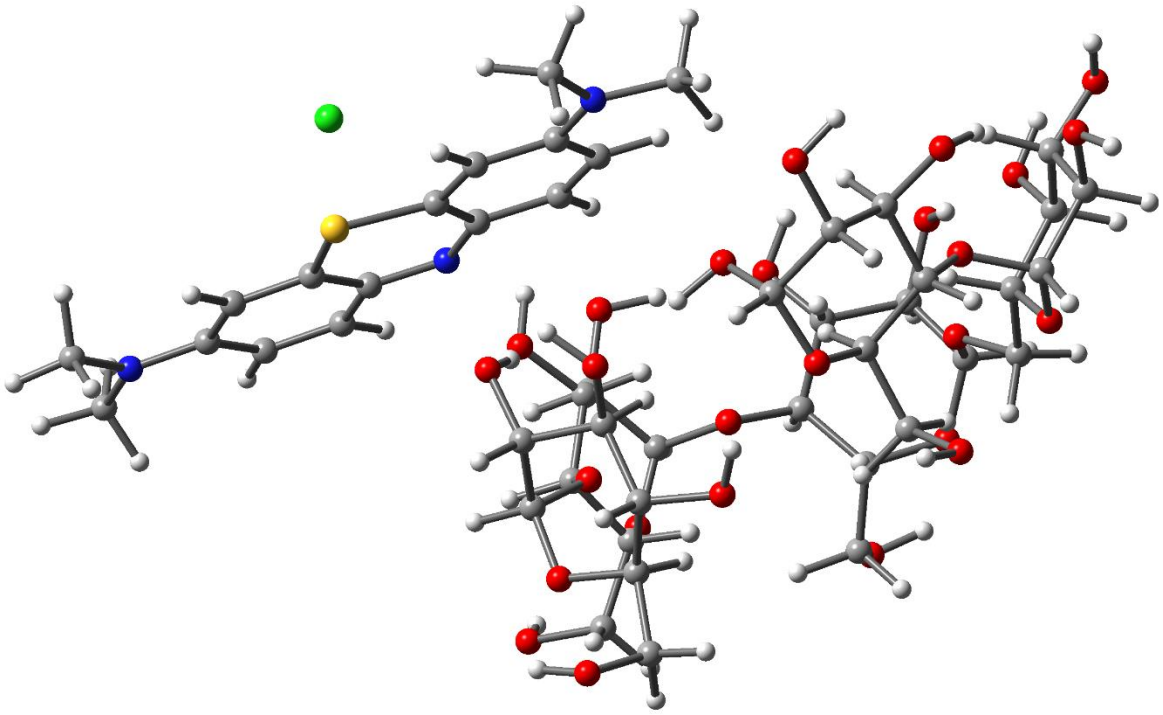

methylene blue /pullulan 47

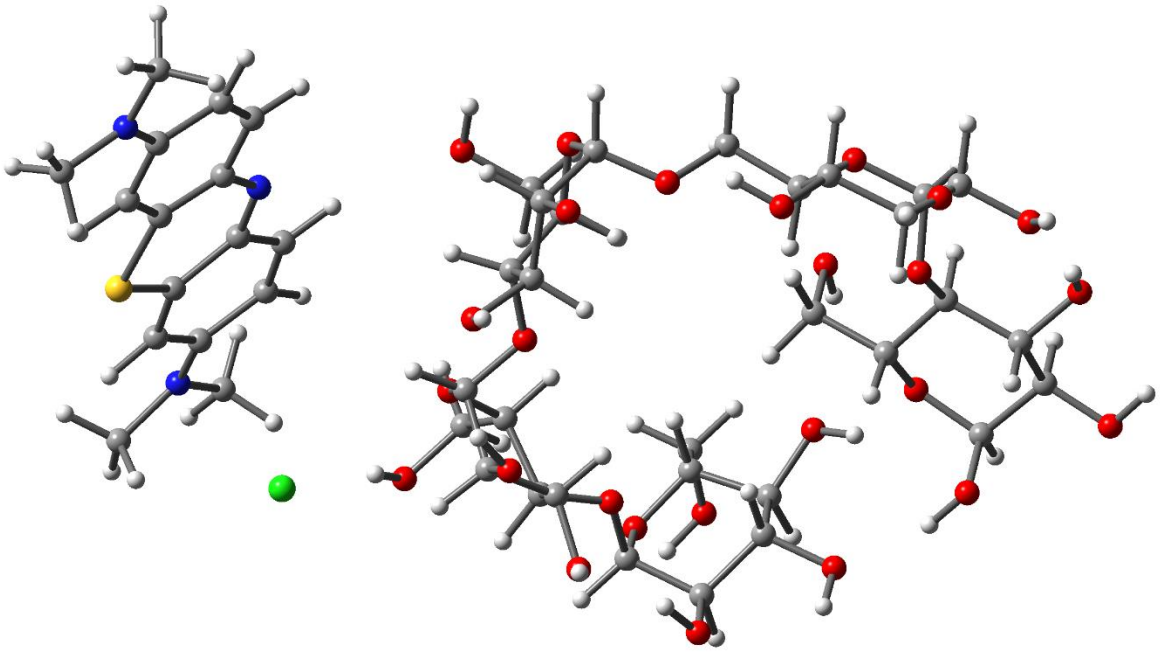

methylene blue /pullulan 50

Fig.4-2. The optimized for the methylene blue /pullulan complexes at the B3LYP/6-31G(d) level of theory.

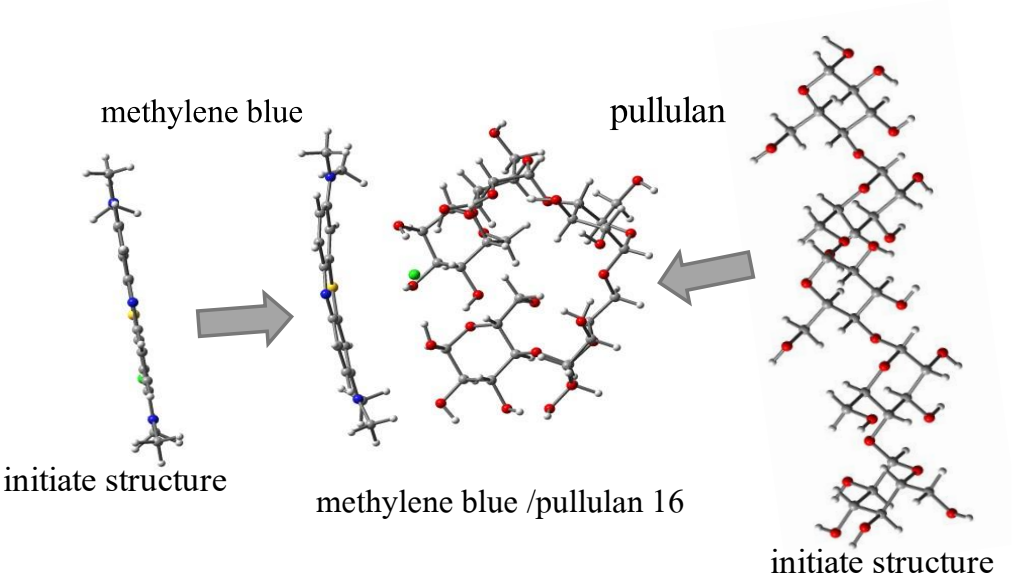

The 3D figure shows the most optimized geometries found using DFT calculations, which were implemented in the B3LYP/6-31(d) level (Fig. 4-2). This allows the change to be identified from its original structure. When calculating the structure of methylene blue and pullulan, particularly pullulan was clearly changed. The figure shows that the pullulan structure is contorted to form a cluster or circle. As for the methylene blue, some structures are slightly bent. Out of all the structural improvements, structure of methylene blue /pullulan 16 was the most stable.

From the B3LYP/6-31G(d) calculations, this technique has been widely used to determine the binding energy of stable molecules. It was found that the binding energy between the methylene blue /pullulan structure was -54.19 to -10.15 kcal/mol respectively. Sorted by the highest to lowest binding energy among all the results are shown in Fig 4-2. methylene blue/pullulan 16 has the highest binding energy of -54.19 kcal/mol, while the lowest binding energy of -10.15 kcal/mol is methylene blue/pullulan structures as from Fig 4-2. It also indicates that the relative energy difference between methylene blue /pullulan 16 compared with methylene blue /pullulan 35 structures is 44.04 kcal/mol. The interaction energy between two molecules methylene blue and pullulan is typically calculated as the energy difference between the product complex methylene blue/pullulan. The small basis sets stabilize the complex more

than the separate components due to the basis set superposition error (BSSE). Since the atoms are closer when involved in chemical bonds than they are in intermolecular complexes, the magnitude of the BSSE. The largest BSSE of methylene blue/pullulan 2 is 10.63 kcal/mol. Whereas the smallest BSSE of methylene blue/pullulan 3 to 5.48 kcal/mol was obtained.

Table 1. Binding energy of methylene blue /pullulan structures at the B3LYP/6-31G(d) level of theory.

Structure Name	**Complexation energy (kcal/mole)**	**Relative energy (kcal/mole)**	**BSSE (kcal/mole)**
MB/PL (16)	-54.19	-10.16	10.63
MB/PL (1)	-44.03	0.00	11.57
MB/PL (29)	-39.26	4.77	5.48
MB/PL (14)	-34.97	9.06	8.48
MB/PL (43)	-32.61	11.42	7.41
MB/PL (31)	-25.95	18.08	12.33
MB/PL (28)	-23.54	20.49	7.31
MB/PL (44)	-21.45	22.58	12.19
MB/PL (36)	-10.27	33.76	7.90
MB/PL (38)	-10.27	33.76	7.90
MB/PL (6)	-10.15	33.88	7.66
MB/PL (20)	-10.15	33.88	7.66
MB/PL (42)	-10.15	33.88	7.95
MB/PL (21)	-7.28	36.75	4.88
MB/PL (39)	-6.85	37.18	4.94
MB/PL (35)	-6.71	37.32	4.87
MB/PL (47)	-6.34	37.69	5.80

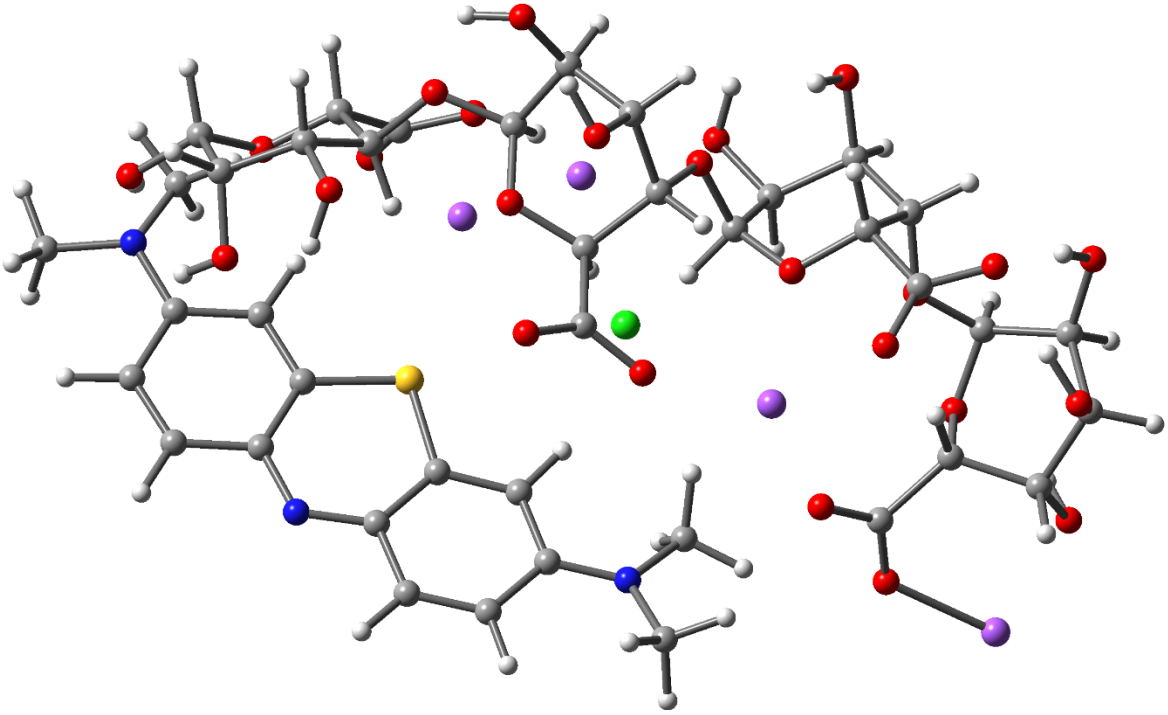

methylene blue /sodium alginate 1

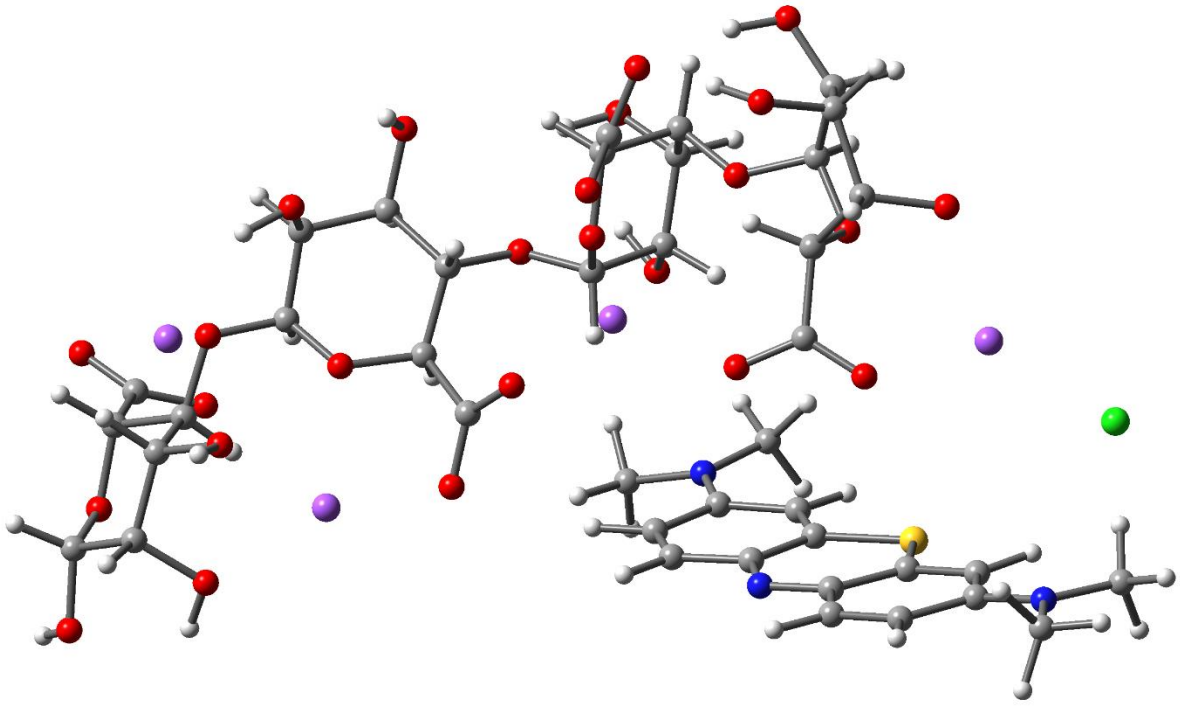

methylene blue /sodium alginate 2

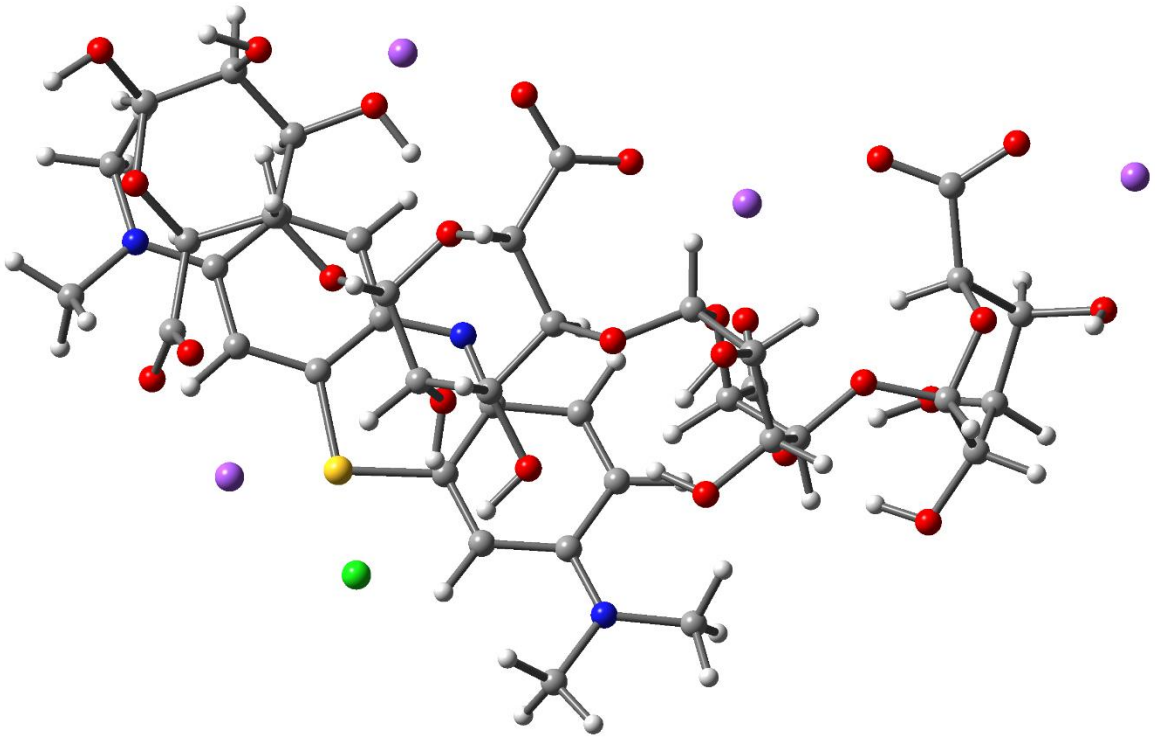

methylene blue /sodium alginate 3

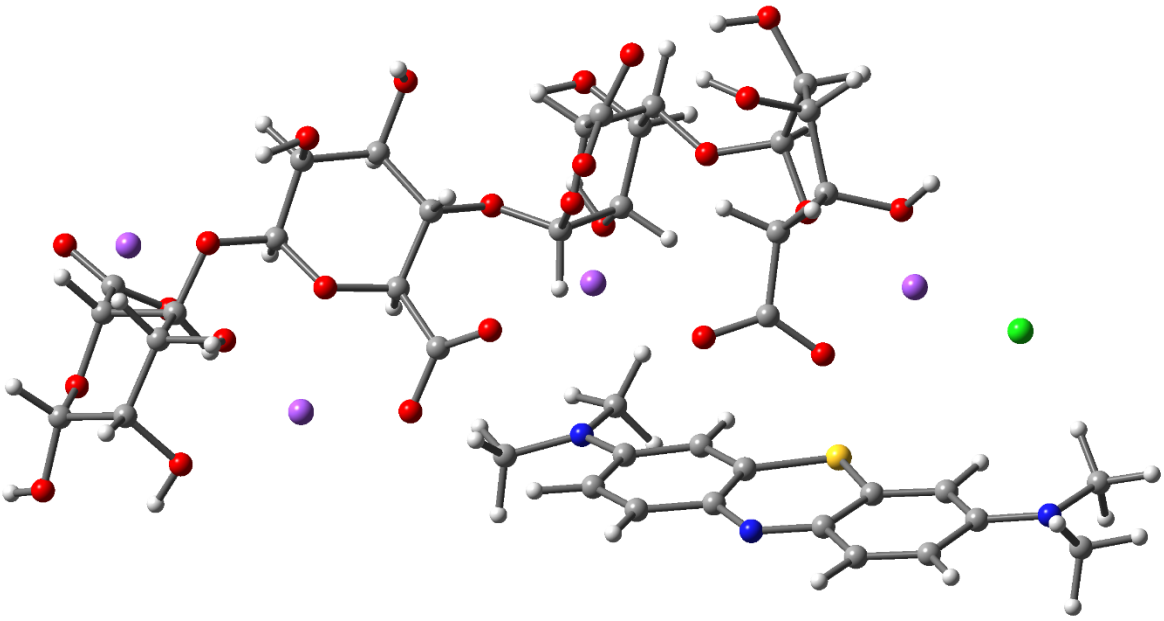

methylene blue /sodium alginate 4

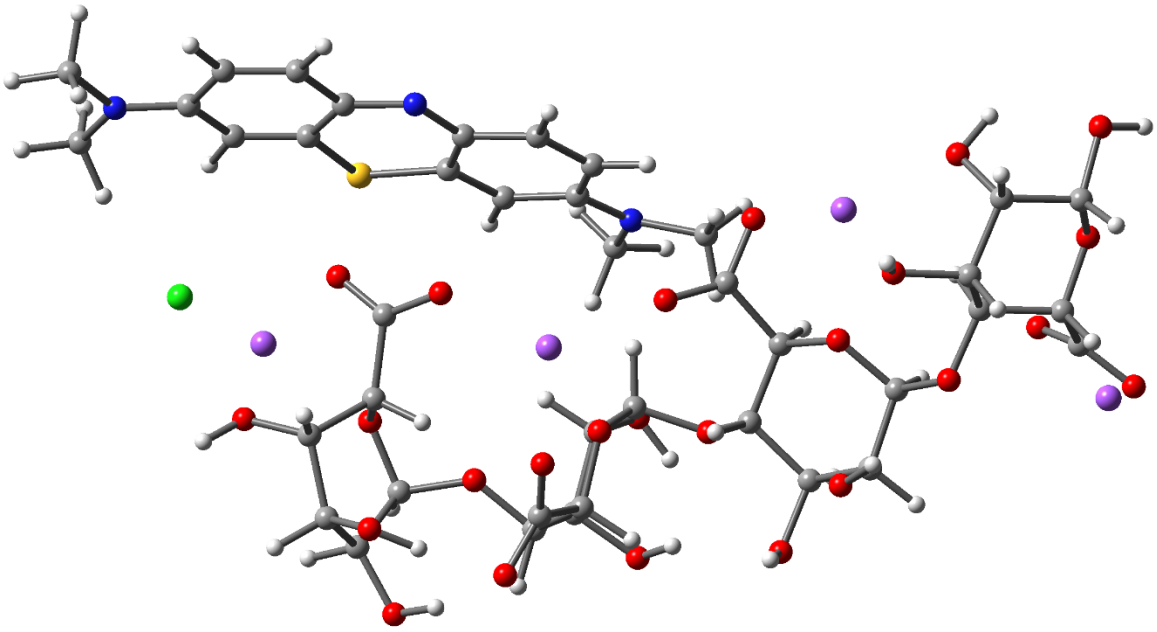

methylene blue /sodium alginate 5

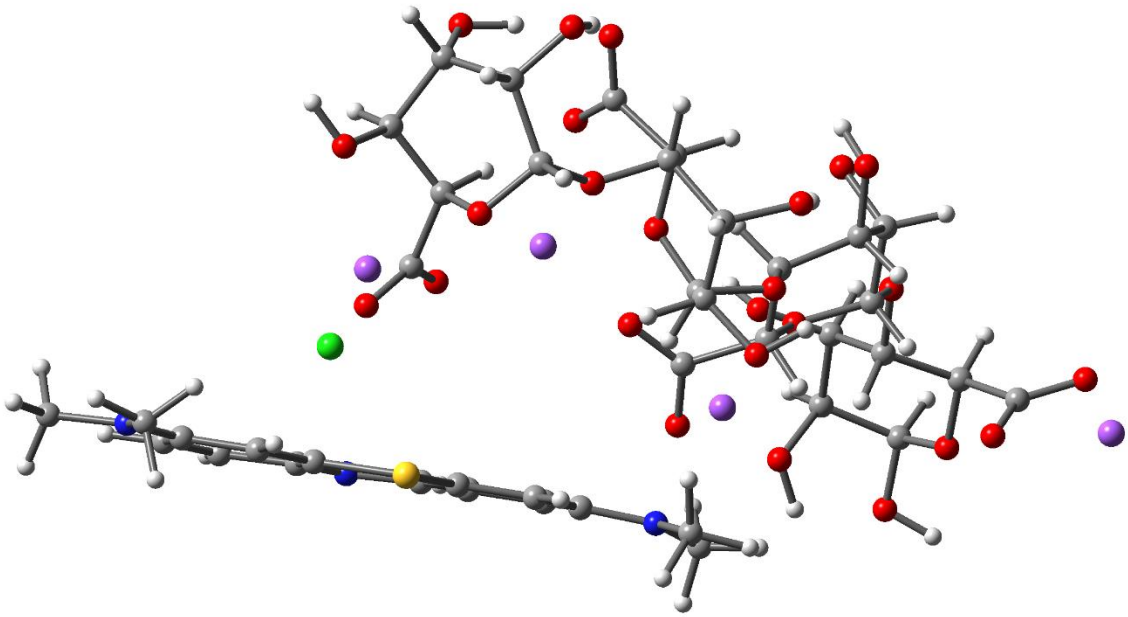

methylene blue /sodium alginate 6

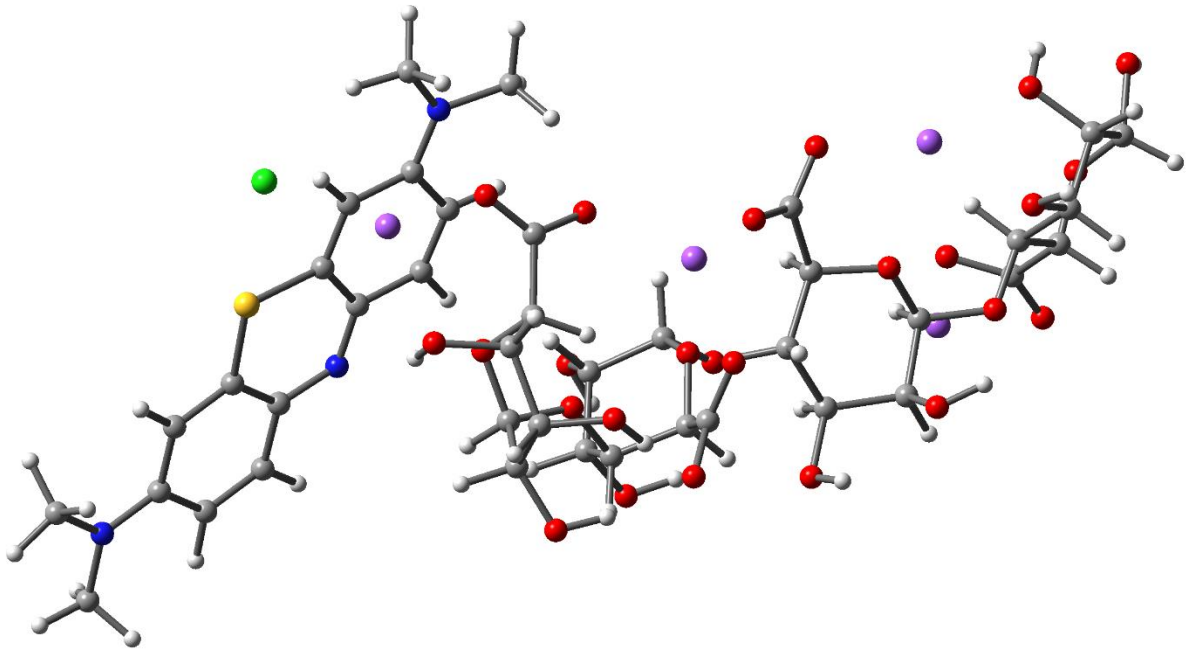

methylene blue /sodium alginate 7

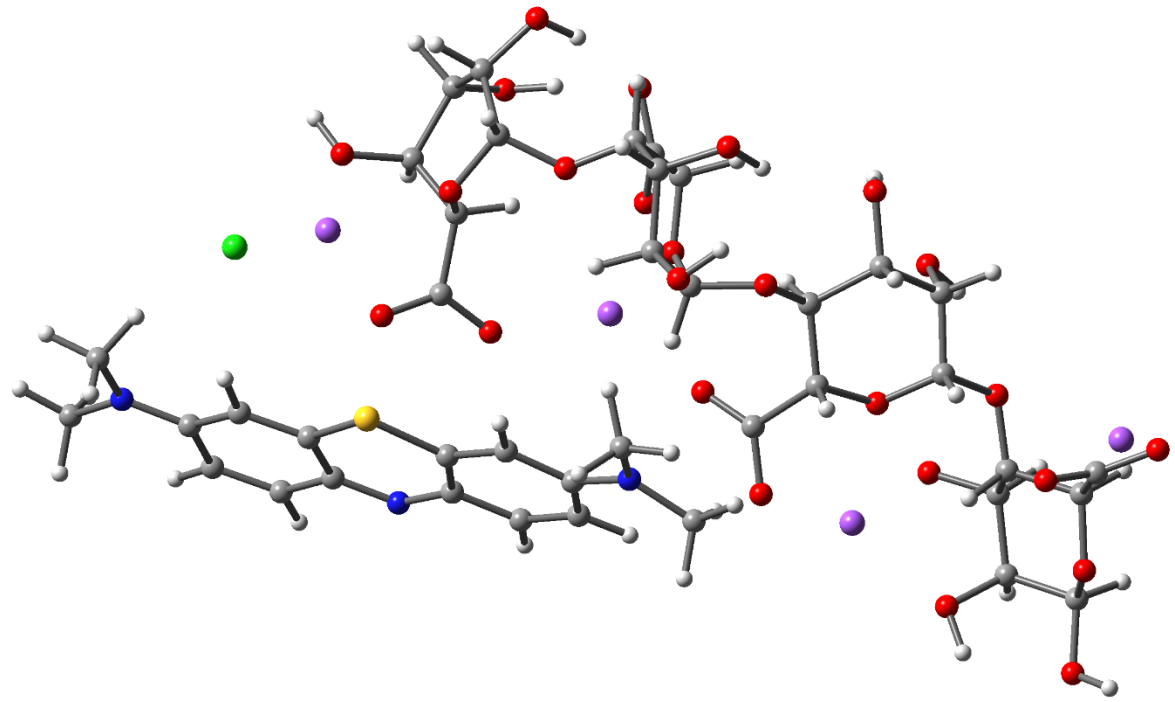

methylene blue /sodium alginate 8

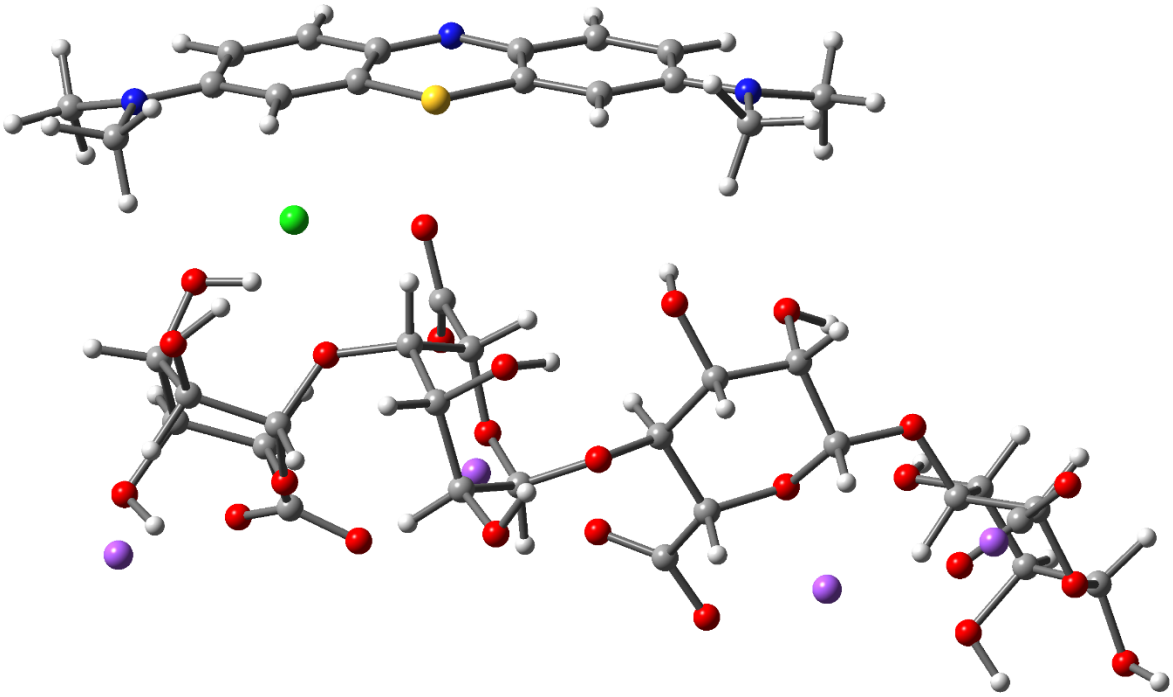

methylene blue /sodium alginate 9

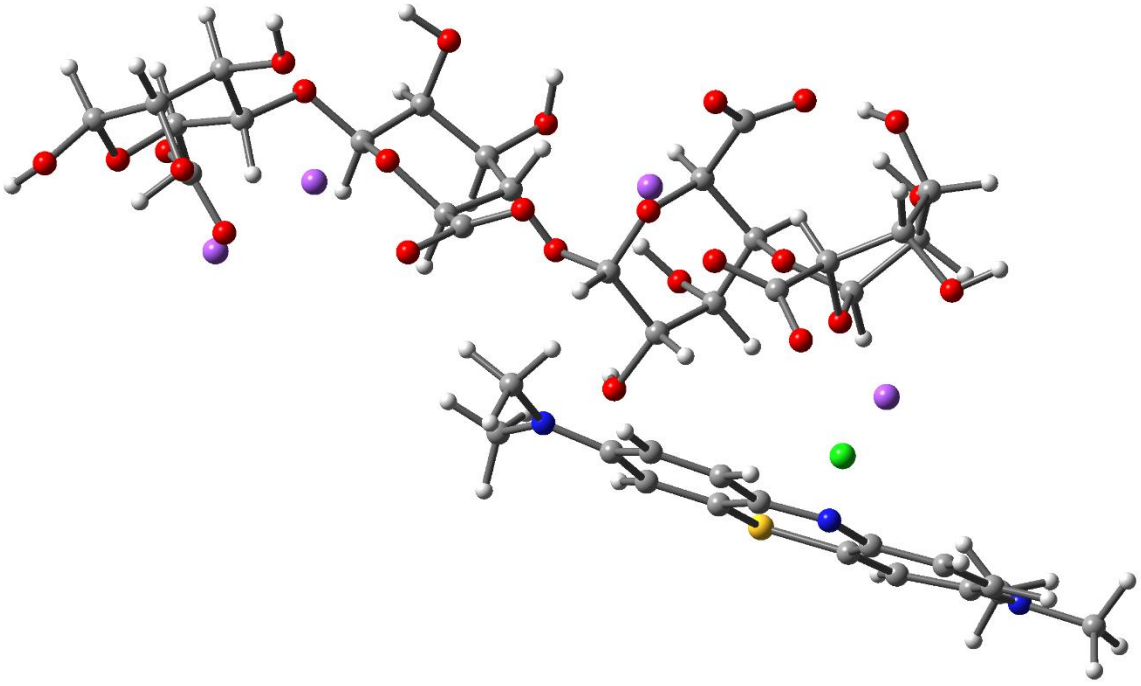

methylene blue /sodium alginate 10

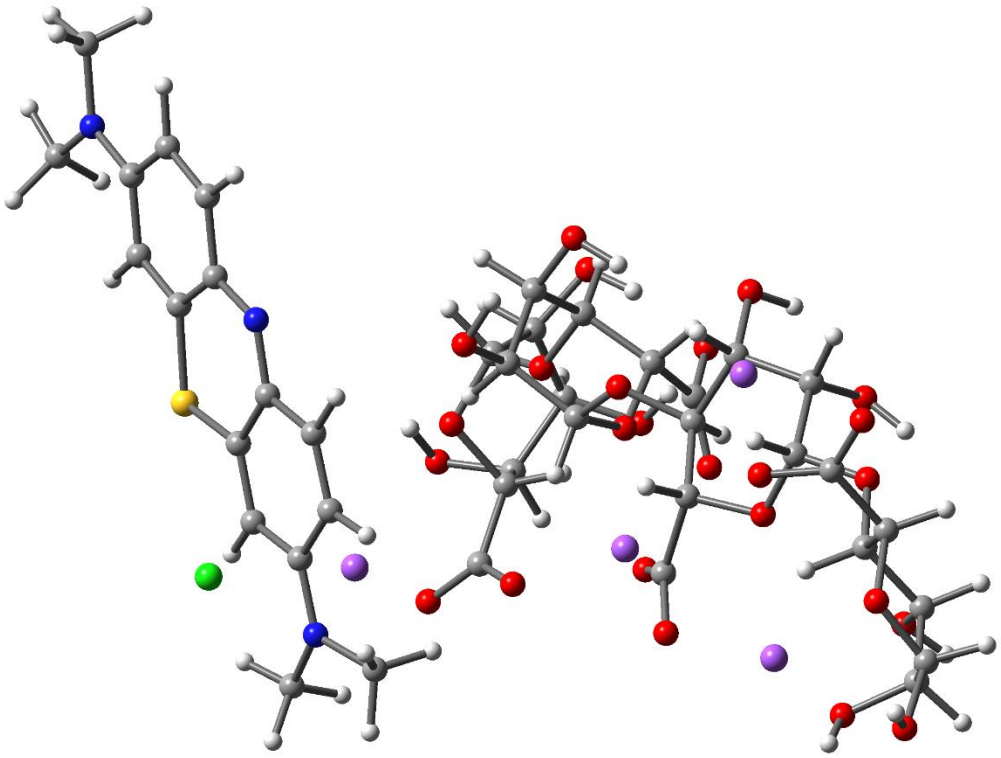

methylene blue /sodium alginate 11

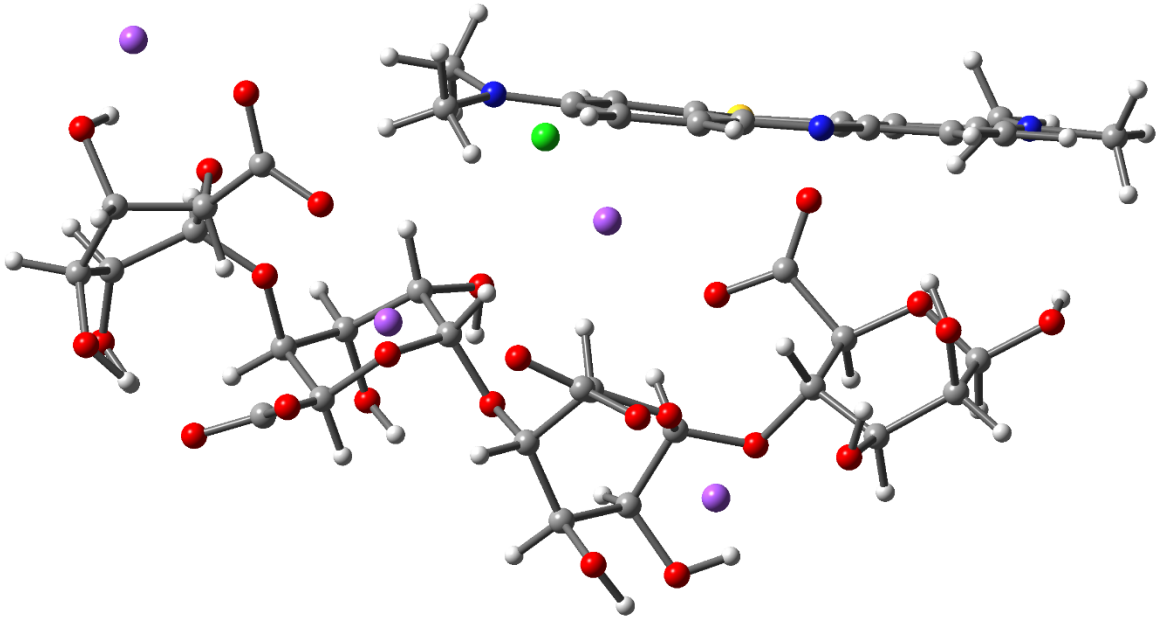

methylene blue /sodium alginate 12

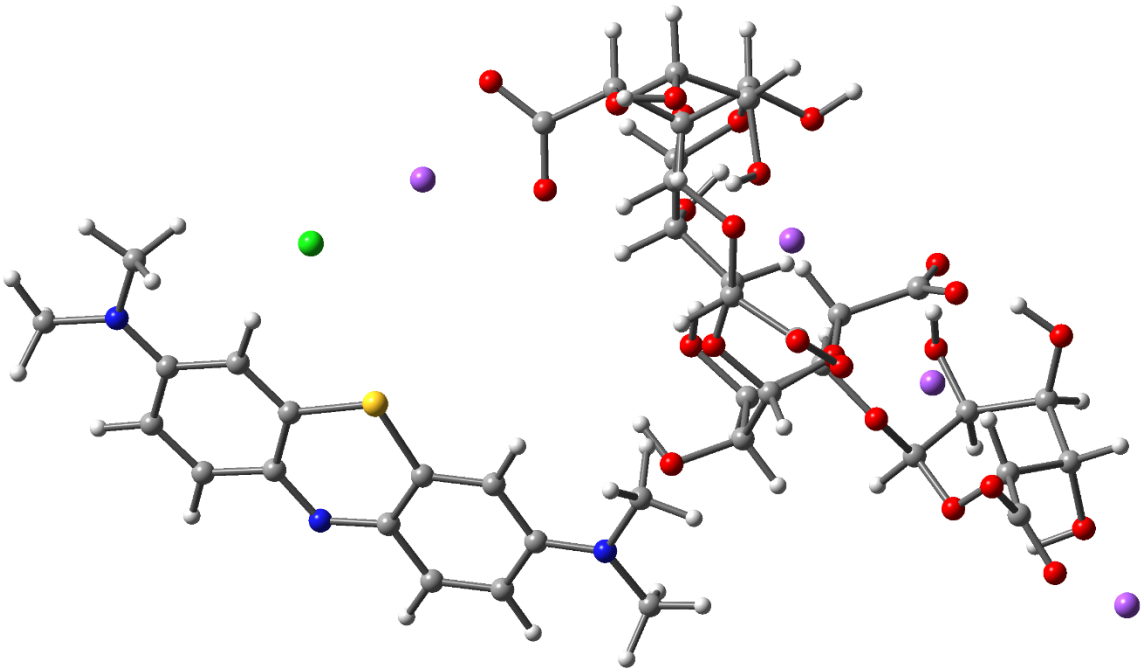

methylene blue /sodium alginate 13

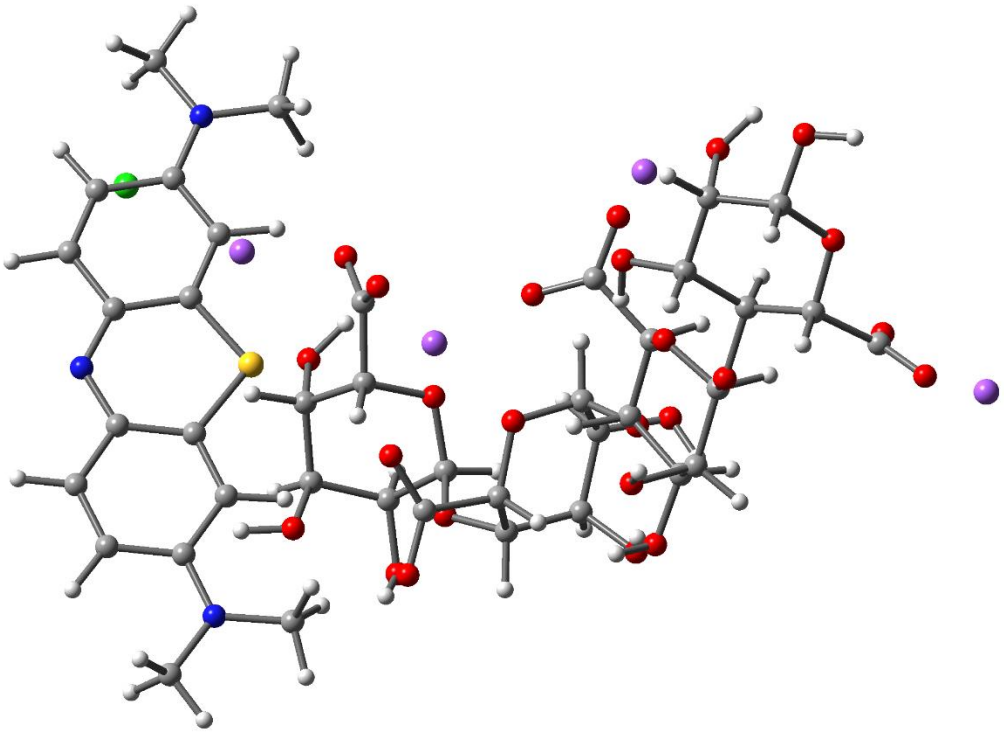

methylene blue /sodium alginate 14

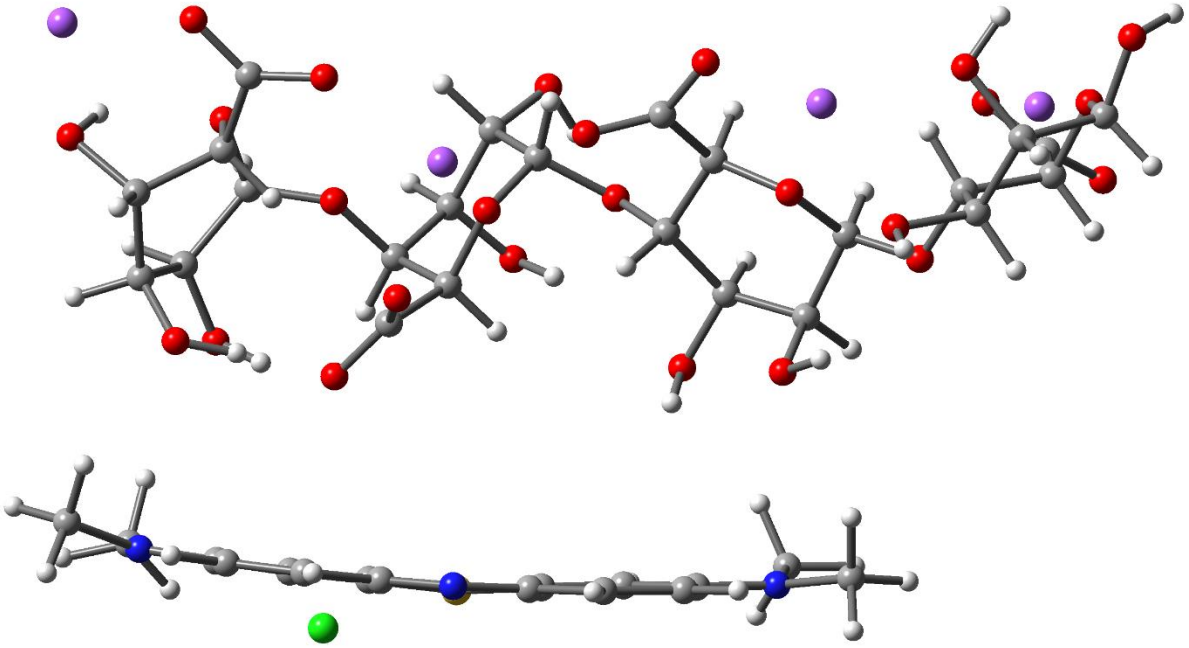

methylene blue /sodium alginate 15

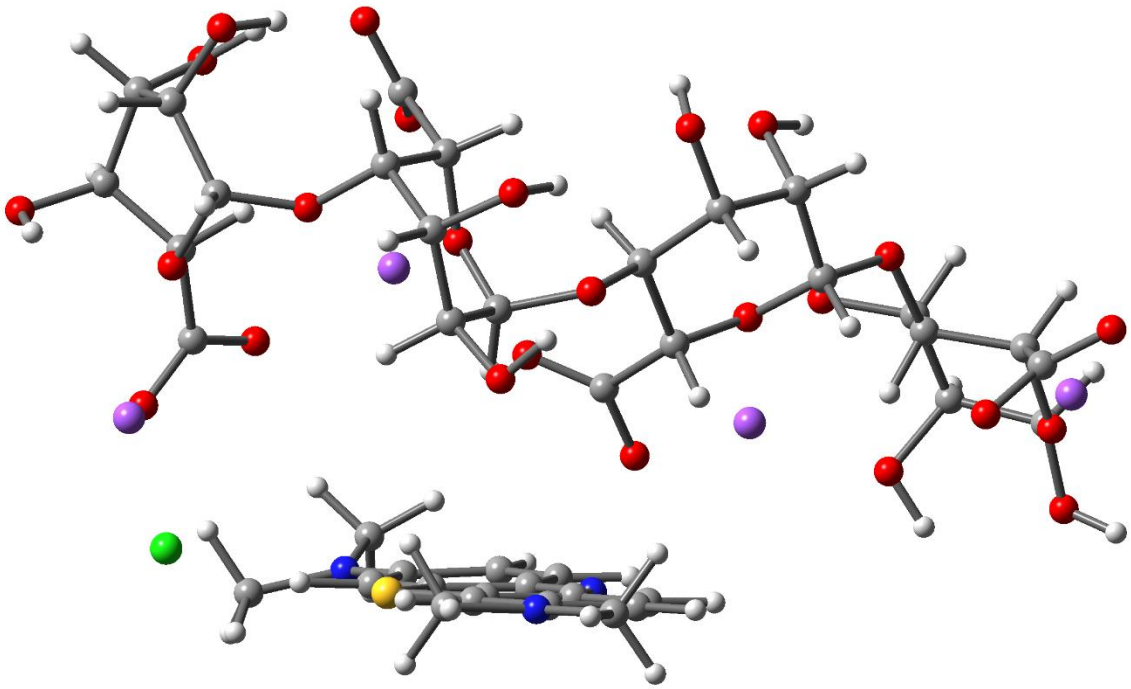

methylene blue /sodium alginate 16

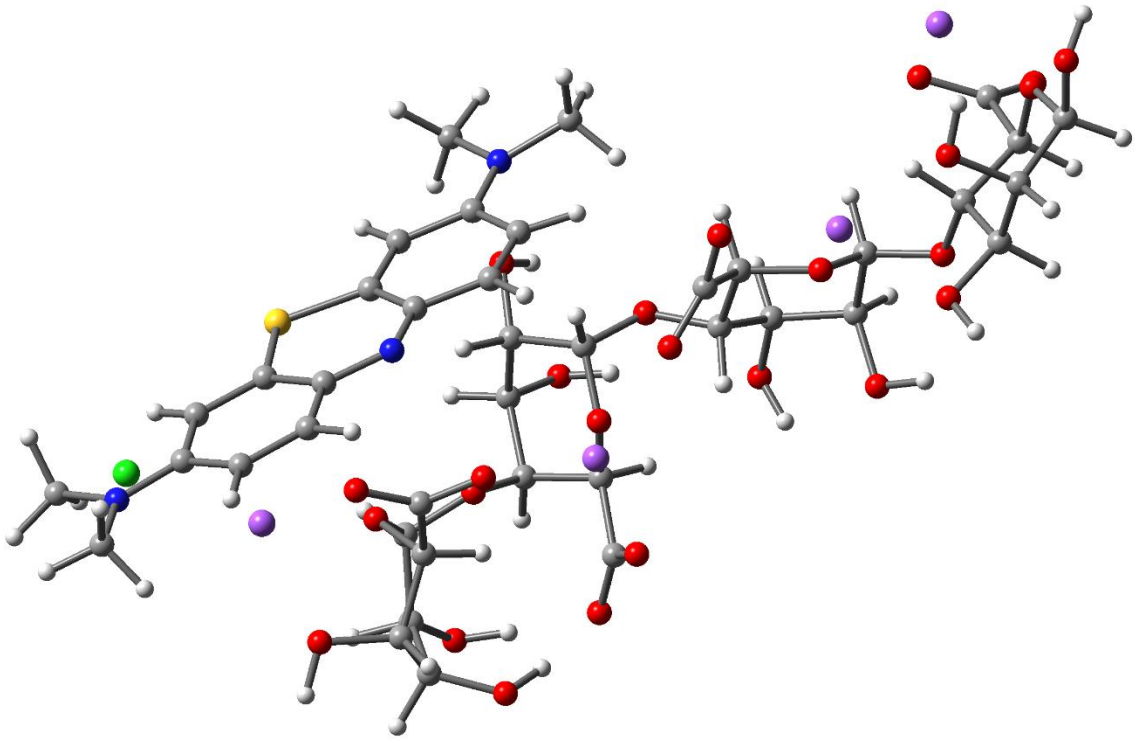

methylene blue /sodium alginate 17

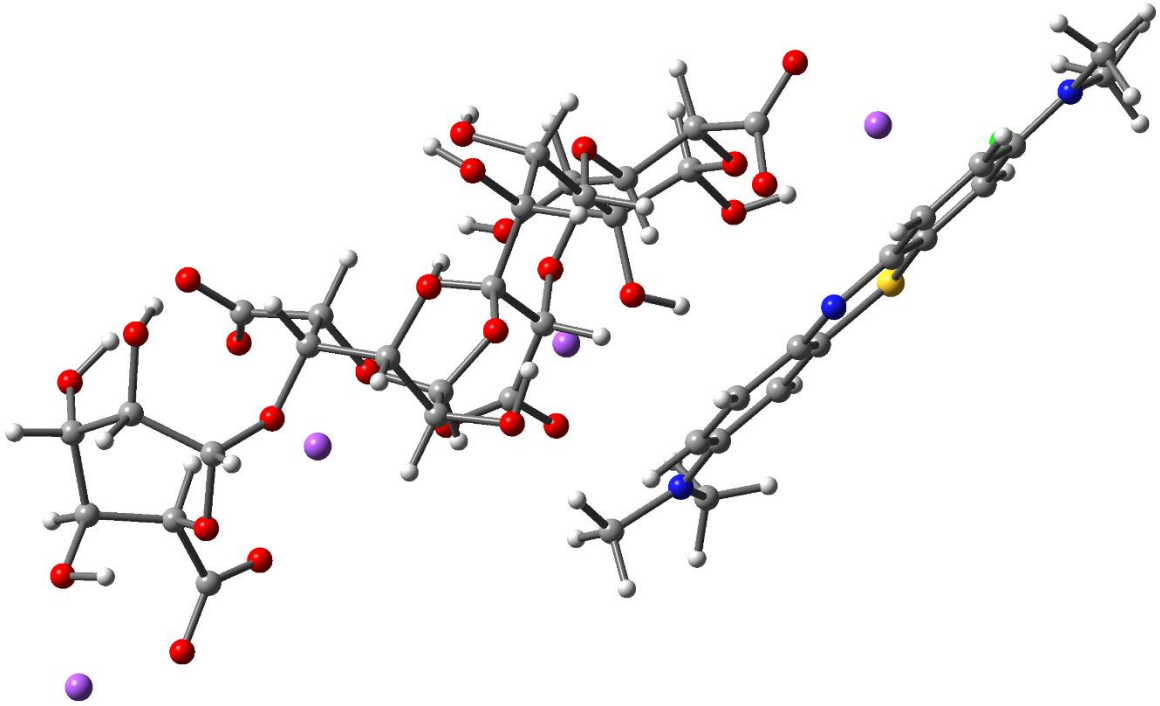

methylene blue /sodium alginate 18

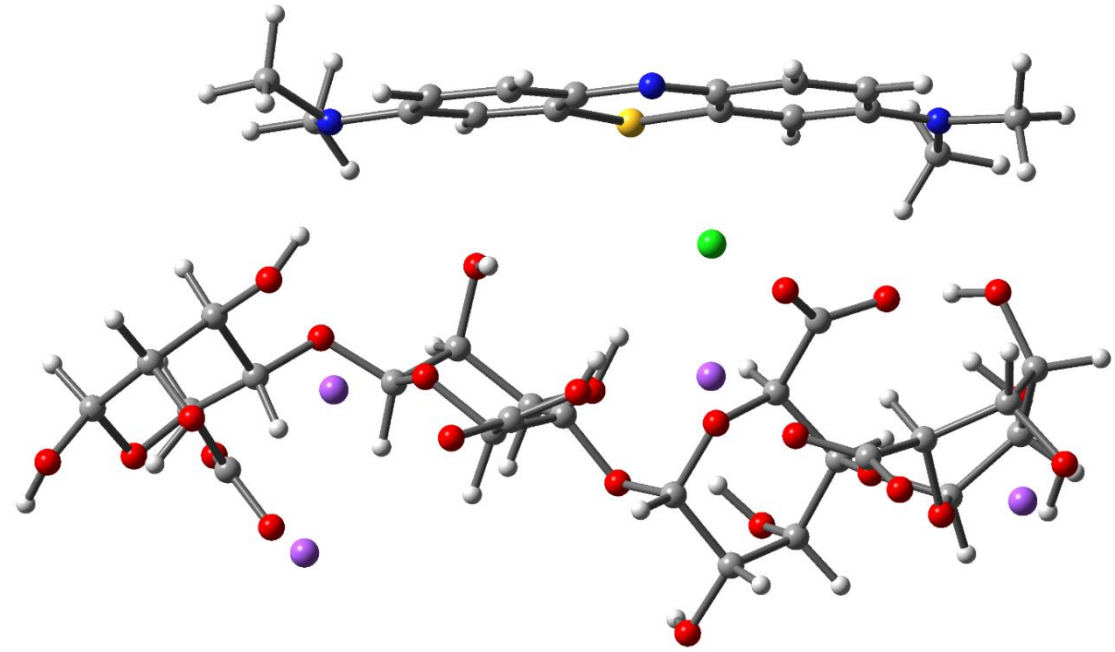

methylene blue /sodium alginate 19

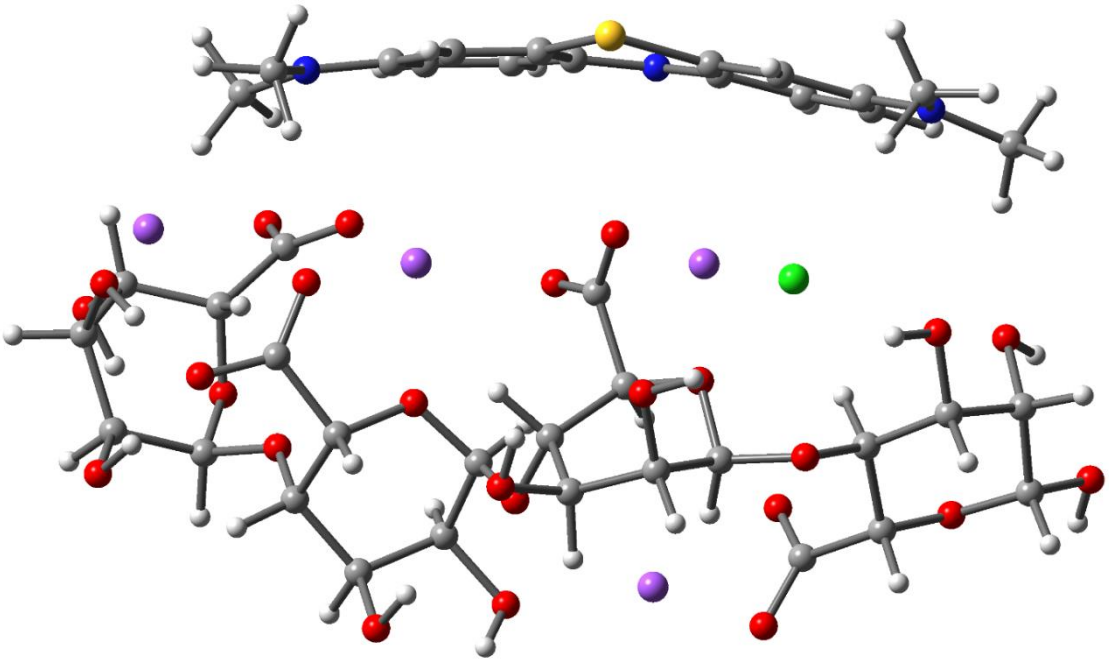

methylene blue /sodium alginate 20

Fig.4-3. the optimized for the methylene blue /sodium alginate complexes at the B3LYP/6-31G(d) level of theory.

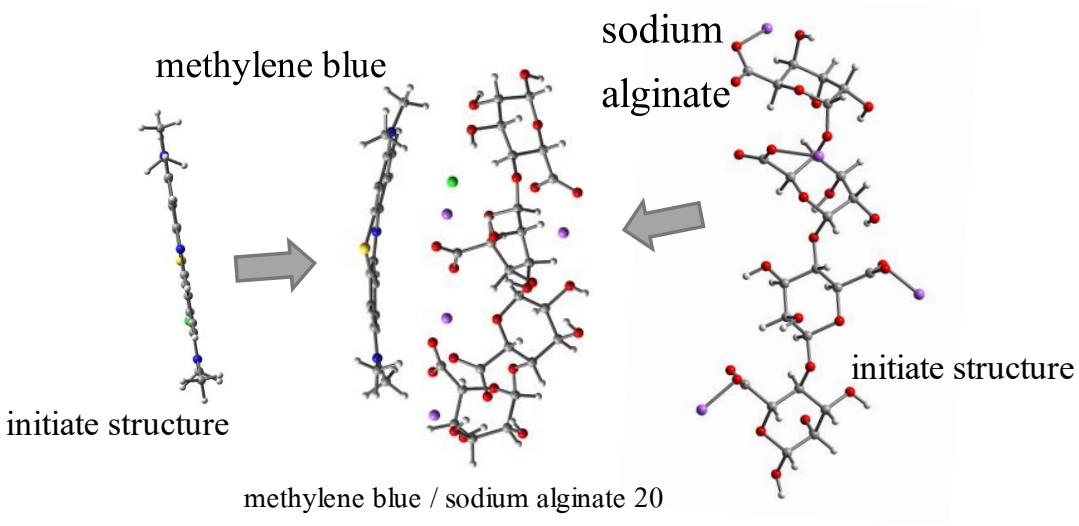

methylene blue / sodium alginate 20

The 3D figure shows the most optimized geometries found using DFT calculations, which were implemented in the B3LYP/6-31(d) level (Fig. 4-3). The complex structure of methylene blue /sodium alginate has differed from its initial structure. Furthermore, the position of methylene blue and sodium alginate structures shifted towards one another, which can analyze the reaction between methylene blue /sodium alginate were investigated by comparing vdW radii. Of all the optimized geometries, the structure of methylene blue /sodium alginate3 is the most stable.

The binding energy is usually obtained from the solution of the Schrödinger equation which is, in turn, complicated by the impossibility to separate the center-of-mass motion. The binding energy is the amount of energy required to separate a particle from a system of particles or to disperse all the particles of the system. This binding energy is shown in Fig.4-3 has presented measurements of the optimization for the methylene blue /sodium alginate complexes structure at the B3LYP/6-31G(d) level of theory. The binding energy results in all 20 complex structures show that the highest value is -81.40 kcal/mol (methylene blue /sodium alginate 3) and the lowest value of the measurement of the complex structure is -44.13 kcal/mol (methylene blue /sodium alginate 5). The relative energy, which shows the difference between the most stable complex structure and the lowest stable complex structure, indicates that the relative energy is -37.27 kcal/mol. In addition, the BSSE results between the methylene blue /sodium alginate structure are 16.18 to 8.54 kcal/mol.

Table 2. Binding energy of methylene blue /sodium alginate structure at the B3LYP/6-31G(d) level of theory.

Structure Name	Complexation energy (kcal/mole)	Relative energy (kcal/mole)	BSSE (kcal/mole)
MB/SA (20)	-69.39	0.00	14.32
MB/SA (3)	-67.56	1.83	11.53
MB/SA (4)	-67.56	1.83	11.53
MB/SA (14)	-64.92	4.47	10.40
MB/SA (1)	-49.58	19.81	12.27
MB/SA (18)	-49.09	20.30	7.06
MB/SA (12)	-47.74	21.65	12.56
MB/SA (13)	-47.06	22.33	6.16
MB/SA (16)	-45.69	23.70	9.80
MB/SA (2)	-44.36	25.03	10.05
MB/SA (7)	-42.49	26.90	8.20
MB/SA (11)	-42.49	26.90	8.20
MB/SA (5)	-39.08	30.31	10.22
MB/SA (8)	-38.13	31.26	9.31
MB/SA (6)	-38.12	31.27	9.31
MB/SA (17)	-38.12	31.27	9.32
MB/SA (19)	-21.84	47.55	11.78
MB/SA (10)	-15.97	53.42	9.07
MB/SA (9)	-13.61	55.78	11.30
MB/SA (15)	-1.19	68.20	8.00

Table 3. The values chemical reactivity of AOS structure at the B3LYP/6-31G(d) level of theory.

Property	Formular	Structure		
		hydroxyl radical	hydrogen peroxide	ozone
LUMO energy (eV)	ELUMO	-6.59	0.57	-4.90
SOMO*, HOMO energy (eV)	EHOMO	-7.26	-6.71	-8.98
energy gap (eV)	Eg = ELUMO – EHOMO	0.67	7.27	4.08
chemical potential	μ = (ELUMO + EHOMO)/2	-6.93	-3.07	-6.94
global hardness	η = (ELUMO – EHOMO)/2	0.34	3.64	2.04
softness	$\sigma = 1/\eta$	2.98	0.27	0.49
electronegativity (EN)	$\chi = -\mu$	6.93	3.07	6.94

In part of Table 3 presents various parameters. The LUMO energy (eV), HOMO energy (eV), energy gap (eV) (The value of the energy difference between HOMO energy and LUMO energy well as HOMO energy and LUMO energy play a very important role in the stability and reactivity of molecules), hardness [4-8),(4-9)], softness (softness is just reciprocal of the hardness), and electro-negativity associated with decolorization mechanisms have been calculated for the OH radical structure, H_2O_2 structure, and ozone structure respectively. Thus, the oxidant power of structures can be estimated by considering all the possible physicochemical characteristics such as orbital. Conceptual density functional theory offers a wide range of chemical reactivity indices for the description of chemical processes. It is clear from Table1, the energy gap for all molecules depends on the number of HOMO and LUMO. The total energy for all study molecules as AOS species. which the structures that were analyzed, it is showing different in results. It is well known that the singly occupied molecular orbital (SOMO) of a radical species is considered to be highly reactive. The global hardness presents the

resistance of a chemical species to change its electronic configuration. The high value of global hardness means a very stable system to accept and donate electrons. The global hardness is positive, and its minimum value is zero. From the results, it can be seen that OH radical structure has the highest hardness (2.39). In addition, the SOMO energy of OH radical structure (-7.26 eV). In terms of electronegativity of OH radical structure (6.93) is also higher than H_2O_2 structure.

Table 4. The values chemical reactivity of structure at the B3LYP/6-31G(d) level of theory.

Property	Structure				
	methylene blue	pullulan	sodium alginate	methylene blue/pullulan	methylene blue/sodium alginate
LUMO energy (eV)	-2.99	0.81	-2.05	-3.48	-3.32
HOMO energy (eV)	-4.08	-6.73	-5.40	-5.57	-5.73
energy gap (eV)	1.09	7.54	3.35	2.09	2.41
chemical potential	-3.54	-2.96	-3.73	-4.53	-4.53
global hardness	0.55	3.77	1.68	1.05	1.21
softness	1.83	0.27	0.60	0.96	0.83
electronegativity (EN)	3.54	2.96	3.73	4.53	4.53

The various parameters LUMO energy (eV), HOMO energy (eV), energy gap (eV), hardness, softness, and electronegativity associated with decolorization mechanisms have been calculated for the methylene blue pullulan and methylene blue /sodium alginate complex structures. The chemical reactivity bases on the cooperation effects of different parameters are presented in Table 4. The HOMO energy of a molecule shows the electron-donating ability as when energetically reacted, found easiest to take away electrons from this orbital path whereas LUMO characterizes electrons accepting ability. We report that as the energy gap of methylene blue structure is 1.09 eV, pullulan structure is 7.54 eV, and sodium alginate structure is 3.35eV. There is indicates methylene blue structure is a smaller gap than the pullulan structure and

sodium alginate structure. Thus, the small energy gap between LUMO and HOMO infers the molecule can reactive more easily. Whereas the large energy gap indicates the molecule is difficult to reactive.

To develop complex structures for AOS detection with enhanced oxidative ability, it is important to stabilize methylene blue by combining it with water-soluble polymers. If the methylene blue is stable, it can protect against AOS attacks. Properties of methylene blue: deep blue in color, highly soluble in water. Methylene blue [4-10] is a colorful organic chloride salt compound used in indicators by us apply as a dye to help them see decolorization under the uniform thin film. methylene blue can cause easy oxidation and reduction agents.

As mentioned above of water-soluble polymers, we choose water-soluble polymers are sodium alginate and pullulan act as a protection layer for methylene blue. Due to the good properties of sodium alginate and pullulan. Sodium alginate [4-1), (4-2)] is obtained from brown algae. The structure is an inorganic salt of alginic acid, the most used type in the food industry is sodium alginate. Alginates are polymers of two substances, β-D-mannuronic acid (M) and α-L-guluronic acid (G) acid. Sodium alginate shows good film-forming properties and low price, due to its popularity in large-scale production in chemical industries. Pullulan [4-11), (4-12)] model is represented by five glucose units to investigate the large and complex pullulan structure. Pullulan is a natural water-soluble polysaccharide with excellent film-forming properties. It is a water-soluble microbial polysaccharide, which is an ideal material for edible films and coatings. Besides being flavorless and having good oxygen barrier properties, and its application for creating films, Pullulan has low transparency.

Hence as for complex structures, the energy gap of methylene blue/sodium alginate structure (2.41 eV) and methylene blue/pullulan structure (2.09 eV) is bigger than the energy gap of methylene blue structure (1.09 eV), which indicates the sodium alginate and pullulan would be a protective layer before the decolorization mechanism occurs. Furthermore, in complex structures, the energy gap of methylene blue/ pullulan structure is smaller than the energy gap of methylene blue/ sodium alginate structure, which indicates a smaller gap allows the electron to easily jump from the lower to a higher energy level. Where the methylene blue/

pullulan structure easily oxidation more than methylene blue/ sodium alginate structure. Furthermore, we find that the pullulan structure has a bigger gap more than the methylene sodium alginate structure, which means the pullulan structure is stable more than the sodium alginate structure. The more stable will be to prevent attacks from AOS. The pullulan structure is excellent to act as a protection layer for MB due to the harder be to react.

However, we compare the result of OH radical structure with methylene blue structure, pullulan structure, sodium alginate structure, and complex structures. While the HOMO of methylene blue structure (-4.08 eV), sodium alginate structure (-5.40 eV) methylene blue/pullulan structure (-5.57 eV) and of methylene blue/sodium alginate structure (-5.73 eV) are higher than the LUMO of OH radical structure, it indicates that the molecule structures can cause oxidation to occur with OH radical structure. Similarly, as for pullulan is lower than the LUMO of OH radical structure slightly. Forasmuch OH radical is singly occupied, it is well known that a radical species is considered to be highly reactive.

4-5 Conclusions

This study was fully optimized using the B3LYP density functional method and 6-31G (d) basis set. The research results are significantly satisfactory and conform with those from former and relevant research. The results confirmed the energetic reaction in decolorization between methylene blue/pullulan and methylene blue/sodium alginate. Furthermore, when analyzing the values of LUMO energy and HOMO energy from the calculation of the structures of methylene blue, pullulan, sodium alginate, methylene blue/pullulan, and methylene blue/sodium alginate, it indicates that OH radical can induce methylene blue, pullulan, sodium alginate, methylene blue/pullulan, and methylene blue/sodium alginate to decolorization. Finally of the results research assumption that OH radical, which has the strongest oxidative ability among AOS. It is easily reacting with methylene blue/pullulan or methylene blue/sodium alginate complex but H_2O_2 and ozone not, which leads decolorization with the OH radicals. According to the species with a highly energetic reaction to molecules due to the high potential in oxidation. Consequently, the selection of these two polymers as detectors of OH radical can help in protecting the invasion of OH radical which finally results in the decolorization of methylene blue.

References

(4-1) P. Temeepresertkij, M. Iwaoka, and S. Iwamori. “Molecular Interactions between Methylene Blue and Sodium Alginate Studied by Molecular Orbital Calculations”. Molecules. 2021, Vol. 26, 7029.

(4-2) S. Yenchit, H. Yamanaka, P. Temeeprasertkij, Y. Oda, O. Kanie, Y. Okamura, T. Inazu, S. Iwamori. “Chemical Stability of a Colorimetric Indicator Based on Sodium Alginate Thin Film and Methylene Blue Dye upon Active Oxygen Species Exposure”. Japanese Journal of Applied Physics. 2020, Vol. 59, p. SDDF09.

(4-3) S. Yenchit, Y. Tadokoro, S. Iwamori. “Measuring Active Oxygen Species across a Nonwoven Fabric Using a Pullulan-Mixed Methylene Blue Thin Film and Electron Spin Resonance”. IEEJ Transactions on Sensors and Micromachines. 2019, Vol. 139, pp. 54-60.

(4-4) A. Kumar, V. Pottiboyina, M.D. Sevilla. “Hydroxyl Radical (OH•) Reaction with Guanine in an Aqueous Environment: A DFT Study”. The Journal of Physical Chemistry B. 2011, Vol.115, pp. 15129–15137.

(4-5) E. Çakmak, D.O. Isin. “A theoretical evaluation on free radical scavenging activity of 3-styrylchromone derivatives: the DFT study”. Journal of Molecular Modeling. 2020, Vol. 26, pp. 98.

(4-6) S. Balachandar, M. Dhandapani, I.V.M.V. Enoch, S. Suganthi. “Structural Analysis, Molecular Docking and DFT Calculations of Bis (Pyrazolium Picrate) Monohydrate Interaction with Calf Thymus DNA and Microbes”. ChemistrySelect. 2017, Vol. 2, pp. 9298– 9311.

(4-7) N. Okutsu, K. Shimamura, E. Shimizu, S. Shulga, V.I. Danilov, N. Kurita. “DFT study on the attacking mechanisms of H and OH radicals to G-C and A-T base pairs in water”. AIP Conference Proceedings 1709. 2016, pp. 020006-1–020006-14.

(4-8) R.G. Parr, R.G. Pearson. “Absolute Hardness: Companion Parameter to Absolute Electronegativity”. American Chemical Society. 1983, Vol. 105, pp. 7512-7516.

(4-9) R.G. Pearson. “Absolute Electronegativity and Hardness: Application to Inorganic Chemistry”. Inorganic Chemistry. 1988, Vol. 27, pp. 734-740.

(4-10) Y. Kuang, X. Zhang, S. Zhou. “Adsorption of Methylene Blue in Water onto Activated Carbon by Surfactant Modification”. Water. 2020, Vol. 12, pp. 587.

(4-11) J. Yan, Z. Li, J. Zhang, C. Qiao. “Preparation and Properties of Pullulan Composite Films”. Advanced Materials Research. 2012, Vol. 476-478, pp 2100-2104.

(4-12) Y. Li, W. Yokoyama, J. Wu, J. M, F. Zhong. “Properties of edible films based on pullulan–chitosan blended film-forming solutions at different pH”. The Royal Society of Chemistry. 2015, Vol. 5, pp. 105844–105850.

Chapter 5
Conclusions

5-1 Conclusions

In this study, the author aimed to elucidate the index for AOS detection by theoretically investigating the decolorization phenomenon, which occurs between AOS and the composite membranes made of methylene blue and water-soluble polymers, such as pullulan or sodium alginate. To clarify the intermolecular interactions between methylene blue, pullulan or sodium alginate, and AOS, molecular orbital calculations were performed using Gaussian09 and GaussView software.

The thesis started from overviewing the historical research background about AOS applications to surface modification technology in industrial environments. Then, the features of the Gaussian and GaussView programs were highlighted along with their principles of operation, including input and output files of the programs. The objective of this thesis was finally described.

In Chapter 2, the author has succeeded in analyzing the interaction patterns of the MB–pullulan complex, which undergoes decolorization upon OH* exposure and thus can be utilized for selective OH* detection, by MO calculation at the HF/6-31G(d) and DFT calculation at B3LYP/6-31G(d) level of theory. The results of the calculations suggested the possible formation of hydrogen bonds between the OH groups of pullulan and the sulfur, carbon, or nitrogen atom of methylene blue. The stabilization energy by the complex formation was also estimated.

In Chapter 3, the author has performed DFT calculations at B3LYP/6-31G (d) level of theory to elucidate the geometrical and energetic features of MB, SA, and MB/SA. The results suggested the presence of intermolecular interactions between the N and C atoms of MB and the O (-OOC-) atoms of SA. The estimated binding energies showed that the stability of the MB/SA complex changes depending on the interaction patterns at the B3LYP/6-31G(d) level of theory. Accordingly, the most preferable interaction sites of MB and SA were identified. Moreover, the molecular orbitals of MB, SA, pullulan, MB/SA, and MB/pullulan was analyzed to get insight into the decolorization mechanism for the methylene blue-dyed thin films of water-soluble polymers. The calculations for MB/O3 and MB/SA or pullulan/O3 complexes showed that O3 can decolorize MB; however, the indicators comprising SA or pullulan mixed with MB cannot be decolorized in O3 exposure.

In Chapter 4, the study was extended to analyze the Fortier orbitals. For the fully optimized structures of methylene blue, pullulan, sodium alginate, methylene blue/pullulan, and methylene blue/sodium alginate obtained at the B3LYP density functional method using the 6-31G(d) basis set, the LUMO and HOMO levels were compared with the SOMO level of OH radical. The results supported the assumption that OH radical, a highly reactive species with a high oxidation potential toward various molecules, can react with methylene blue even in the polymer matrix to decolorize it. The result was satisfactory and conform with the previous experimental observations.

All these research results help us understand the decolorization phenomenon of the methylene blue-dyed thin films upon exposure to AOS at the atomic level and thus provide us a theoretical validity to use the film to detect AOS. The weak interactions, which were found in this study to play roles in the decolorization of MB, will be useful for developing efficient AOS-based disinfection and surface modification technologies in industrial processes.

Acknowledgement

Throughout the writing of this dissertation, I have received a great deal of support and assistance.

I would like to express my sincere gratitude to my supervisor, Professor Satoru Iwamori, whose expertise was invaluable in formulating the research questions and methodology. Your insightful feedback pushed me to sharpen my thinking and brought my work to a higher level.

I would like to offer my special thanks to my supervisor, Professor Michio Iwaoka, for their valuable guidance throughout my studies. You provided me with the tools that I needed to choose the right direction and successfully complete my dissertation.

I am deeply grateful to my colleagues from my senior and junior students at Professor Iwamori's laboratory at Tokai university. I want to thank you for your support and for all the opportunities I was given to further my research.

In addition, I would like to extend my sincere thanks to my parents for their wise counsel and sympathetic ear. You are always there for me and provide stimulating discussions as well as happy distractions to rest my mind outside of my research.